ABSTRACT

WIGGIN, MICHAEL BRUCE. Characterizing Optimal Performance of a Passive Elastic Ankle Exoskeleton during Human Locomotion. (Under the direction of Gregory S. Sawicki).

Perhaps because humans are already so well-tuned for locomotion, no autonomous, wearable device intended to assist walking or running has succeeded in reducing metabolic energy consumption for healthy individuals during typical walking conditions. The ankle provides the majority of positive mechanical work during walking and much of this work is delivered via elastic recoil from the Achilles' tendon, which may serve as an energy savings mechanism. My goal for Chapter 1 was to develop a portable ankle exoskeleton taking inspiration from the passive elastic mechanisms at play in the human triceps surae-Achilles' tendon complex during walking.

The exoskeleton was designed to be as transparent to the user as possible having minimal interference with gait kinematics and lightweight enough to minimize the metabolic penalty of adding mass to the user. I designed the exoskeleton to provide plantarflexion torque during stance, and not interfere with toe clearance during swing. To do this I developed a lightweight custom composite frame and two clutches that can engage and disengage a parallel spring based only on ankle kinematic state. The primary system is purely passive containing no motors, electronics or external power supply. A secondary clutch has an additional low power, servomotor to control the timing of engagement of the clutch, which still passively provides assistance but is more versatile and can handle dynamically

changing gait (e.g. increases in speed, asymmetry due to impairment).

To test the validity of our exoskeleton design I performed a variety of studies of individuals walking in many conditions with and without the exoskeleton, on a split belt instrumented treadmill. Kinetic, kinematic, electromyography, and oxygen consumption and carbon dioxide expiration were recorded during all trials. Initial testing of the exoskeleton in Chapter 1 suggests the utility of the clutch, to act in series with the parallel spring. My results indicate the clutched exoskeleton design addresses all three of our design criteria: (1) it does not hinder natural gait kinematics, (2) it is lightweight enough so that added mass has minimal effect on net metabolic energy consumption, and (3) it can produce significant plantarflexor torque assistance during stance, but does not resist toe clearance during swing.

In Chapter 2 I studied the user adaptation to the exoskeleton. Regression fits to indirect calorimetry data indicate that users began to decrease their metabolic energy use below normal walking after ~18.5 min of training with intermediate exoskeleton parallel spring stiffness. These data also suggest that users could decrease their metabolic energy consumption even more than the values we reported with additional training.

In Chapter 3 I took a more in depth view of the neuromechanics and energetics of walking with a passive elastic exoskeleton. Study participants (n=9) reduced their net metabolic power by 7% below normal walking with an intermediate spring stiffness after 28 minutes of walking in the exoskeleton. Kinetic analysis indicates the exoskeleton offloads plantar flexor muscle forces during stance and assists in plantarflexion, which might be key to reducing metabolic energy expenditure. Electromyography (EMG) data indicate that reductions in plantarflexior muscle activation (e.g. soleus) plays a role in decreased net metabolic power, but increases in dorsiflexor (e.g. tibialis anterior) EMG activity at high parallel spring stiffness confounds this reduction and ultimately leads to an increase in net metabolic power for the stiffest exoskeleton parallel springs. Future studies with direct muscle level measurements will be necessary to identify the exact mechanism of energy savings.

© Copyright 2014 Michael Bruce Wiggin

All Rights Reserved

Characterizing Optimal Performance of a Passive Elastic Ankle Exoskeleton during Human Locomotion

by
Michael Bruce Wiggin

A dissertation submitted to the Graduate Faculty of
North Carolina State University
in partial fulfillment of the
requirements for the degree of
Doctor of Philosophy

Biomedical Engineering

Raleigh, North Carolina

2014

APPROVED BY:

Gregory Sawicki Committee Chair	Elizabeth Loboa
Ola Harrysson	Richard Goldberg
Steven Collins	

DEDICATION

This is dedicated to all the members of the Human PoWeR lab, past and present who have helped make this research possible. Without all of your help and support over the years of testing, rebuilding, and testing again this project would never have succeeded.

BIOGRAPHY

Bruce Wiggin is from High Point, NC. He attended high school at Westchester Academy in High Point, NC in 2005. Bruce received his Bachelors of Science in Biomedical Engineering from North Carolina State University in 2009 graduating magna cum laude with a concentration in bioinstrumentation. He is a design engineer specializing in mechatronic, robotic, and medical device design. Bruce's designs have received many national awards including a Da Vinci Award (2001), the President's Award from the American Society of Biomechanics (2012), NCSU Chancellor's Innovation Funding (2012), and several local and national awards and grants. In 2009 Bruce began to pursue his Ph.D. at the Joint Department of Biomedical Engineering at North Carolina State University and the University of North Carolina, Chapel Hill.

ACKNOWLEDGMENTS

I would like to thank my friends and family for their support on this long journey. A special thanks to Rodney Barr for being an awesome mentor and teaching me to be an effective mechanical design engineer. Thanks to Steve Collins for teaching me mechanical design optimization and challenging me to be a better engineer. Thanks to all Human PoWeR lab members for their countless hours spent helping me on this project. Thanks to Audrey Westbrook and Lexis Smith for being the best undergraduate researchers I've had. Finally, a special thanks to Greg Sawicki, you taught me how to be a scientist, a researcher, an investigator, and an academic. Thank you for your mentorship, your advice, and your friendship over the past 5 years.

Table of Contents

LIST OF TABLES vii

LIST OF FIGURES viii

CHAPTER 1: 1

A passive-elastic ankle exoskeleton using controlled energy storage and release to aid human walking 1

Introduction 1

Methods 4

Clutch Design 9

Frame Design 21

Human Walking Testing Methods 23

Results 27

Discussion 38

CHAPTER 2: 41

Characterizing the energetic adaptation to mechanical assistance from a passive elastic exoskeleton during human walking 41

Introduction 41

Methods 43

Results 48

Discussion 48

CHAPTER 3: 50

Stiffness matters: A passive elastic ankle exoskeleton with optimal compliance can reduce the metabolic cost of human walking 50

Summary 50

Methods 55

Results 57

Discussion 76

APPENDICES 87

Appendix A 88

Mechanical Clutch Drawings 88
Appendix B 100
Electromechanical Clutch Drawings 100
Appendix C 111

LIST OF TABLES

Table 1: Comparison of Ankle Exoskeleton Peak Power, Mass, and Power Density. 35
Table 2: Exoskeleton Mass Distribution 36
Table C1: Regression equations for key outcome metrics vs. normalized spring stiffness during walking at 1.25 m/s. 111
Table C2: Regression equations for net metabolic power vs. time training with elastic ankle exoskeletons of varying spring stiffness during walking at 1.25 m/s. 113

LIST OF FIGURES

Figure 1: Passive Exoskeleton Design 5
Figure 2: Exoskeleton Phases, Ankle Angle and Moment, Exoskeleton Torque 7
Figure 3: Passive Clutch Design 10
Figure 4: Active Clutch Design 13
Figure 5: Active Clutch Timing 19
Figure 6: Experimental Methods across Clutch Conditions 25
Figure 7: Joint Angle Kinematics across Clutch Conditions 28
Figure 8: Biological Ankle Moments & Mechanical Powers; and Exoskeleton Torques & Mechanical Powers 30
Figure 9: Torque Angle Curves across Clutch Conditions 32
Figure 10: Electromyography (EMG) across Clutch Conditions 33
Figure 11: Net Metabolic Power across Clutch Conditions 37
Figure 12: Experimental Setup: Training 45
Figure 13: Net Metabolic Power vs. Time during Training 46
Figure 14: Exoskeleton Functional Diagram 53
Figure 15: Net Metabolic Power vs. Exoskeleton Spring Stiffness 59
Figure 16: Functional Stages of Exoskeleton Function and Kinetic Analysis 61
Figure 17: Ankle Joint Muscle Electromyography (EMG) vs. Exoskeleton Spring Stiffness 63
Figure 18: Lower-limb Joint Moments vs. Exoskeleton Spring Stiffness 67
Figure 19: Lower-limb Joint Mechanical Powers vs. Exoskeleton Spring Stiffness 70
Figure 20: Lower Limb Joint Angles 74
Figure 21: Step Length and Width vs. Exoskeleton Spring Stiffness 75

CHAPTER 1:

A passive-elastic ankle exoskeleton using controlled energy storage and release to aid human walking

In preparation for submission to the Journal of Biomechanical Engineering

Initial design concepts published in IEEE Int Conf Rehabil Robot, 2011 [1]

This research has led to one US Utility Patent: US20130046218 A1 and one provisional patent awaiting review (10/15).

Introduction

Efficient human walking is made possible by precisely coordinated ankle propulsion [2]. The ankle provides the majority of positive mechanical work during walking and much of this work is delivered via elastic recoil from the Achilles' tendon, which may serve as an energy savings mechanism [2-4]. Even though the human ankle plays a central role in propulsion, body-weight support and swing initiation during walking [5, 6], most exoskeletal devices do not include ankle plantarflexion assistance. Our goal was to develop a portable ankle exoskeleton taking inspiration from the passive elastic mechanisms at play in the human triceps surae-Achilles' tendon complex during walking.

Current assistive devices tend to be either fully powered [7-10] or purely passive [11, 12]. Fully-powered devices typically employ motors under high gain force control that can mimic the normal torque output of the lower-limb joints over the full gait cycle. Some major downsides to this approach are that powerful motors are heavy, require bulky gears and mounting frames, and rely on finite power sources that must be worn by the user. The consequence of this added mass is a marked decrease in walking economy [13] (i.e. no metabolic savings) during assisted locomotion with portable powered devices.

Purely passive devices (e.g. dynamic ankle-foot orthoses (DAFOs)) can store and release elastic energy in rigid, non-hinged frames to assist walking without assistance from motors. The main advantages of DAFOs are that they are lightweight, relatively low cost and easy to maintain. Furthermore, recent work has shown that DAFOs can lead to small increases in both walking speed and economy post-stroke [11, 14, 15]. There are two key downsides to current DAFO designs in non-clinical use. First, most rigid, non-hinged DAFOs restrict full ankle joint range of motion, allowing only limited rotation in the sagittal plane limiting plantarflexion during push-off. Second, and perhaps more crucial, current DAFOs do not allow free ankle rotation during swing, making it difficult to dorsiflex in preparation for heel strike. Inability to dorsiflex freely during swing could impose a significant metabolic penalty.

Key components from both the purely passive and fully powered wearable ankle devices can be combined in a ‘hybrid’ approach that offers optimized mobility assistance. For example, by actively controlling the passive elastic properties of an ankle exoskeleton it may be possible to produce the normal torque output of the ankle joint during walking with minimal actuation. This concept is analogous to the elastic ‘muscle activated latch’ observed in the human ankle during walking [16, 17]. This ‘muscle actuated latch’ allows natural rotation of the center-of-mass over the ankle joint (i.e. inverted pendulum motion [2]) during single limb support to transfer energy to the Achilles tendon as it is stretched performing negative work. Then, at terminal stance the stored strain energy in the Achilles’ is rapidly returned to the body, powering push-off. During swing phase plantar flexor muscles relax, and ankle dorsiflexors can reposition the foot for heel strike with no resistance from antagonists. Our approach is motivated by the fact that humans generate nearly half of the mechanical energy to walk with their ankles [4] and more than half of that comes from recycled elastic energy in the Achilles’ tendon and aponeurosis [3].

We designed a device to utilize parallel springs to provide ankle joint mechanical assistance during the stance phase but allow free ankle rotation during swing phase [18, 19]. To do this we developed a novel exoskeleton, consisting of a lightweight custom composite frame and a clutch that can engage and disengage a parallel spring based only on ankle kinematic state. This energy-neutral ankle exoskeleton could not only be used to restore symmetry and reduce metabolic energy expenditure of walking in populations with weak ankle plantar flexors (e.g. stroke, spinal cord injury, normal aging), but also shows benefits to healthy populations as well. We had three design goals when developing the exoskeleton. (1) The exoskeleton should be as transparent to the user as possible having minimal interference with gait kinematics and should be lightweight, to minimize increased metabolic energy expenditure from adding mass to the lower limbs. (2) The exoskeleton should provide plantarflexion torque during stance. (3) The exoskeleton should not interfere with toe clearance during swing.

Methods

We developed a passive elastic ankle exoskeleton incorporating a lightweight composite frame with a clutch to control storage and return of energy in a parallel spring (Fig. 1). Our ankle exoskeleton is designed to recycle energy from human walking in a manner that does not hinder natural gait using two systems, a mechanical clutch and an adaptive low power electromechanical clutch. The frame is designed to be lightweight, while still carrying all loads necessary to assist plantarflexion. It was also important to ensure proper interfacing and alignment with the user to minimize any alterations of gait kinematics. In order to provide plantarflexion torque during stance and not hinder dorsiflexion during swing it was important to develop a clutch that would respond at key events during walking. With proper clutch timing, the exoskeleton should be able to store and return energy during stance and allow a freely rotating joint during swing (Fig. 2), which we hypothesize, is a key step in assisting natural gait.

Figure 1: Passive Exoskeleton Design

This system comprises three main components, a lightweight composite frame, a passive clutch, and a parallel spring. The lightweight composite frame transmits forces, from the anterior shank to the passive clutch and parallel spring which is in series with the passive clutch. The forces applied to the thrust bearing by the parallel spring are transmitted through the rigid frame to the ball of the foot. During walking the passive clutch engages a ratchet and pawl immediately before heel strike at a set angle. A tension spring takes up slack in the system before foot flat to allow for energy storage and return during the remaining stance phase of gait. After push off, the clutch disengages the ratchet and pawl mechanism, decoupling the spring, and allowing free ankle rotation during swing. The clutch is engaged and disengaged by timing pins set at predetermined ankle angles. The parallel spring stores energy during dorsiflexion and returns that stored energy during push off.

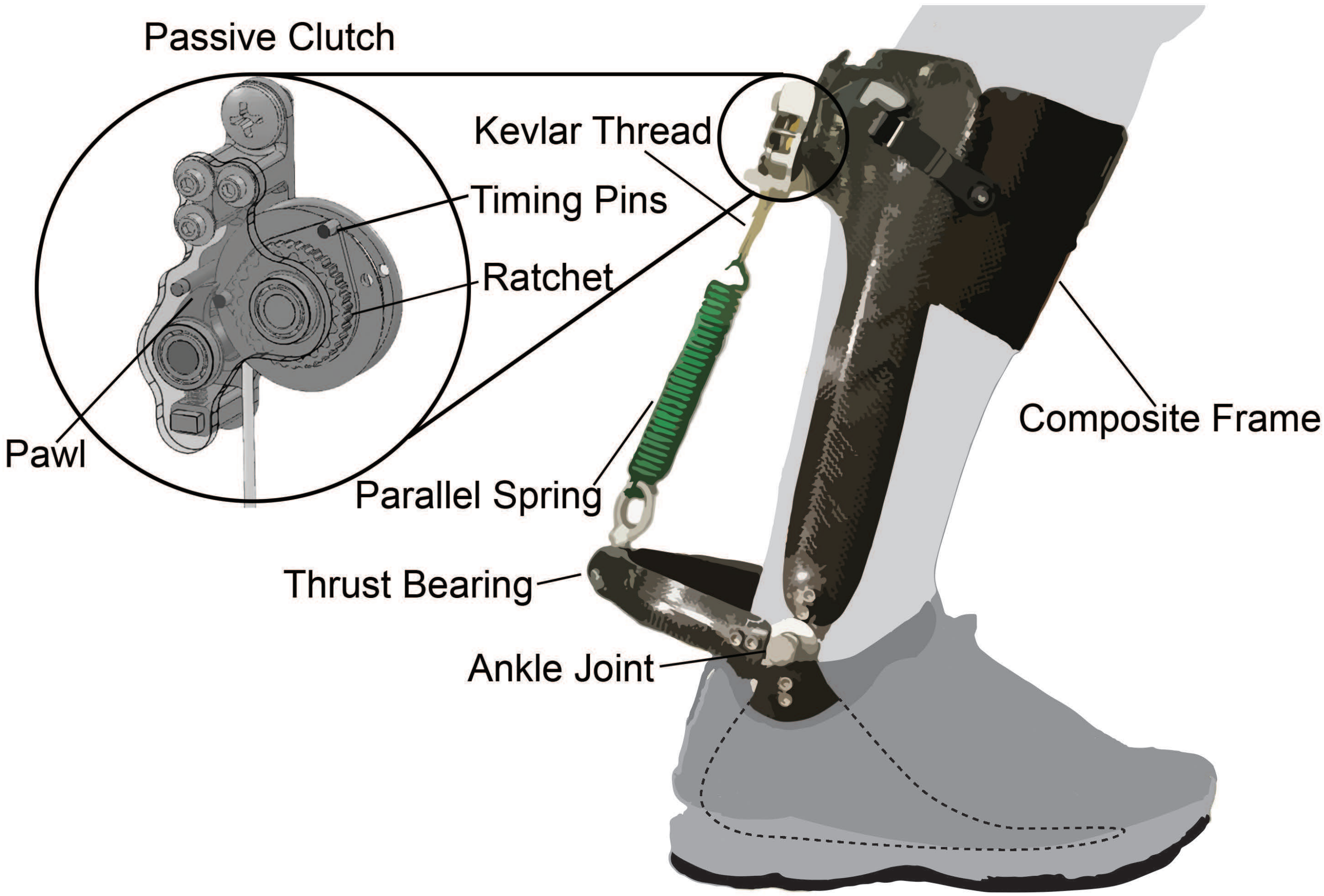
Passive Clutch
Kevlar Thread
Timing Pins
Ratchet
Pawl
Parallel Spring
Composite Frame
Thrust Bearing
Ankle Joint

Figure 2: Exoskeleton Phases, Ankle Angle and Moment, Exoskeleton Torque

Exoskeleton configuration and key ankle joint angle during stance phase of normal walking from heel strike to heel strike (top). Colors coordinate to phases of gait. Before heel strike the clutch is unlocked allowing free ankle rotation. When the user reaches a set dorsiflexion angle, right before heel strike, the clutch engages, only allowing motion in the proximal (upwards) direction. As the user plantarflexes to foot flat, the clutch takes up slack in the parallel spring. As soon as the user begins to dorsiflex the clutch locks and the spring stretches, storing mechanical energy. During push-off, spring energy is returned to the ankle, assisting plantarflexion. Finally, the clutch disengages during push-off to allow free rotation during swing. A kinetic analysis (bottom) shows exoskeleton torque overlaid on total ankle joint moment produced during an average gait cycle.

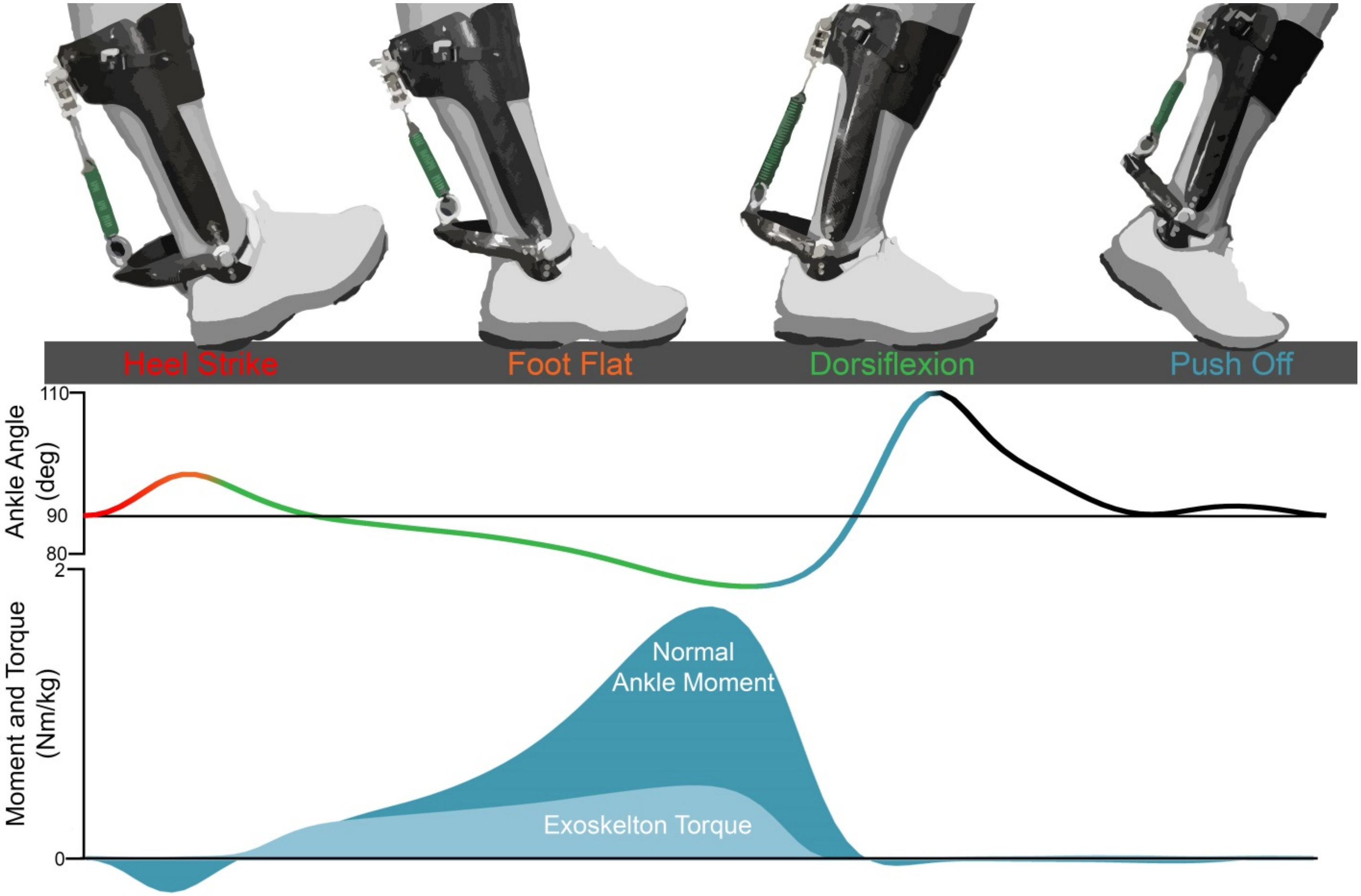
Heel Strike
Foot Flat
Dorsiflexion
Push Off
Ankle Angle (deg)
110
90
80
Moment and Torque (Nm/kg)
2
0
Normal Ankle Moment
Exoskelton Torque

Clutch Design

To address two of our design goals of assisting plantarflexor torque during stance and not interfering with toe clearance during swing we developed two clutches to act in series with our parallel spring. One a mechanical clutch contains no motors or electronics and can engage and disengage the parallel spring based off of direct mechanical feedback from the ankle angle (Fig. 3). The passive clutch is designed for normal gait patterns over a small range of walking speeds near 1.25 m/s. In order to accommodate various terrain, walking speeds, or clinical gaits, we developed an active clutching system as well. The active clutch uses a small microcontroller and micro-servo to set the timing of the ratcheting mechanism, which also controls energy storage and return. This is highly energy efficient as all the holding forces in the clutches are transmitted to mechanical members.

Figure 3: Passive Clutch Design

The key components of the passive clutch lie in a unique ratchet and pawl mechanism. The pawl (17-4 Stainless Steel) has a triangular cam face that interacts with a detent pin, keeping the pawl compliantly held against the ratchet (17-4 Stainless Steel) or disengaged. The ratchet is coupled to a spring-loaded pulley (7075 Aluminum) which keeps tension in the Kevlar (0.038” Dia. x4) strands during all phases of gait. The pulley is also coupled to a set of timing pins (7075 Al). The pins are designed so that at a set angle the disengage pin will contact the underside of the pawl and press it away from the ratchet which will lock the pawl outwards due to the cam’s interaction with the detent pin allowing free ankle rotation. At the set engagement angle, the engagement pin which is located further out in diameter on the pulley will contact on top of the pawl forcing it onto the ratchet where it will be held by the detent pin’s spring force on the cam allowing ratcheting and slack retention. Engineering drawings are available in Appendix A.

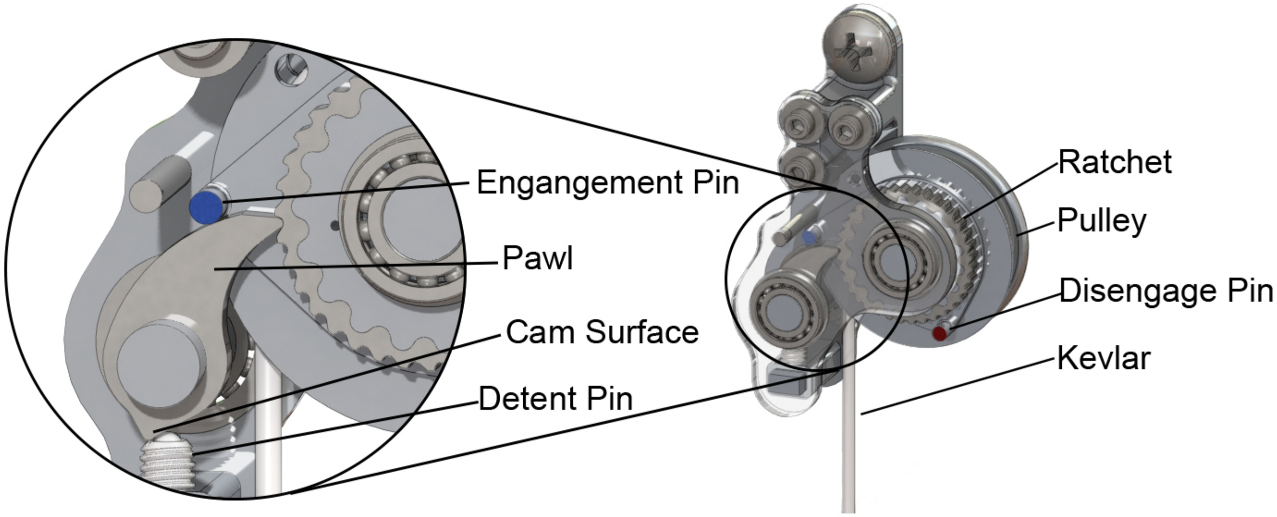
Engangement Pin
Pawl
Cam Surface
Detent Pin
Ratchet
Pulley
Disengage Pin
Kevlar

While our passive clutch is an effective means for controlling a truly energy neutral exoskeleton, it is very limited in its ability to accommodate varying gaits and would not be an effective control strategy outside the laboratory environment. To address this, an electromechanical clutch was designed using a similar force transmission strategy as in the passive clutch but incorporating a small motor to engage and disengage the ratchet and pawl instead of timing pins. The motor (HITEC, HS-35) can be driven directly from a microcontroller without the need for a transistor or servo driver making it very energetically efficient (Fig. 4). Additionally, all holding forces in the electromechanical clutch are transmitted to passive components, as in the mechanical clutch.

Figure 4: Active Clutch Design

The active clutch uses a four pawl, ratchet and pawl system (7075 Aluminum) to engage and disengage to clutch. The pawls are machined with geared teeth to control their position. When the clutch is engaged, the servo drives a PMMA disk which is attached to a through shaft. The disk is compliantly attached via compression springs to a central gear which freely rotates around the through shaft. The spring force in the gear engages the pawl to the ratchet and allows unidirectional rotation of the ratchet. When disengaged the pawls rotate inward away from the ratchet face and allow free rotation of the ratchet. A small return spring can be attached to the clutch to keep tension in the Kevlar during the swing phase of gait. Engineering drawings are available in Appendix B.

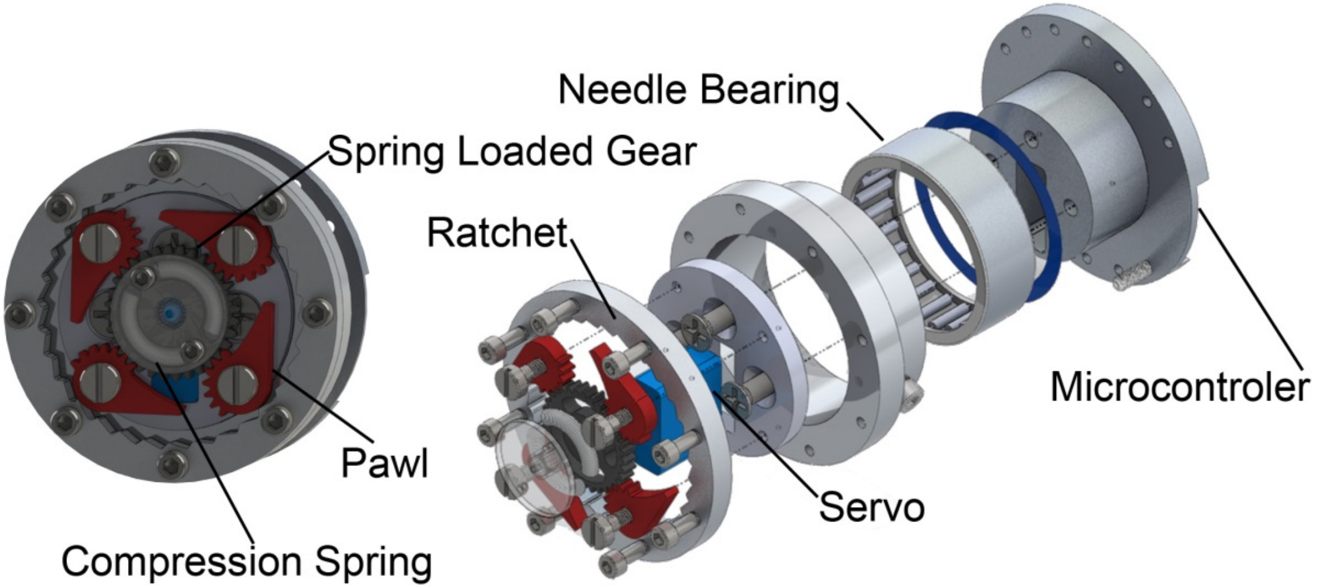
Needle Bearing
Spring Loaded Gear
Ratchet
Microcontroler
Pawl
Servo
Compression Spring

The active clutch is controlled by an integrated microcontroller (ATmega32U4 5V/16MHz) located on the back side of the clutch. The microcontroller has 4 channels of 10-bit ADC, 5 PWM pins, 12 DIOs and a direct USB transceiver which can be used for easy control and attachment of sensors and inputs. For our exoskeleton we integrated both a footswitch (Interlink Electronics force sensitive resistor, 10KΩ resistor voltage divider to digital in) located under the heel of the foot and a digital absolute miniature magnetic encoder (US Digital MAE3) integrated into the ankle joint. The microcontroller directly drives the servo turning the pawls to engage and disengage the ratchet.

We considered three strategies to control timing of the electromechanical clutch: (1) heel strike detection, (2) myoelectric control (EMG), and (3) monitoring ankle angle. A study using pneumatic ankle exoskeletons compared the use of both a footswitch and proportional myoelectric control (PMC) [20] to control ankle assistance. The study concluded that users respond quicker and adapt much faster to a footswitch than with proportional myoelectric control when analyzing time to steady state EMG and kinematic joint angles. However, that study also showed proportional myoelectric control resulted in more efficient use of the exoskeleton and users had significantly lower electromyography (EMG) activity after several thirty minute sessions of training (a possible but not direct indicator of reduced metabolic cost). Proportional myoelectrically controlled exoskeletons have been shown to help reduce the metabolic expenditure of walking with respect to the elevated cost due to added mass, but none show results of metabolic consumption below that of normal walking [21].

On the other hand, a recent study has shown reductions in metabolic cost below that of normal walking with a foot-switch controlled pneumatic ankle exoskeleton [22]. The difference in this study was that the onset of activation of the pneumatic muscle was adjusted until an optimum engagement time was determined. This shows how imperative it is to have a proper timing of engagement and disengagement of assistance. In contrast to a pneumatic exoskeleton, a passive exoskeleton cannot only apply positive work during push off, but negative work as well, possibly reducing forces on plantarflexor muscles.

A third control strategy is to use ankle angle to detect gait events and control engagement and disengagement. While monitoring ankle angle for gait events has been a strategy implemented in some pneumatic exoskeletons [23] it has not been shown as a technique that can lower the metabolic cost of walking below normal.

Our current passive clutch uses mechanical feedback from ankle angle position to control the engagement and disengagement of the clutch. This has been an effective control strategy for steady state walking and can easily be incorporated into an active clutching system using a digital encoder at the ankle joint. The main drawback to simply monitoring ankle angle is that the encoder would not be able to accommodate for when the exoskeleton is used on varying slopes as the user's ankle angles would shift.

A myoelectricaly controlled exoskeleton would not be ideal. Ensuring proper electrode placement would require carefully placed electrodes built in to each exoskeleton in a region that could cause rubbing throughout the day. In addition, motion artifacts in the EMG signal could lead to skin irritation.

The control strategy we chose can accommodate both minimal user setup and accurate timing during walking. We simply attached a pressure sensor under the heel of the foot to set the engagement of the clutch. Our foot pressure monitor is essentially a flexible force sensitive resistor integrated into the microcontroller with a pull down resistor and has been proven to be very reliable at determining stance phases of gait.

Fortunately because of the mechanical design of the clutch there are several fail safes built in. First if the clutch is engaged too early in stance the ratcheting feature will take up the slack in the system as the user goes from heel strike to foot flat, and will mechanically lock once the user dorsiflexes. If the clutch is disengaged too early, the clutch is designed so that it cannot unlock under high force loads meaning that the force in the springs must be released before the clutch unlocks and allows free rotation. These two built in mechanical fail safes make the control of the clutch a much simpler operation.

During use, the microcontroller determines if the exoskeleton is in swing or stance phase of gait based off of foot pressure values. In swing the microcontroller monitors the foot-switch, if it is detected that the user is beginning stance phase with a heel strike, the microcontroller engages the clutch to capture and return as much energy in the spring as possible without hindering the gait (e.g. Fig. 5; orange curve). Thanks to the built in mechanical fail safes, as long as the user is not running or walking on steep slopes, the microcontroller simply needs to disengage after push off when the foot pressure monitor indicates swing phase. To accommodate for other variations in gait mechanics (e.g. rough terrain) it will be necessary to use a more advanced control strategy that relies on magnetic encoders built into the ankle joints. Current efforts focused on creating a device which could optimize the timing of engagement during normal walking as it has been shown that simply controlling the timing of assistance of a pneumatic ankle exoskeleton can significantly lower the metabolic cost of walking [22].

Figure 5: Active Clutch Timing

To test the ability to control timing, the active clutch was used with one study participant and set to engage at three different gait events: (1) after heel strike, (2) after foot flat, and (3) at mid stance while attached to an intermediate 182 Nm/Rad spring (~50% normal ankle stiffness at 1.25 m/s). Ankle moment without an exoskeleton (dashed black line) and exoskeleton torque (solid colored graphs) were calculated using inverse dynamics and load cells in series with the a compression spring. By tuning the timing of engagement and choosing an optimum spring stiffness we aim to assist walking in a way that reduces the metabolic cost of walking.

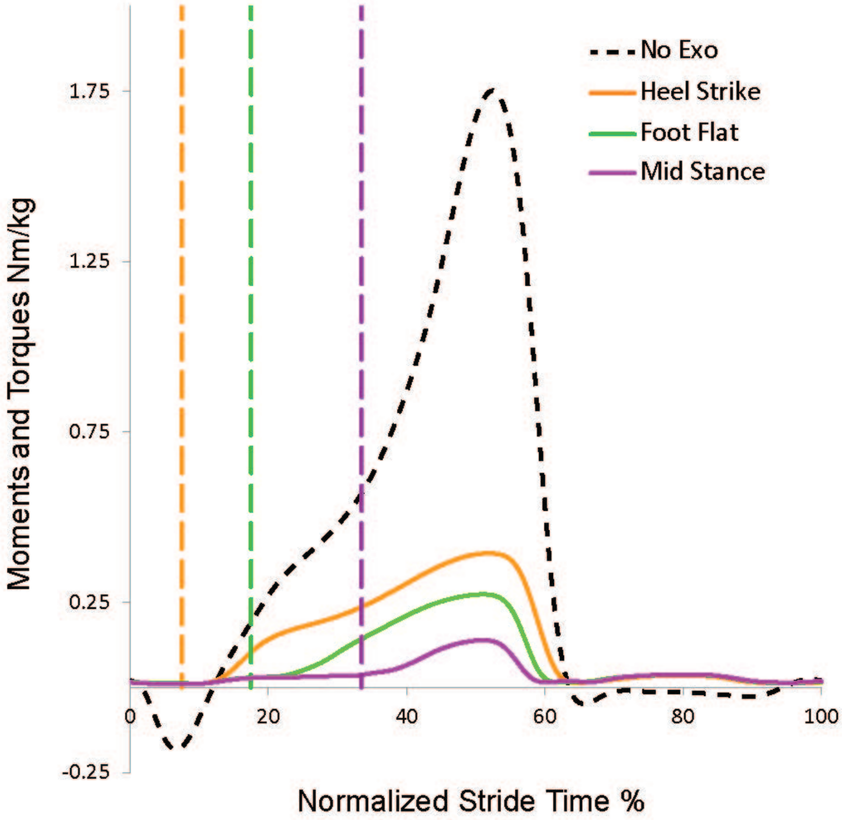
No Exo
Heel Strike
Foot Flat
Mid Stance
1.75
1.25
0.75
0.25
-0.25
0
20
40
60
80
100
Moments and Torques Nm/kg
Normalized Stride Time %

Frame Design

Increased weight on the lower-limbs causes a marked increase in metabolic energy consumption [13]. Studies with pneumatic exoskeletons report a marked increase in metabolic cost when user's simply wear the device, due to the added mass [21]. In order to overcome this added mass, the exoskeleton must provide enough assistance to not only offset its own weight, but to additionally assist the user. In order to address this added mass setback we have developed a custom composite frame design of fiberglass (4 oz/yard^2 S Glass), carbon fiber (5.7oz/yard^2 in plain and twill weaves) and kevlar held in an epoxy nano resin (Acsys Nano-Res) that reduced the total mass of the exoskeleton frame to 275g-360g (size 8US to size 13US shoe), total mass with clutch and spring 392g-477g (Table 2). Previous studies have been performed with pneumatic carbon fiber exoskeletons with frames over 1kg without hardware [9, 20, 21, 24-28]. By developing advanced composite fabrication techniques, with a woven composite truss infrastructure using pre-tensioned fibers before lamination we have produced an ultra-light exoskeleton in order to reduce the added mass cost of wearing an exoskeleton. Our current design utilizes quickly interchangeable steel extension springs as a test bed to be able to characterize an ideal parallel spring stiffness.

In addition to reducing the mass of the exoskeleton it was important that the exoskeleton did not hinder natural gait kinematics or harm the user. Proper anatomical alignment and a comfortable fit of the exoskeleton were main design concerns. The frame was designed to be ridged in load bearing directions but compliant when fitting around the user. The frame could not have sharp edges or surfaces that rubbed the user's skin during walking causing blistering. The frontal shank section of the frame was designed to sit 2 cm below the medial condyle to avoid pressure on the tibial nerves, which could harm the user. Mechanical joint alignment with the ankle joint proper, line of rotation was also important in ensuring natural kinematics were observed when using the exoskeleton.

Considering our design criteria it was necessary that each study participant had a custom exoskeleton. Exoskeletons were built on plaster molds of the users legs formed from a negative cast. The mold was then hand carved and sanded, then built up with more plaster in areas of negative space to ensure a tight vacuum during lamination. Plaster was also added to areas such as the sides of the foot which expanded during walking and the back of the heel (to predetermined dimensions) to form the posterior beam connected to the ankle joint and tension spring. It was also important to remove any small radii to ensure vacuum sealing was relatively even and didn't pull any bearings causing a miss alignment. This also prevented air pockets from forming during lamination. Ankle joints were also drilled into the plaster mold in line with the natural alignment of the joint to ensure they did not shift during lamination.

Many types of carbon fiber weaves were used when forming the exoskeleton. A twill weave was chosen for areas of more complex geometry as it conformed easier than other weaves. The downside of this weave was ensuring the fibers, which shifted easier than other weaves, were in line with where we determined tensional strength was needed. Other less complex areas were covered with a square weave. Uniaxial and biaxial carbon fiber tape and tubing were used in most structural members to create composite beams. Structural members undergoing bending had increased carbon fiber density on the side of tension. A custom carbon fiber truss was woven by hand for each test subject. After taking measurements of the subject's shank, a weave template was designed and laser cut to keep fibers in tension while the truss structure was being woven. This structure was then strengthened by adding unidirectional and biaxial carbon fiber, and inserting the entire structure into a biaxial carbon fiber tube where all fibers were tensioned and secured before lamination. Fiberglass composites were used in the foot section of the exoskeleton under the heel to allow more compliance and user comfort. Thrust bearings and threaded inserts were also sealed and laminated in the carbon fiber frame being held in place by Kevlar strands to ensure they did not shift during lamination.

Human Walking Testing Methods

Four able-bodied subjects (male, height =1.86 ± 0.04 m , mass =81.3 ± 9.3 kg, 25 ± 5 years) performed a series of walking test (Fig. 6) on a split belt treadmill instrumented with two separate force platforms, one under each treadmill belt (BERTEC, Columbus, OH, USA). Rates of oxygen consumption and carbon dioxide production during trials were collected using a portable metabolic system (OXYCON MOBILE, VIASYS Healthcare, Yorba Linda, CA, USA). Prior to walking, metabolic measurements were taken during 5 min of quiet standing and values from the last 2 minutes were used to calculate the rate of metabolic energy consumption (watts) while standing. For the walking trials data from the last 2 of the 7 minutes were used for the calculation of metabolic rate. Visual inspection of rates of oxygen consumption with time (averaged over 30 second intervals) confirmed that participants were at steady-state during this period. Using standard equations detailed by Brockway [29], rates of oxygen consumption and carbon dioxide production were converted to metabolic rates. Net metabolic powers during test conditions were calculated by subtracting the standing metabolic power from the metabolic power during testing conditions, these values were then normalized to individual body mass. Kinematics and kinetics data were collected with an eight camera motion analysis system (VICON, Oxford, UK) used to capture the positions of 33 reflective markers attached to the pelvis, and legs of each study participant. Force data were captured using the two force platforms integrated into the split-belt treadmill. Kinematic, kinetic, and EMG analysis was performed using Visual 3D software (C-motion Inc., Germantown, MD, USA). Surface EMG was used to record muscle activity from the soleus (SOL) and tibialis anterior (TA) of each leg. All four channels were recorded using wired electrodes (Biometrics, Newport, UK) that were placed over muscle bellies. DC offsets were removed from raw signals, which were then high pass filtered, rectified, and smoothed by low pass filtering. Signals were then integrated across step time and averaged. Time series data for study participants were recorded and averaged to the mean of at least 10 steps for all participants. Error bars represent ± SE for the whole group.

Figure 6: Experimental Methods across Clutch Conditions

Custom bilateral ankle exoskeletons were built for 4 study participants. After subjects became accustomed to walking in the exoskeletons they were asked to walk at 1.25m/s during four randomized conditions, 1) normal walking without the exoskeletons, 2) walking with the exoskeleton frame with no assistance (no spring), 3) walking with the exoskeleton frame with a mechanically clutched intermediate spring (182 Nm/rad spring, ~50% quasi-ankle stiffness), and 4) walking with the exoskeleton with the intermediate spring rigidly attached by locking out the mechanical clutch at an engagement angle matched to that of the mechanical clutch engagement during clutched walking.

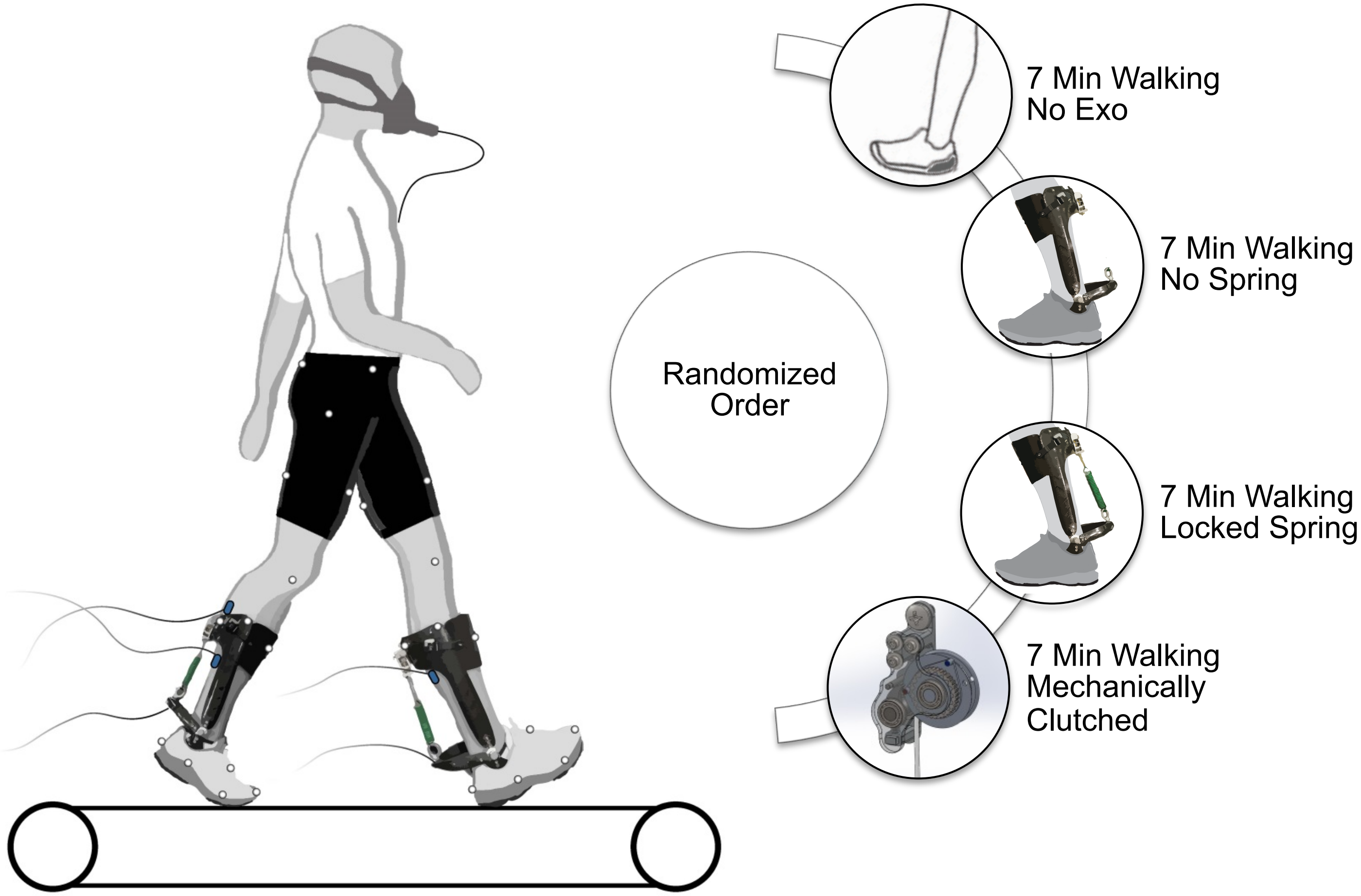
Randomized
Order
7 Min Walking
No Exo
7 Min Walking
No Spring
7 Min Walking
Locked Spring
7 Min Walking
Mechanically
Clutched

Results

Kinematic measurements show a slightly increased plantarflexion angle (~3 deg.) when the user wears the exoskeleton. The design of the exoskeleton does slightly raise the user's heel, however changing marker placement from the exoskeleton trials to the no exoskeleton trials could also cause this shift. We did not report any other major derivations from normal walking joint ankle kinematics in the no spring and mechanically clutched trials. However, when the clutch is locked out user's changed their gait considerably by increasing knee and hip flexion, presumably to put the limbs in a better position for toe clearance (Fig. 7).

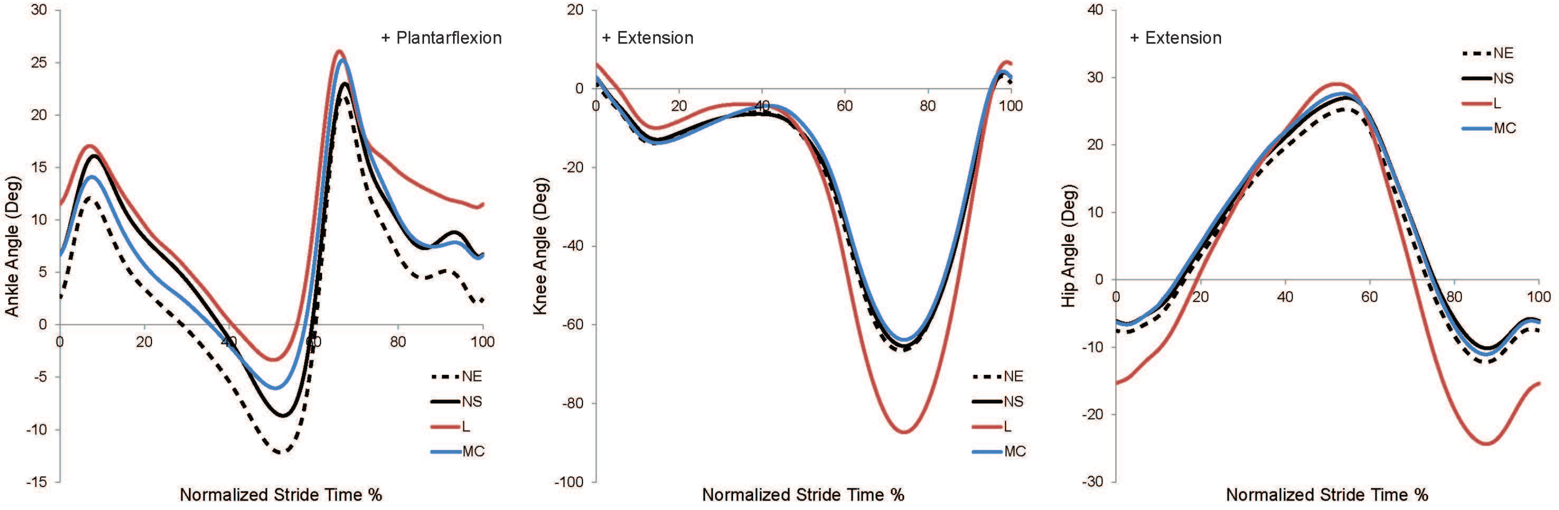

Figure 7: Joint Angle Kinematics across Clutch Conditions

Group mean (n=4) joint angle time series data for the ankle, knee, and hip joints (left to right) from heel strike to heel strike (0-100%). Max ankle plantarflexion angles: 21.9, 22.9, 26.1, & 25.2 (deg), max dorsiflexion angles: -12.2, -8.65, -3.3, & -6.0 (deg) for no exo (NE), no spring (NS), locked (L), and mechanically clutched (MC) conditions, respectively. During the locked condition knee flexion increased by 22 degrees and hip flexion by 12.1 degrees from normal walking however, when using the mechanical clutch, flexion only changed by -2.7 and 2.3 degrees at the knee and hip, respectively.

Kinetics data show the exoskeleton is able to produce 20% of the total average ankle moment when walking with an intermediate spring. In addition the exoskeleton contributes ~23% of the average negative mechanical power and ~17% of the average positive mechanical power during exoskeleton assisted walking at 1.25 m/s. Most importantly, average negative biological mechanical power was reduced by 40% during pre-push off stance (Fig. 8).

Figure 8: Biological Ankle Moments & Mechanical Powers; and Exoskeleton Torques & Mechanical Powers

Average group (n=4) biological moment and exoskeleton torque time-series data from heel strike to heel strike (0-100%) (left). Average group mechanical power time-series data from heel strike to heel strike (0-100%) (middle). The no exoskeleton condition, ankle moment and mechanical power (NE), no spring condition, ankle moment and mechanical power (NS), locked condition, biological moment and mechanical *power* (L Bio), mechanically clutched condition, biological moment and mechanical power (MC Bio), locked condition, exoskeleton torque and mechanical power (L Exo), and mechanically clutched condition, exoskeleton torque and mechanical power (MC Exo) were plotted against percent stride. Average moments, and mechanical powers of the biological ankle were calculated by integrating time-series data and dividing by stride time, for no exo (NE), no spring (NS), locked (L), and mechanically clutched (MC) conditions. The mechanical clutch causes the largest reduction in biological ankle average moment and average positive and negative mechanical powers, closely followed by the locked condition. The no spring (NS) condition causes a marked increase in biological moments and mechanical powers.

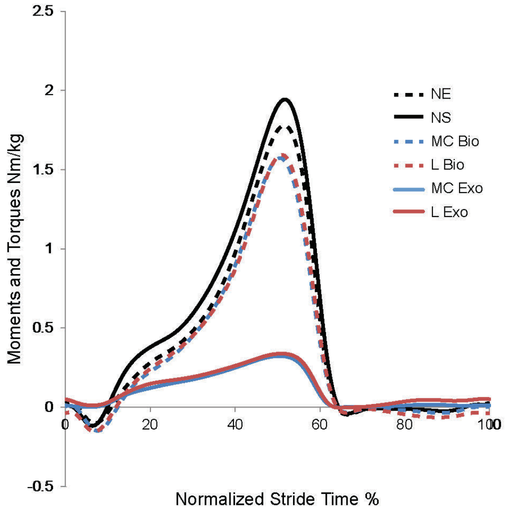

2.5
2
1.5
1
0.5
0
-0.5
0
20
40
60
80
100
Moments and Torques Nm/kg
Normalized Stride Time %
NE
NS
MC Bio
L Bio
MC Exo
L Exo

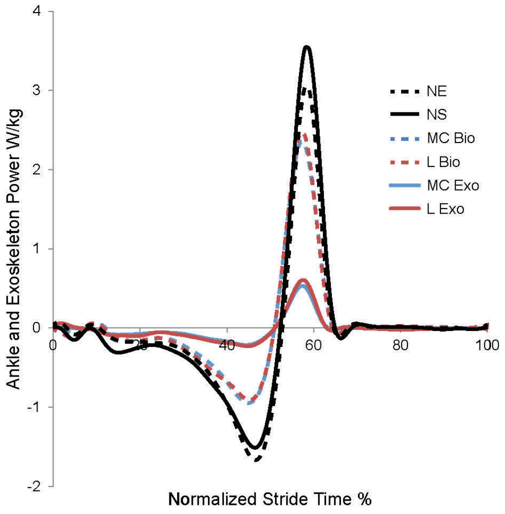

4
3
2
1
0
-1
-2
0
20
40
60
80
100
Ankle and Exoskeleton Power W/kg
Normalized Stride Time %
NE
NS
MC Bio
L Bio
MC Exo
L Exo

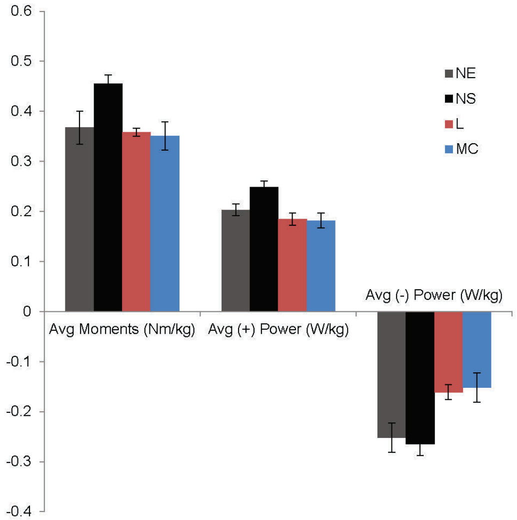

0.6
0.5
0.4
0.3
0.2
0.1
0
-0.1
-0.2
-0.3
-0.4
Avg Moments (Nm/kg)
Avg (+) Power (W/kg)
Avg (-) Power (W/kg)
NE
NS
L
MC

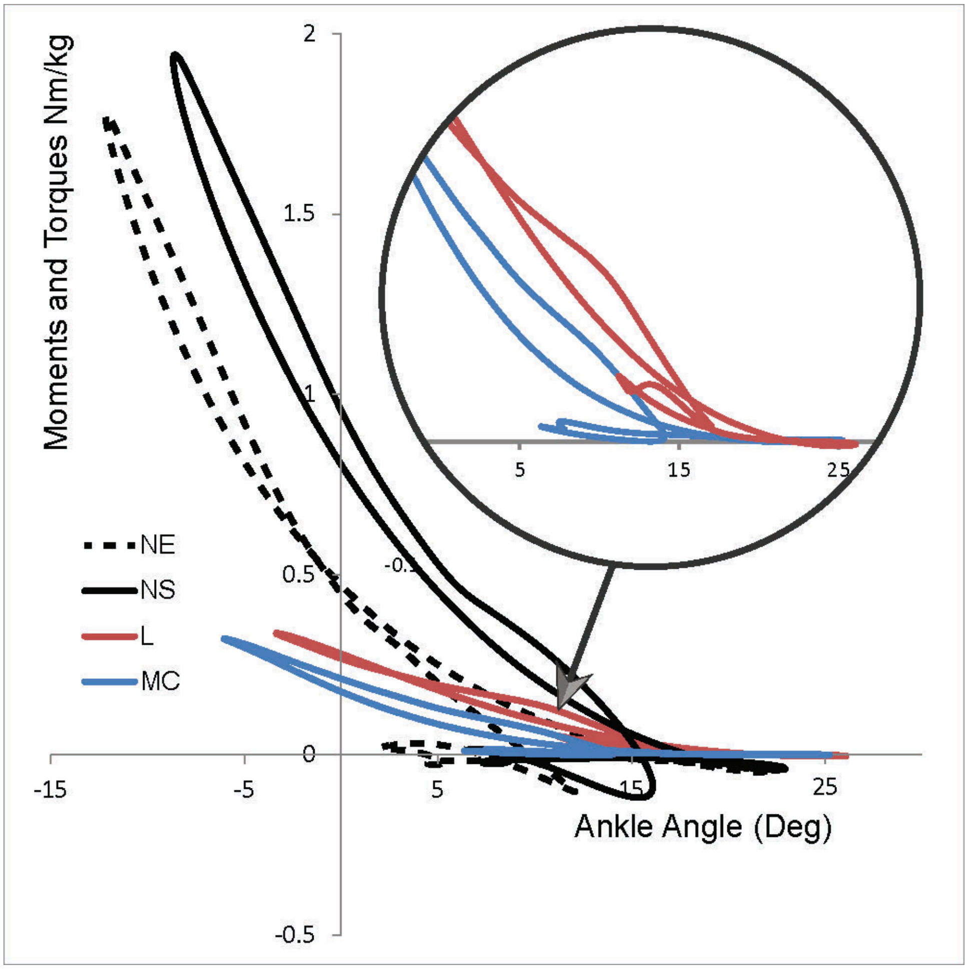

Figure 9: Torque Angle Curves across Clutch Conditions

Ankle moments (no exoskeleton (NE), dotted black and no spring (NS), solid black) and exoskeleton torques (locked (L, red) and mechanical clutch (MC, blue)) plotted against ankle angle in degrees (n=4). During swing (lower portion of inset), the mechanical clutch shows little to no torque production while the locked clutch shows loading similar to when its engaged during stance, indicating it is not slack..

Figure 10: Electromyography (EMG) across Clutch Conditions

Processed electromyography (EMG) time-series signals were averaged over a normalized stride (heel strike to heel strike) and then scaled from 0-1 for each individual based off of maximum EMG amplitude for each signal. Normalized signals were then averaged across subjects and plotted against percent stride time (soleus (SOL), left and tibialis anterior (TA), middle). In addition, individual subject's signals were integrated over the stride, normalized to normal walking values and then averaged across all subjects (right). The locked condition (L) reduced SOL EMG activity by ~20%, but increased TA EMG by ~43%. The time-series data for TA (middle) shows increased activity during early swing, suggesting subjects work against the spring to actively dorsiflex the ankle. The mechanical clutch condition (MC) reduced SOL EMG activity by ~16% while only increasing TA activity by ~24%. Because the SOL has over 2.5 times the cross-sectional area of the TA [30], changes in the SOL EMG activity should have a stronger impact on net metabolic cost than changes in TA activity, although there is no direct correlation between EMG activity and metabolic cost.

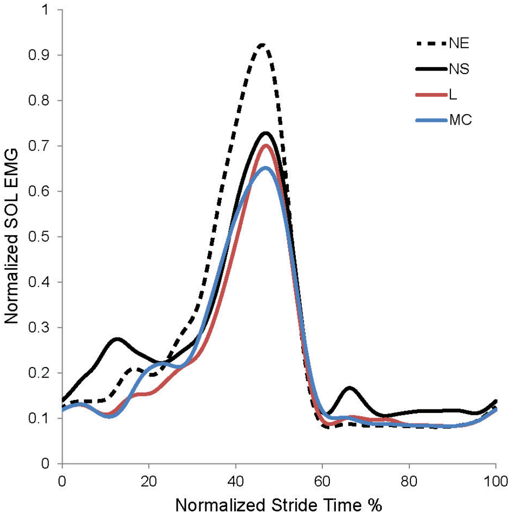

Normalized SOL EMG
1
0.9
0.8
0.7
0.6
0.5
0.4
0.3
0.2
0.1
0
0
20
40
60
80
100
Normalized Stride Time %
NE
NS
L
MC

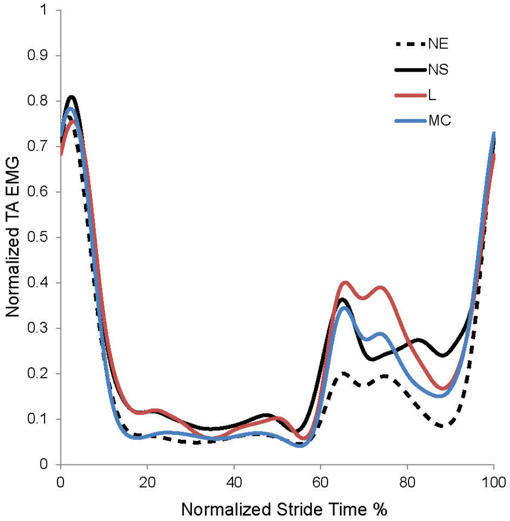

Normalized TA EMG
1
0.9
0.8
0.7
0.6
0.5
0.4
0.3
0.2
0.1
0
0
20
40
60
80
100
Normalized Stride Time %
NE
NS
L
MC

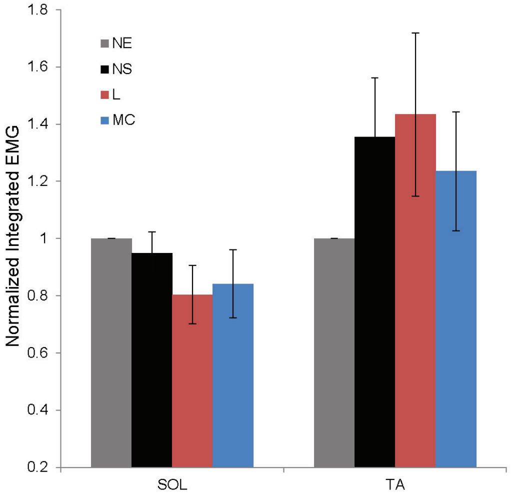

Normalized Integrated EMG
1.8
1.6
1.4
1.2
1
0.8
0.6
0.4
0.2
SOL
TA
NE
NS
L
MC

Table 1: Comparison of Ankle Exoskeleton Peak Power, Mass, and Power Density.

Author	Mass of Exoskeleton (per leg)	Max Positive Power	Power Density
Mooney et al. [31]	2,000g (including all hardware)	3.5 W/kg	1.75 W/kg^2
Sawicki et al. [21]	1,210 g (not including tethered hardware)	1.09 W/kg	.901 W/kg^2
Malcolm et al. [22]	760g (not including tethered hardware)	1.2 W/kg	1.57 W/kg^2
Wiggin et al. (size 8 US)	392g (including hardware)	0.38 W/kg	0.969 W/kg^2
Wiggin et al. (size 13 US)	477g (including hardware)	0.38 W/kg	0.797 W/kg^2

Table 2: Exoskeleton Mass Distribution

Segment	US Size 8	US Size 13
Carbon Fiber Foot Section	130g	155g
Aluminum Ankle Joints (x2)	40g	40g
Carbon Fiber Shank Section	105g	165
Mechanical Clutch	57g	57g
Average Spring	60g	60g
Frame Mass	275g	360g
Total Mass	392g	477g

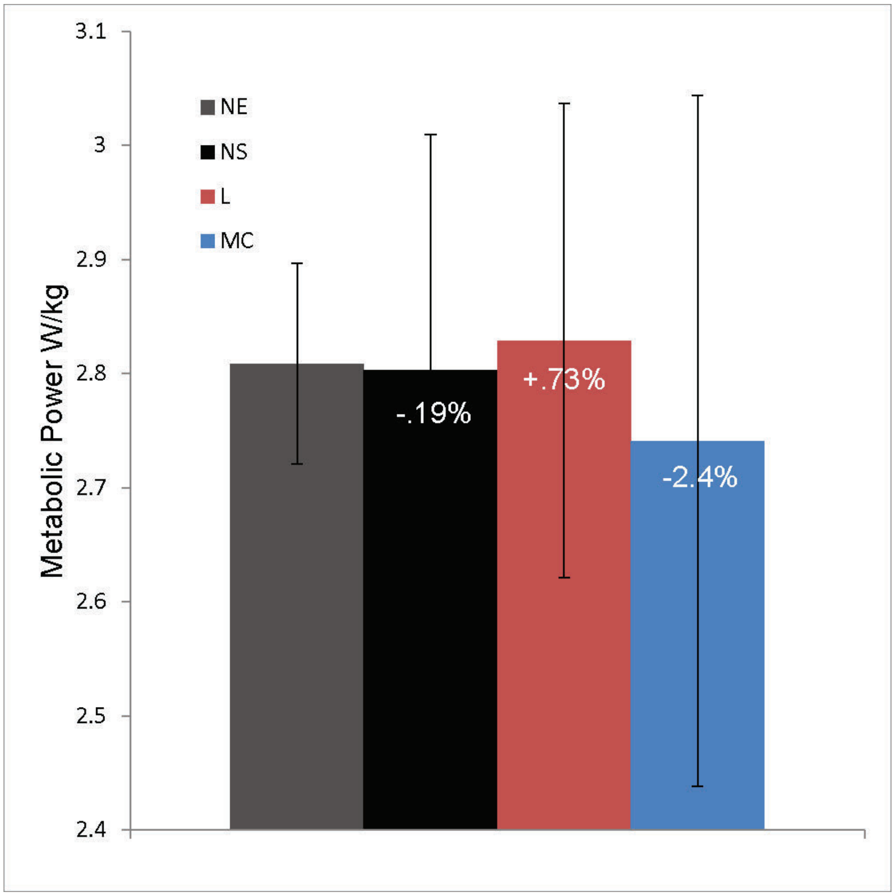

Figure 11: Net Metabolic Power across Clutch Conditions

Net metabolic power was averaged over the last two minutes of walking trials (n=4). Initial results suggest the locked condition (L) causes a small increase in net metabolic power while the mechanical clutch (MC) causes a decrease in net metabolic power from the no exoskeleton trial (NE). Measurements indicate little change in net metabolic power during trials walking with the exoskeleton frame without a spring (NS), a key finding indicating ensuring our frame has negligible added mass cost, a crucial design criteria.

Discussion

Initial testing of the exoskeleton suggests the utility of the clutch, to act in series with the parallel spring. Our results indicate the clutched exoskeleton design (Fig. 1) addresses all three of our design criteria by not hindering natural gait kinematics (Fig. 7), remaining lightweight enough to have minimal effect on net metabolic energy consumption (Fig. 11), producing plantarflexor torque during stance, and not hindering toe clearance during swing (Figs. 2, 8, 9).

Alternatively, the locked condition appears to change the kinematics of the study participants by forcing them to increase both knee and hip flexion and hinders toe clearance during swing, failing two major design criteria (Figs. 7, 8, 9) Increased hip and knee flexion could lead to increased energy consumption by the hip and knee flexor muscles during swing. In addition the inability to dorsiflex could be a tripping hazard, forcing individuals to compensate by using their hip and knee flexors to allow for greater ground clearance. Analysis of the torque angle curves during the locked condition also shows a near linear trend and slight torque production during swing suggesting that dorsiflexion is restricted by the locked spring (Fig. 9). Increased TA EMG activation during early swing also suggests the user dorsiflexes against the locked spring (Fig. 10). Though we tested only a small sample, and there is only a small increase in net metabolic power x during the locked condition compared to the clutched condition (Fig. 11), we feel the trends shown promote the need for a clutched spring when walking in a passive ankle exoskeleton that assist plantarflexion.

For an exoskeletal device to be transparent to the user it should act in a way that does not hinder natural gait kinematics. By adding a clutch with precisely tuned timing it is possible to provide plantarflexion assistance with minimal alteration of normal joint kinematics. Kinetics analysis of ankle moment and exoskeleton torque also suggests the exoskeleton only provides torque during stance and does not produce hindering torque during swing, which is critical to satisfying our design criteria. In addition mechanical power analyses suggest the clutched exoskeleton is capable of offloading muscle force during the stance phase of gait (seen as negative power) and then can return that energy during push off. Powered ankle assistive devices mainly focus on providing positive power [9, 21, 22, 31, 32] our device provides both positive and negative power. Simulation studies indicate that the phase of gait where negative ankle power occurs is the most metabolically intensive period for the plantarflexor muscles [33, 34]. While there is only a small decrease in metabolic power with the mechanically clutched exoskeleton, perhaps better timing of clutch engagement and a precisely tuned spring stiffness could provide a larger net metabolic reduction.

To date there has not been a published autonomous exoskeleton that when used in an unpowered state does not raise the metabolic cost of walking [9, 22, 24, 28, 35, 36]. While we have a limited sample size in reporting a near even net metabolic cost of walking with the unpowered exoskeleton (no spring trials); kinetic, kinematic, and EMG data also suggest that the exoskeleton frame might not have a hindering effect. While both average ankle moment and mechanical power increase when users don the exoskeleton, the soleus EMG activity actually decreases. A larger sample size would be necessary to draw conclusions on this result, however these results are very promising.

Future work will explore the effects of adjusting the timing of energy storage and return using the electromechanical clutch in series with a spring (e.g. Fig. 5). . In addition we plan to recruit a larger sample size and test a larger range of spring stiffness's ranging from 32-97% of normal ankle quasi-stiffness during walking at 1.25 m/s to build upon these results.

CHAPTER 2:

Characterizing the energetic adaptation to mechanical assistance from a passive elastic exoskeleton during human walking

Introduction

Exoskeletons have been used previously to understand the time-course of motor adaptation to novel mechanical environments [21, 24]. In order to drive designs to target optimal user performance, it becomes necessary to study the rate of adaptation to a passive exoskeleton as compared to previous studies in active exoskeletons.

Studies of walking with powered ankle devices [9, 16, 21] indicate that even when assistance is provided in a biologically inspired manner, extensive practice is essential to maximize the metabolic benefit [24]. For users walking with electromyography (EMG)-controlled, pneumatically powered ankle exoskeletons, muscle EMG amplitudes, joint kinematics, and exoskeleton mechanics did not reach new steady values until at least two, thirty minute sessions of powered walking [20, 24]. Furthermore, metabolic cost was reduced by the end of the second 30 minute training session, but continued to show improvement with a third session of training [21].

Initially it was thought that people adapt faster to an exoskeleton controlled using direct human interface (e.g. via EMG) [20], however a recent study has shown better adaptation and energetics data using a footswitch and a better tuned pneumatic interface [22]. It is still not clear whether the pneumatic tuning or the control method was responsible for the improved adaptation. While previous studies have analyzed the way in which people adapt to pneumatic exoskeletons [24], it is not known if humans will respond the same way to passive exoskeletons and how fast they may reduce their metabolic energy expenditure.

We ultimately aim to determine the time course and extent of adaptation to a passive elastic ankle exoskeleton over a range of absolute spring stiffnesses and then identify the normalized (non-dimensional) stiffness using anthropometric data (weight/leg length) that provides the greatest reduction in metabolic energy expenditure. A recent passive elastic ankle foot orthosis (AFO) simulation study predicted that a spring of intermediate stiffness that could store significant elastic energy and still allow normal walking without altering gait, would reduce metabolic energy consumption the most [15]. Springs with higher and lower stiffnesses resulted in higher metabolic cost. In addition, rehabilitation and simulation studies indicate that while using a passive ankle assistive device, the device must be optimized to the user's physiology (e.g. leg length, body mass, and tendon stiffness), so that it can store and return energy in the most metabolically efficient manner [14, 15]. We also contend that properly tuned exoskeleton stiffness may speed the rate of metabolic adaptation to its use. Based on previous studies using powered devices [37], we hypothesize that (1) humans will need >=21 minutes of training to adapt to mechanical assistance from passive elastic ankle exoskeletons and reach steady state net metabolic rates and (2) that there is an intermediate (i.e. optimal) exoskeletal spring stiffness that provides the maximum metabolic benefit during assisted walking.

Methods

Nine individuals (2 female, 7 male, height =1.83 ± 0.11 m , mass =77.4 ± 9.1 kg, 23 ± 4 years) were asked for written informed consent to participate in this study. Ethical approval for all experimental procedures was granted by an institutional review board at the University of North Carolina, Chapel Hill, and all procedures were in line with the Declaration of Helsinki.

Participants completed four days of walking trials with a day of rest in between sessions. Each day study participants walked on a split belt instrumented treadmill (Bertec, Columbus, OH, USA) at 1.25m/s during seven randomized conditions: normal walking without the exoskeletons, walking with the exoskeleton frame with no assistance (no spring), and walking with the exoskeleton frame with five springs ranging from 129-397 Nm/rad (Fig. 12). Rates of oxygen consumption and carbon dioxide production during trials were collected. Prior to walking, metabolic measurements were taken during 5 min of quiet standing and values from the last 2 minutes were used to calculate the mass specific rate of metabolic energy consumption (Watts/kg) while standing using standard equations [29]. For the walking trials data from the last 2 minutes of the 7 minute trials were used for the calculation of mass specific net metabolic rate (net=walking-standing). Visual inspection of rates of oxygen consumption with time (averaged over 30s intervals) confirmed that participants were at steady-state during the recording period.

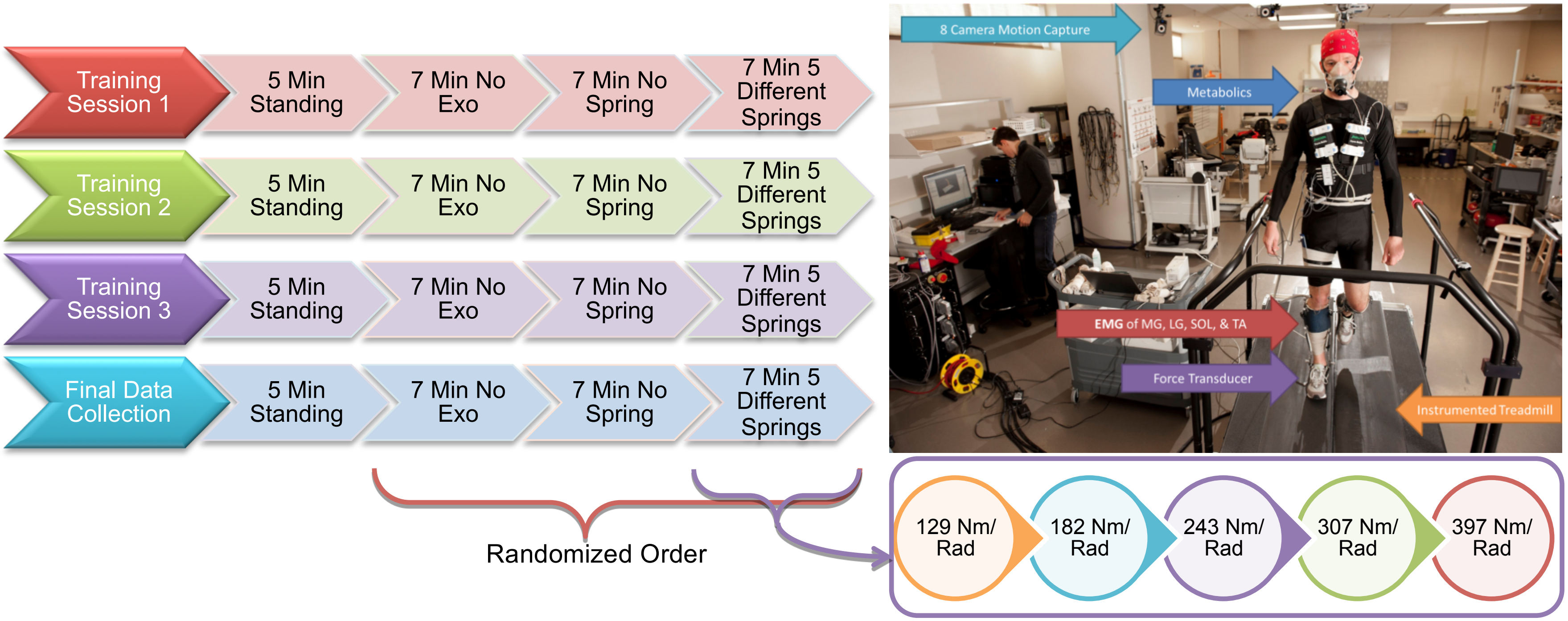
Training Session 1
5 Min Standing
7 Min No Exo
7 Min No Spring
7 Min 5 Different Springs
Training Session 2
5 Min Standing
7 Min No Exo
7 Min No Spring
7 Min 5 Different Springs
Training Session 3
5 Min Standing
7 Min No Exo
7 Min No Spring
7 Min 5 Different Springs
Final Data Collection
5 Min Standing
7 Min No Exo
7 Min No Spring
7 Min 5 Different Springs
Randomized Order
8 Camera Motion Capture
Metabolics
EMG of MG, LG, SOL, & TA
Force Transducer
Instrumented Treadmill
129 Nm/ Rad
182 Nm/ Rad
243 Nm/ Rad
307 Nm/ Rad
397 Nm/ Rad

Figure 12: Experimental Setup: Training

Exoskeleton walking during seven randomized conditions: normal walking without the exoskeletons, walking with the exoskeleton frame with no assistance (no spring), and walking with the exoskeleton frame with five springs ranging from 129-397 Nm/rad = 32%-97% of the average ankle quasi-stiffness during loading phase of walking (i.e. 405 Nm/rad) at 1.25 m/s).

Figure 13: Net Metabolic Power vs. Time during Training

Net metabolic power was calculated for the last 2 minutes of each 7 minute trial using standard equations detailed by Brockway [29]. Rates of oxygen consumption and carbon dioxide production were converted to metabolic rates. Net metabolic powers during test conditions were calculated by subtracting the standing metabolic power from the metabolic power during testing conditions, these values were then normalized to individual body mass. The Δ net metabolic power was calculated from the difference between each exoskeleton trial and the normal walking condition. Each subject is represented by a different color. Each shape represents a different trial condition. (n=7 at 7min, n=8 at 14min and 21 min, n=9 at 28min). We used least-squares regression to fit second order polynomial curves to the data for each condition. Equations for curve fits are available in Appendix C, Table 1.

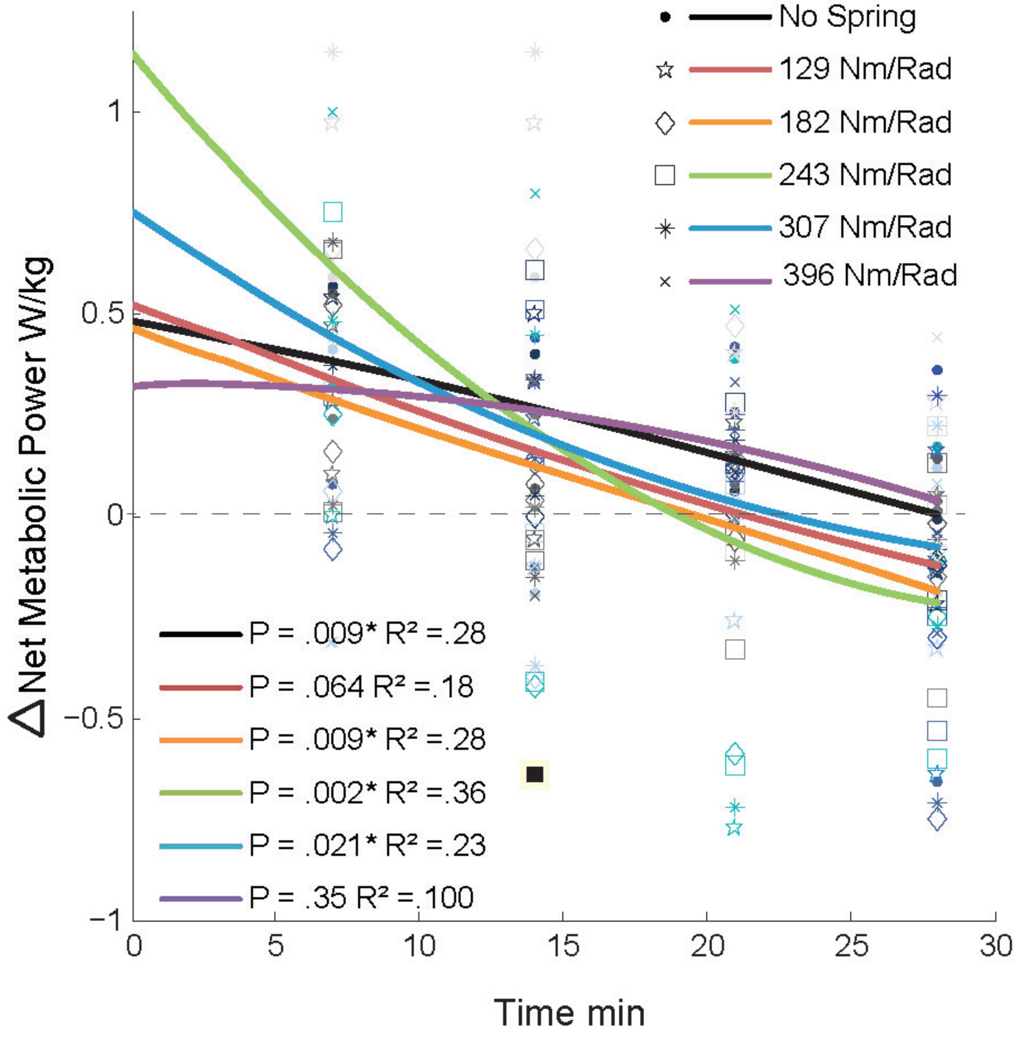
No Spring
129 Nm/Rad
182 Nm/Rad
243 Nm/Rad
307 Nm/Rad
396 Nm/Rad
P = .009* R² =.28
P = .064 R² =.18
P = .009* R² =.28
P = .002* R² =.36
P = .021* R² =.23
P = .35 R² =.100
△Net Metabolic Power W/kg
Time min
1
0.5
0
−0.5
−1
0
5
10
15
20
25
30

Results

While some subjects were able to quickly accommodate to the exoskeletons during the first session (i.e. after 7 min) and reduce their metabolic cost below normal, the group average did not reduce their metabolic energy expenditure until session 3 or~21min of walking with a parallel spring. The second order polynomial curve fits indicate that for intermediate spring stiffness it takes between18.5-19 min (for 182-243Nm/rad springs) to get below the metabolic cost of normal walking. We note however, that only the No Spring, 182 Nm/Rad, 243 Nm/Rad, and 307 Nm/Rad springs had statistically significant curves fits.

Discussion

Our initial hypothesis was that people would quickly adapt and reach steady state net metabolic energy cost after 21 min of walking in a passive elastic ankle exoskeleton. In contrast, our data indicate that users only began to decrease their metabolic energy use below normal walking after ~18.5 min and second order polynomial fits to our data of Δ net metabolic power over time suggest that users could decrease their metabolic energy consumption even more with additional training.

While early studies on adaptation to a pneumatic exoskeleton suggested that it would take several long trials to accommodate to an exoskeleton, [20, 21, 24] a more recent study using a highly tuned pneumatic exoskeleton reports steady state accommodation occurs at 18.5 min with a large SE of ± 5min [22, 38]. It was also reported that on average individuals could lower their metabolic cost below normal walking by 16.5min of walking in the exoskeleton. It seems that accommodation to a passive exoskeleton that assists both positive and negative ankle power could take more time to reach steady state accommodation.

There are a number of potential reasons why adaptation in a passive device may be slower than in an active device. Pneumatic exoskeleton research emphasizes the importance of precisely timing ankle assistance to improve walking economy which we did not carefully control. This may have negatively influenced adaptation, Future studies that more closely control timing of assistance in our device with an electromechanical clutch (see Chapter 1) could address this possibility. Next, our study did not carefully control for cross-learning (i.e. training with one spring stiffness impacting training with a different spring stiffness) but we did randomize all trials to reduce its potential effect to slow adaptation. Finally, by breaking up the trials into 7 min bouts it is possible that we slowed adaptation. Pneumatic exoskeleton studies with the quickest reported accommodation times ran continuous trials until the subject reached steady state accommodation [37]. It might be more beneficial to test subjects walking in each spring stiffness for 30 min or more while measuring metabolic rates to more accurately measure accommodation.

CHAPTER 3:

Stiffness matters: A passive elastic ankle exoskeleton with optimal compliance can reduce the metabolic cost of human walking

In preparation for submission to Nature

Summary

Perhaps because humans are already so well-tuned for locomotion [39], no autonomous, wearable device intended to assist walking or running [32, 40-42] has succeeded in reducing metabolic energy consumption for healthy individuals during typical walking conditions. Here we show that the energy cost of human walking can be reduced using a lightweight exoskeleton. We have built and tested an autonomous lightweight wearable robot which acts in parallel with the human ankle to make walking easier. Our device uses a passive mechanism with clutches and springs to reduce force in ankle muscles. This design uses no chemical or electrical energy, yet reduces the energy cost of walking by 7% when worn on both legs. Minimizing device mass and restrictiveness was important for both results. Ultrasound data from other studies suggest that muscle force reduction, rather than work reduction, could be the primary energy-saving mechanism [43, 44]. Producing force has no energy cost in theory, a fact utilized by this device, but muscles consume metabolic energy whenever contracted. This device demonstrates that, although evolution and learning have tuned gait for economy, engineered systems

can still augment human performance. We anticipate these results will lead to improved techniques for locomotion rehabilitation and enhancement.

Introduction

For at least a century, engineers have designed machines intended to reduce the metabolic energy that humans use to walk [32, 40, 42]. Locomotion is one of the most energy-intensive activities of daily life [45, 46], especially for individuals with disabilities [47]. To date there has not been a reported autonomous device capable of reducing the metabolic energy consumption of healthy individuals during normal walking. A recent study by Malcolm et al. reported a 6% improvement in metabolic energy consumption using an exoskeleton with a pneumatic artificial muscle to assist plantarflexion [22], however this device requires a tethered power source and substantial motors, pumps, valves, and controls which were not worn by the user and would not be practical for use outside of a laboratory environment. This key finding motivates the idea that assisting human plantar flexion during walking is a strategic step in reducing metabolic energy expenditure. Moreover this presents a design challenge, to apply assistance to the ankle joint but in a lightweight and untethered manner. To do this we explored the idea that human muscles require metabolic energy to carry force, however mechanical structures do not; thus it may be possible to reduce metabolic energy expenditure by offloading forces onto mechanically engineered structures.

We designed an autonomous exoskeleton utilizing springs in parallel with the human triceps surae muscle tendon unit that during stance. This device is intended to offload muscle force and provide ankle joint mechanical assistance but allow free ankle rotation during swing phase [18, 19]. To do this we developed a completely passive exoskeleton that uses no motors, batteries, or external energy sources. The device consists of a lightweight custom composite frame and a mechanical clutch that can engage and disengage a parallel spring based only on ankle kinematic state (see Chapter 1 for details; Fig. 14). Before heel strike the clutch is unlocked allowing free ankle rotation. When the user reaches a set dorsiflexion angle, right before heel strike, the clutch engages to allow unidirectional motion upwards and restrict downward motion. As the user plantarflexes to foot flat, the clutch takes up slack in the coupling to the parallel spring. As soon as the user begins to dorsiflex, the clutch locks and the spring stores energy. This energy is captured in the spring and offloads a portion of forces normally held by the muscles. During push-off, spring energy is returned to the ankle assisting plantarflexion. Simulation studies indicate that a parallel spring slightly stiffer than the one which produces the most torque will reduce metabolic energy consumption by the highest degree [15]. Thus, we hypothesize that there will be an ideal parallel spring stiffness for reducing net metabolic energy consumption that is slightly stiffer than the parallel spring which provides the largest ankle torque.

Figure 14: Exoskeleton Functional Diagram

Exoskeleton diagram (top) and photos of exoskeleton in use (bottom). The composite frame transmits forces generated from the center of mass rotating over the ankle, from the anterior shank to the passive clutch and inline parallel spring. The forces applied by the parallel spring are transmitted through the rigid frame to the ball of the foot offloading forces on the triceps surae muscle tendon group and assisting plantarflexion during push off. Timing pins in the clutch engage a ratchet and pawl mechanism to store and return energy during stance and disengage the parallel spring during swing. Bottom left photo shows user's left foot at foot flat before the parallel spring is stretched and right foot in swing. Bottom right photo shows user's left foot during push off as spring energy is being returned and right foot at heel strike. Wires are from exoskeleton load cells used to calculate assistive torque generated by springs and electromyography (EMG) sensors monitoring calf muscle activity.

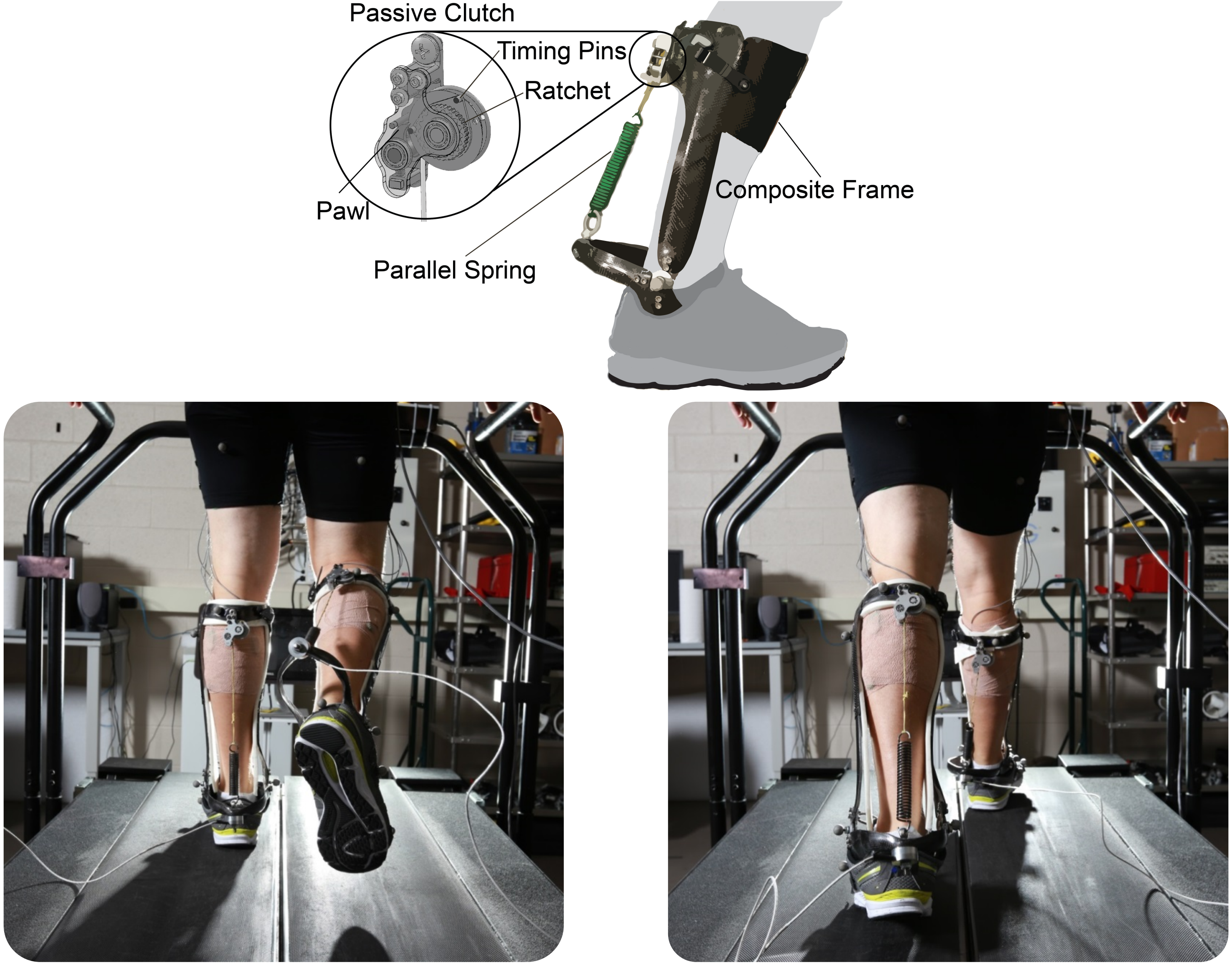
Passive Clutch
Timing Pins
Ratchet
Pawl
Composite Frame
Parallel Spring

Methods

Custom exoskeletons were built for nine able-bodied study participants (2 female, 7 male, height =1.83 ± 0.11 m, mass =77.4 ± 9.1 kg, 23 ± 4 years). Subjects were asked to walk in the exoskeletons with five parallel springs ranging from 129 Nm/rad to 396 Nm/rad for seven minutes each over three training sessions (21 minutes) to become accustomed to walking in the exoskeleton before testing (Chapter 2; Fig. 12). After training, study participants walked on a split belt instrumented treadmill (Bertec, Columbus, OH, USA) at 1.25m/s during seven randomized conditions: normal walking without the exoskeletons, walking with the exoskeleton frame with no assistance (no spring), and walking with the exoskeleton frame with five parallel springs described above.

Rates of oxygen consumption and carbon dioxide production during trials were collected. Prior to walking, metabolic measurements were taken during 5 min of quiet standing and values from the last 2 minutes were used to calculate the mass specific rate of metabolic energy consumption (watts/kg) while standing using standard equations [29]. For the walking trials data from the last 2 minutes of the 7 minute trials were used for the calculation of mass specific net metabolic rate (net=walking – standing). Visual inspection of rates of oxygen consumption with time (averaged over 30s intervals) confirmed that participants were at steady state during the recording period.

Kinematics and kinetics data were collected with an eight camera motion analysis system (Vicon, Oxford, UK) used to capture the positions of 33 reflective markers attached to the pelvis, and legs of each study participant. Force data were captured using the two force platforms integrated into the split-belt treadmill. Marker data were interpolated and low pass filtered with a second order Butterworth filter (6Hz). Inverse dynamics techniques were used to calculate joint moments and exoskeleton torques by determining the moments responsible for holding individual limbs segments considering inertial properties of segments, mass, and external forces from ground reaction forces and exoskeleton load cells. Marker tracking was used to calculate joint angles and velocities. Joint and exoskeleton powers were calculated by crossing joint moments and exoskeletal torques with angular velocity. Time series data for study participants were recorded and averaged to the mean of at least 10 steps for all 9 participants. Error bars represent ± SE for the whole group.

Surface electromyography (EMG) was used to record muscle activity from the soleus (SOL), medial gastrocnemius (MG), lateral gastrocnemius (LG), and tibialis anterior (TA) of each leg. All 8 channels were recorded using wired electrodes (Biometrics, Newport, UK) that were placed over muscle bellies. DC offsets were removed from raw signals, which were then high pass filtered, rectified, and smoothed by low pass filtering at 6Hz. Signals were averaged by stride time (heel strike to heel strike) and scaled from 0-1 for each individual based off of maximum EMG amplitude for each signal.

Results

Walking in the exoskeleton caused a significant reduction in net metabolic power of walking at 1.25 m/s. With an intermediate spring stiffness (~45% of normal ankle quasi-stiffness during loading phase of stance) net metabolic power was reduced by 7% (Fig. 15). This metabolic reduction is comparable to reducing body weight by 28% [48]. Because a set parallel spring stiffness will have a different effect on users of different stature we normalized spring stiffness to individuals' height and weight ($\overline{K_\theta}$). We compared this normalized spring stiffness, $\overline{K_\theta}$, to the change in net metabolic power and used least squares regression to fit a second order polynomial curve to the data (p=.026, R^2 =.134, equation in Appendix C, Table 2.)). In addition, to verify the significant regression, we ran a three factor mixed effects ANOVA with (subject (random), normalized stiffness, and normalized stiffness^2 as the model effects (p=.0075 for stiffness^2). The metabolic cost curve indicates that any normalized spring stiffness below $\overline{K_\theta}$ =.29 should cause a reduction in metabolic cost below normal walking (Fig. 15). This is also a critical point as $\overline{K_\theta}$ =.29 is also equivalent to 405 Nm/rad or ~100% ankle quasi-stiffness during loading phase of normal walking at 1.25 m/s (i.e. 405 Nm/rad during loading, 263 Nm/Rad during unloading, 329 Nm/Rad during stance from linear fit of average ankle moment- angle curve at 1.25 m/s).

By testing a range of parallel springs from 32% to 97% normal ankle quasi-stiffness during loading phase of stance during, we found that when subjects used an intermediate spring stiffness (307 Nm/rad) the exoskeleton provides up to 0.13 Nm/kg of average torque, which is 30% of the average ankle moment (.44Nm/kg) during normal walking at 1.25 m/s. As spring stiffness increased, biological ankle moment decreased linearly. Exoskeleton torque increased to a peak at a normalized spring stiffness of 0.25 (86% ankle stiffness during loading) (Fig. 16).

Figure 15: Net Metabolic Power vs. Exoskeleton Spring Stiffness

Average net metabolic power for the last two minutes of 7 minute walking trials for nine study participants. Absolute spring stiffness (top) and normalized spring stiffness (bottom) are shown compared to net metabolic power (±SE) and Δ net metabolic power from normal walking respectively. Change in net metabolic power was compared with normalized spring stiffness (bottom). We used least squares regression to find the best fit polynomial to the scatter plot with different colors representing individual subjects (fit order=2, p= 0.026 and R^2 =0.134). Regression equation is available in the Appendix C, Table 2. (*n=9)

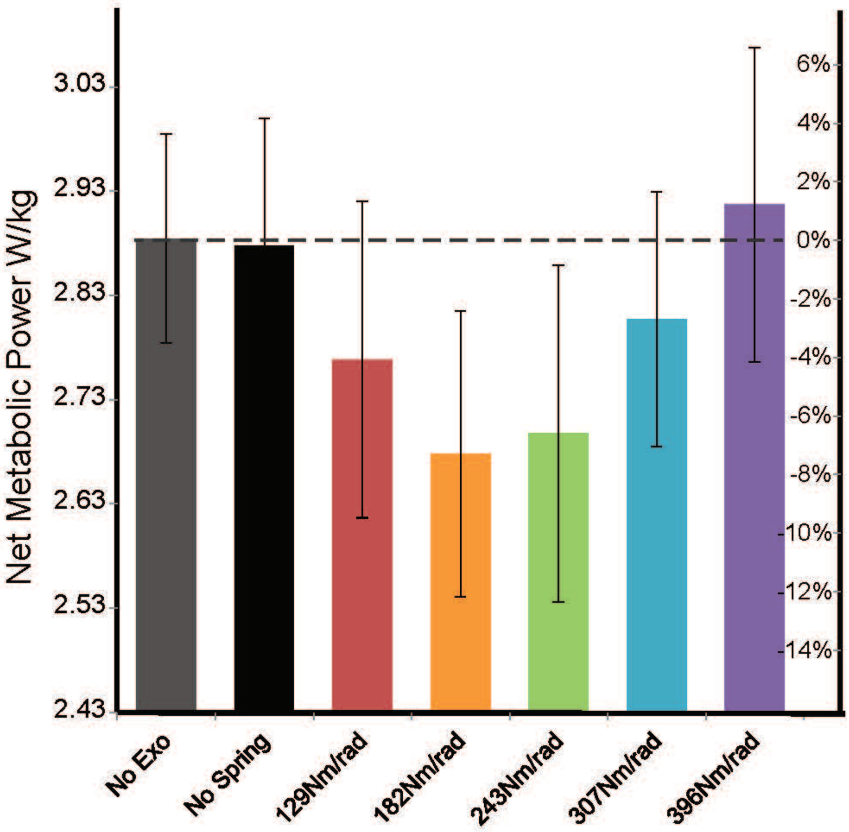
Net Metabolic Power W/kg
3.03
2.93
2.83
2.73
2.63
2.53
2.43
6%
4%
2%
0%
-2%
-4%
-6%
-8%
-10%
-12%
-14%
No Exo
No Spring
129Nm/rad
182Nm/rad
243Nm/rad
307Nm/rad
396Nm/rad

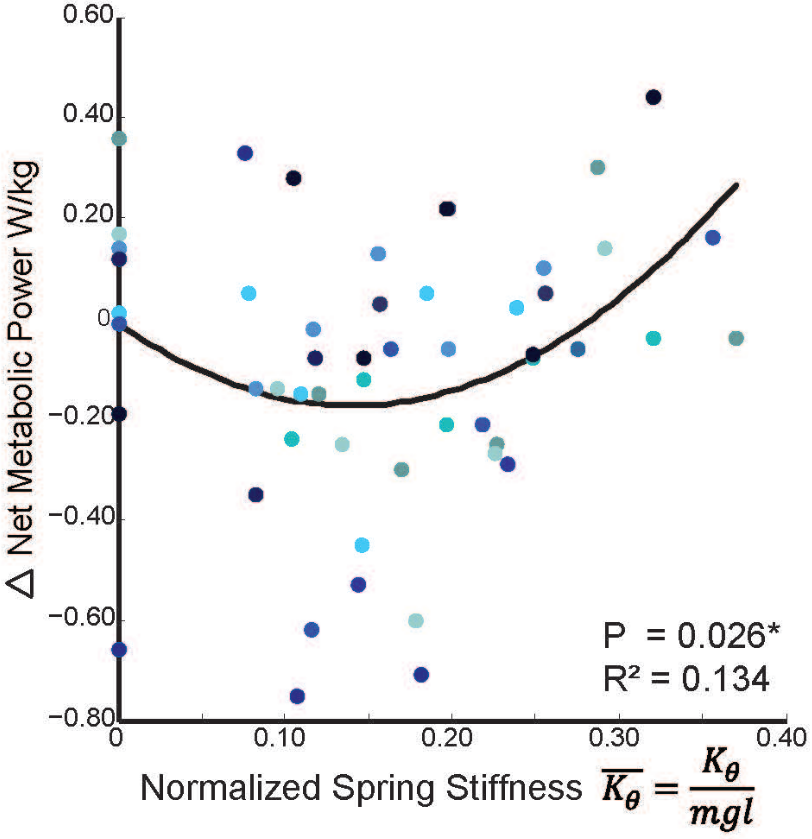
0.60
0.40
0.20
0
−0.20
−0.40
−0.60
−0.80
△ Net Metabolic Power W/kg
0
0.10
0.20
0.30
0.40
Normalized Spring Stiffness $\overline{K_\theta} = \frac{K_\theta}{mgl}$
P = 0.026*
R² = 0.134

Figure 16: Functional Stages of Exoskeleton Function and Kinetic Analysis

Ankle angle over a stride (heel strike to heel strike) with corresponding exoskeleton phases (top). Time-series of biological ankle moment over a stride (left middle) reveals that as parallel spring stiffness increases average biological ankle moment significantly decreases by up to 27%. Biological ankle moment time series data was integrated over the stride and divided by stride time to calculate the average biological ankle moment which was compared against the normalized spring stiffness (right middle). We used least squares regression to find the best-fit polynomial to the scatter plot with different colors representing individual subjects (fit order= 1, p= 0.002 and R^2 = 0.166). Exoskeleton torque (left bottom) and average torque (right bottom) were calculated and compared to absolute and normalized spring stiffness respectively. Best fit to the average exoskeleton torque scatter was a second order polynomial (p = 0.0001 and R^2 = 0.546). Regression equations are available in the Appendix C, Table 2. (n=9*).

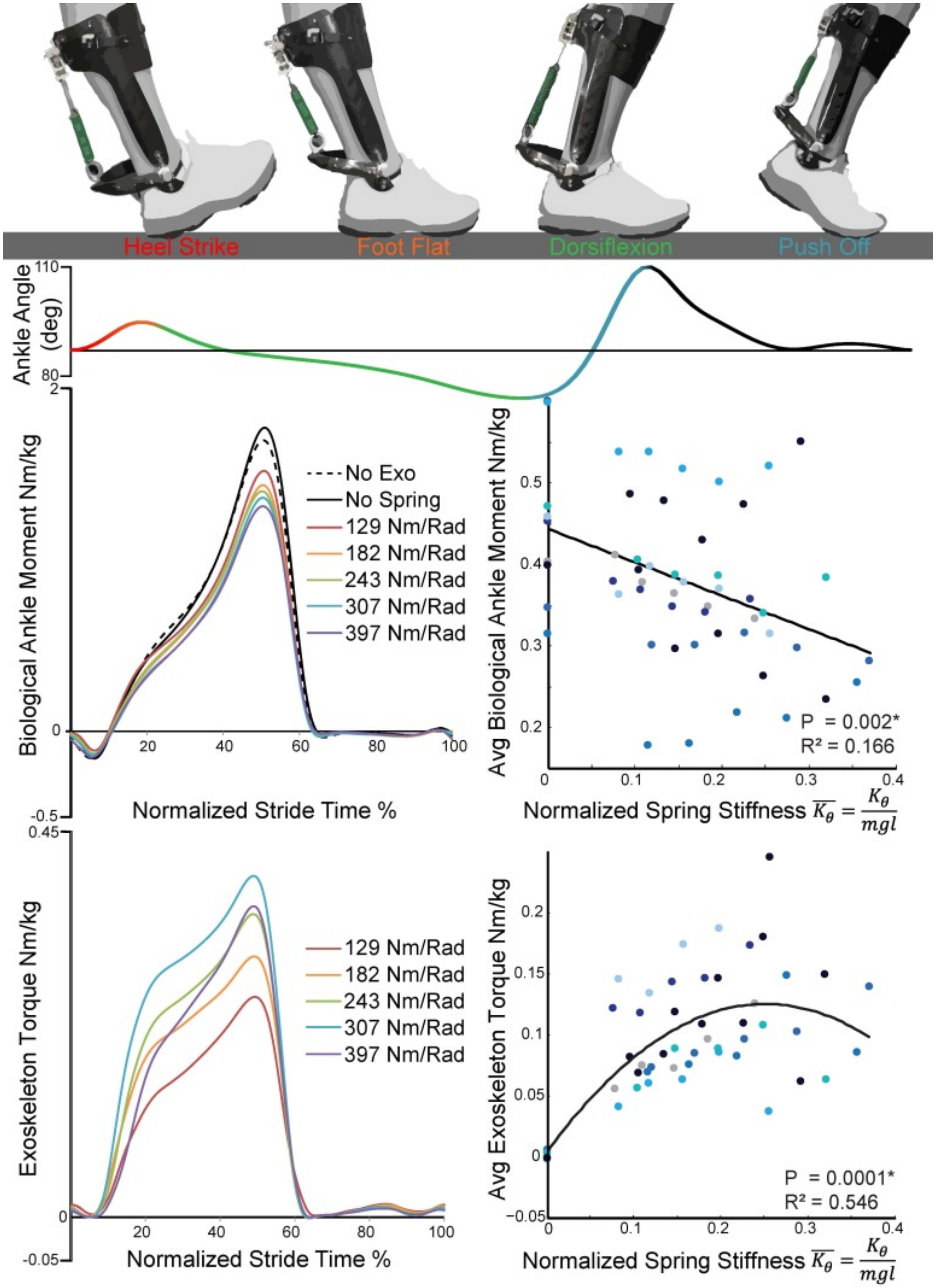
Heel Strike
Foot Flat
Dorsiflexion
Push Off
Ankle Angle (deg)
110
80
Biological Ankle Moment Nm/kg
2
0
-0.5
20
40
60
80
100
Normalized Stride Time %
No Exo
No Spring
129 Nm/Rad
182 Nm/Rad
243 Nm/Rad
307 Nm/Rad
397 Nm/Rad
Avg Biological Ankle Moment Nm/kg
0.5
0.4
0.3
0.2
0
0.1
0.2
0.3
0.4
P = 0.002*
R² = 0.166
Normalized Spring Stiffness $\overline{K_\theta} = \frac{K_\theta}{mgl}$
Exoskeleton Torque Nm/kg
0.45
0
-0.05
129 Nm/Rad
182 Nm/Rad
243 Nm/Rad
307 Nm/Rad
397 Nm/Rad
20
40
60
80
100
Normalized Stride Time %
Avg Exoskeleton Torque Nm/kg
0.2
0.15
0.1
0.05
0
−0.05
0
0.1
0.2
0.3
0.4
P = 0.0001*
R² = 0.546
Normalized Spring Stiffness $\overline{K_\theta} = \frac{K_\theta}{mgl}$

Figure 17: Ankle Joint Muscle Electromyography (EMG) vs. Exoskeleton Spring Stiffness

EMG signals of soleus (SOL), medial gastrocnemius (MG), lateral gastrocnemius (LG), and tibialis anterior (TA) were averaged over a stride (heel strike to heel strike) and scaled from 0-1 for each individual based off of maximum EMG amplitude for each signal. Normalized signals were then averaged across subjects and plotted against percent stride time (left). Signals were then integrated across the stride, and normalized with 1 representing integrated EMG levels for normal walking (No Exo). Subject averaged, normalized, integrated EMG values were then plotted against normalized spring stiffness and least squares regression was performed to find the best-fit polynomial to each scatter plot (right). Different color dots represent different individuals. Regression equations are available in the Appendix C, Table 2. (n=8*)

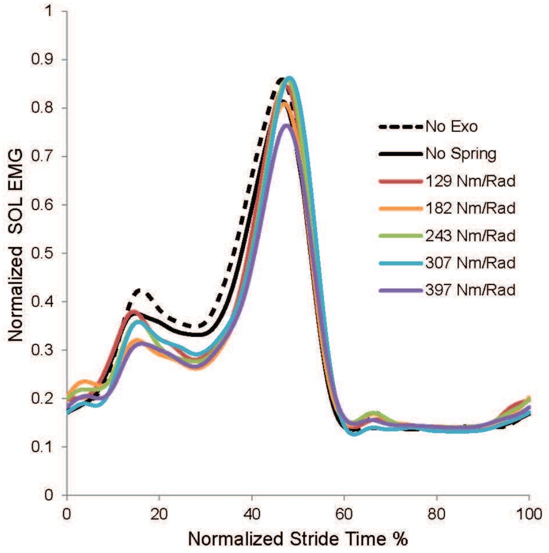
Normalized SOL EMG
Normalized Stride Time %
No Exo
No Spring
129 Nm/Rad
182 Nm/Rad
243 Nm/Rad
307 Nm/Rad
397 Nm/Rad
0
0.1
0.2
0.3
0.4
0.5
0.6
0.7
0.8
0.9
1
0
20
40
60
80
100

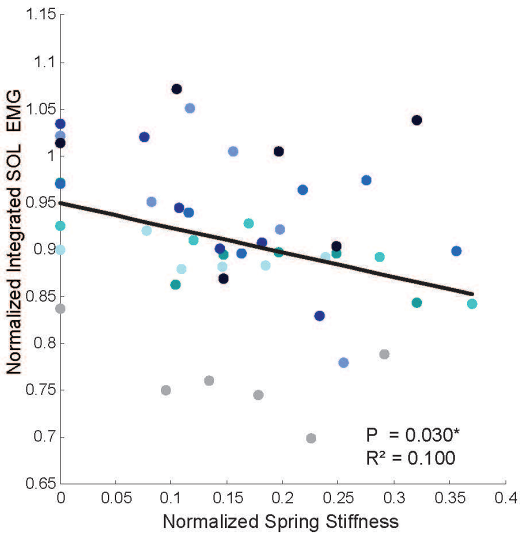
Normalized Integrated SOL EMG
Normalized Spring Stiffness
P = 0.030*
R² = 0.100
0.65
0.7
0.75
0.8
0.85
0.9
0.95
1
1.05
1.1
1.15
0
0.05
0.1
0.15
0.2
0.25
0.3
0.35
0.4

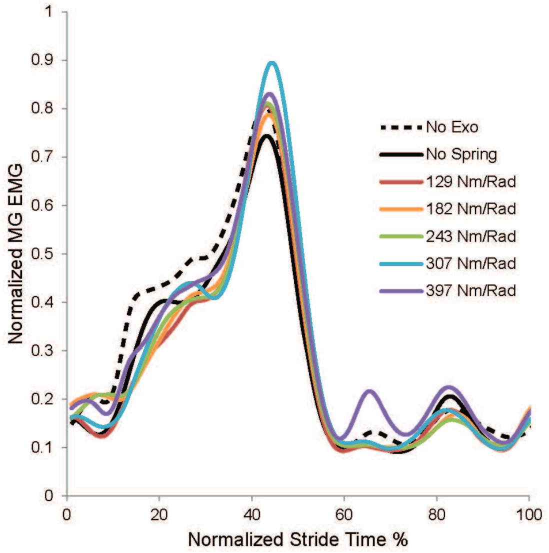
Normalized MG EMG
Normalized Stride Time %
No Exo
No Spring
129 Nm/Rad
182 Nm/Rad
243 Nm/Rad
307 Nm/Rad
397 Nm/Rad
0
0.1
0.2
0.3
0.4
0.5
0.6
0.7
0.8
0.9
1
0
20
40
60
80
100

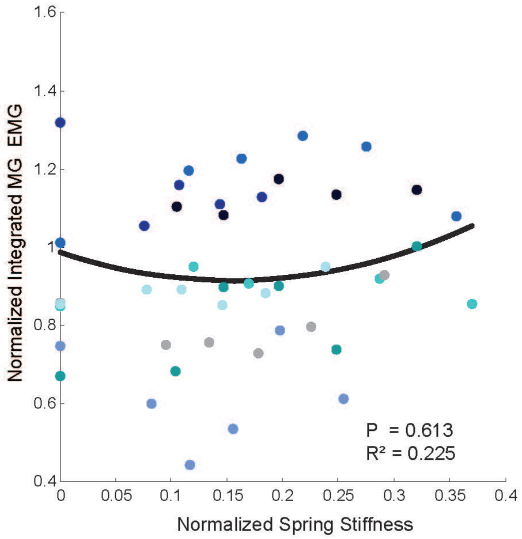
Normalized Integrated MG EMG
Normalized Spring Stiffness
P = 0.613
R² = 0.225
0.4
0.6
0.8
1
1.2
1.4
1.6
0
0.05
0.1
0.15
0.2
0.25
0.3
0.35
0.4

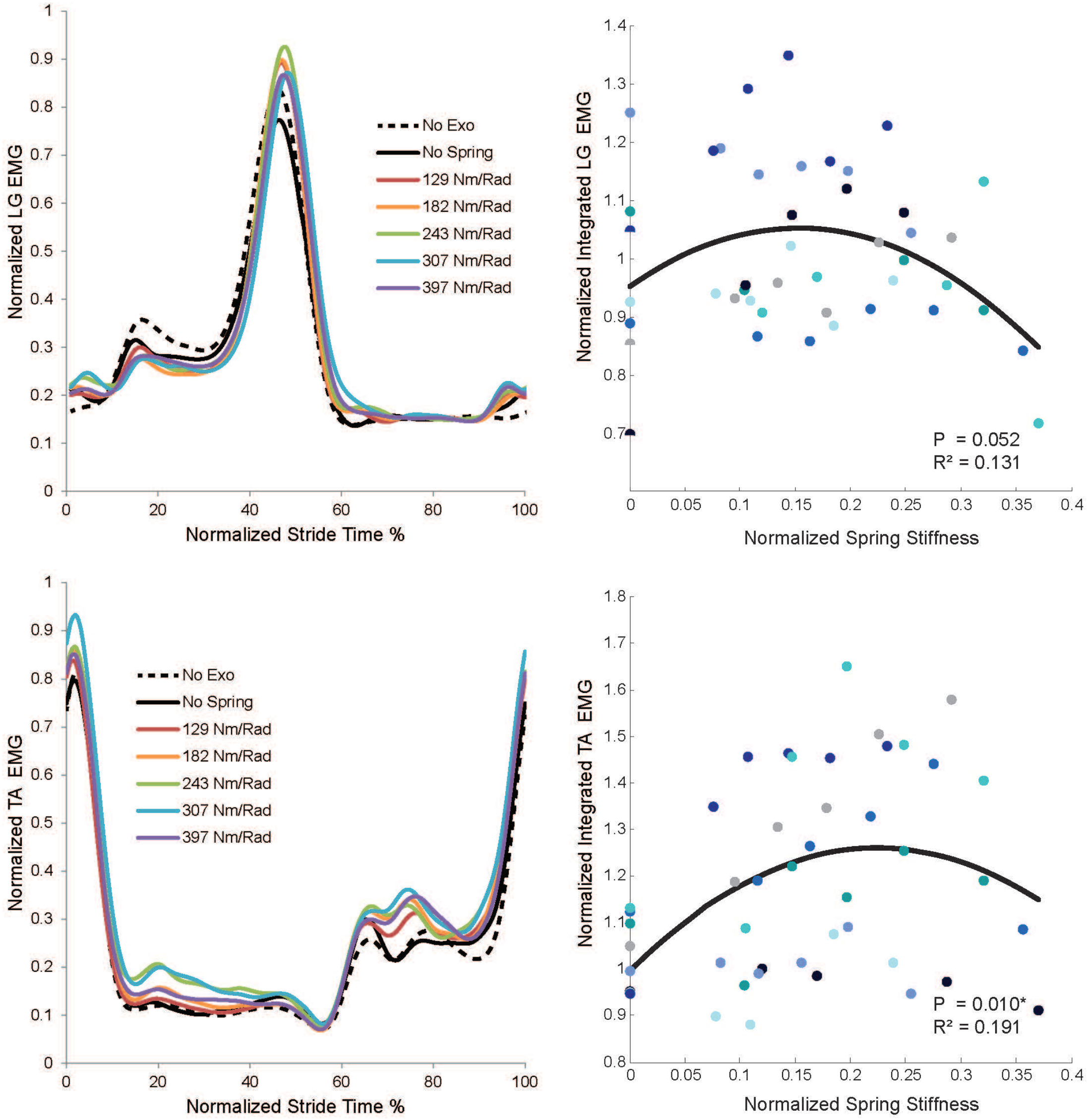
Normalized LG EMG
Normalized Stride Time %
No Exo
No Spring
129 Nm/Rad
182 Nm/Rad
243 Nm/Rad
307 Nm/Rad
397 Nm/Rad
Normalized Integrated LG EMG
Normalized Spring Stiffness
P = 0.052
R² = 0.131
Normalized TA EMG
Normalized Stride Time %
No Exo
No Spring
129 Nm/Rad
182 Nm/Rad
243 Nm/Rad
307 Nm/Rad
397 Nm/Rad
Normalized Integrated TA EMG
Normalized Spring Stiffness
P = 0.010*
R² = 0.191

While there is not a direct correlation between EMG activity and total metabolic energy expenditure we can determine which muscles are more or less active during assisted walking. The soleus (SOL) EMG activity significantly decreases linearly by 5% to 13% as normalized spring stiffness increases from 0 to 100% of the ankle quasi-stiffness during loading (normalized spring stiffness = 0.29) (Fig. 17). While the medial gastrocnemius (MG) curve fit was not statistically significant (Fig. 17), the data indicate that for most subjects MG EMG levels decreased below normal walking. The lateral gastrocnemius (LG) curve fit was not statistically significant either (Fig. 17). While several study participants showed decreased EMG activity, some were higher than normal walking as well. Both the MG and LG are biarticular muscles meaning they both aid in knee flexion and plantarflexion. Looking at time series data we can see that at the region of increased MG and LG activity (40-50% stride) there is also an increase in knee moment from the normal walking to the assisted walking trials.

Figure 18: Lower-limb Joint Moments vs. Exoskeleton Spring Stiffness

Ankle, knee and hip moments and ankle exoskeleton torque were averaged over a stride (heel strike to heel strike) and normalized by body mass, then plotted against percent stride time (left). Average moments and torques were calculated by integrating time-series data (impulse) over the stride and dividing by stride time. This was then plotted against normalized spring stiffness (right). We used least squares regression to find best fit polynomial curves to the scatter plot data with different color circles representing individual subjects. Biological ankle moment is calculated from the difference in total ankle moment and exoskeleton torque. Regression equations are available in the Appendix C, Table 2. (n=9*)

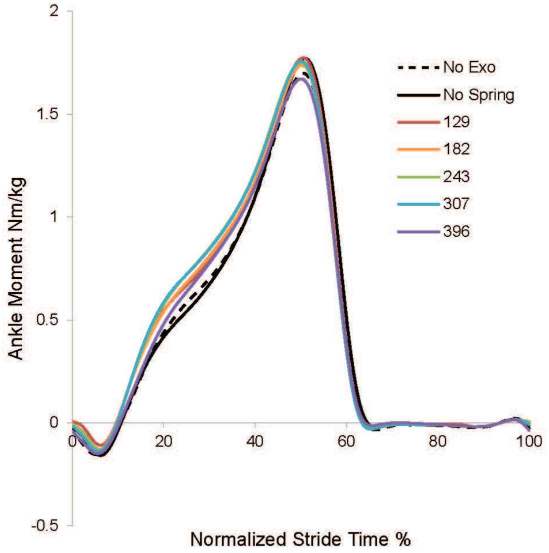

No Exo
No Spring
129
182
243
307
396
Ankle Moment Nm/kg
Normalized Stride Time %
2
1.5
1
0.5
0
-0.5
0
20
40
60
80
100

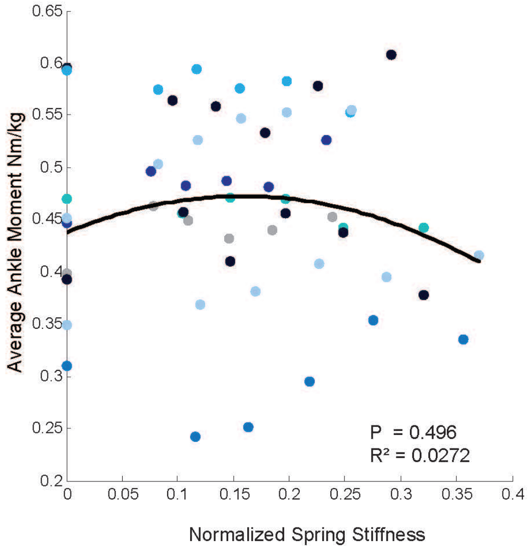

Average Ankle Moment Nm/kg
Normalized Spring Stiffness
P = 0.496
R² = 0.0272
0.65
0.6
0.55
0.5
0.45
0.4
0.35
0.3
0.25
0.2
0
0.05
0.1
0.15
0.2
0.25
0.3
0.35
0.4

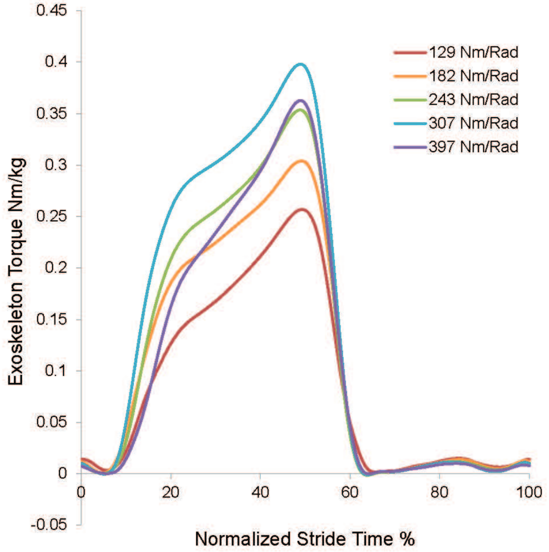

129 Nm/Rad
182 Nm/Rad
243 Nm/Rad
307 Nm/Rad
397 Nm/Rad
Exoskeleton Torque Nm/kg
Normalized Stride Time %
0.45
0.4
0.35
0.3
0.25
0.2
0.15
0.1
0.05
0
-0.05
0
20
40
60
80
100

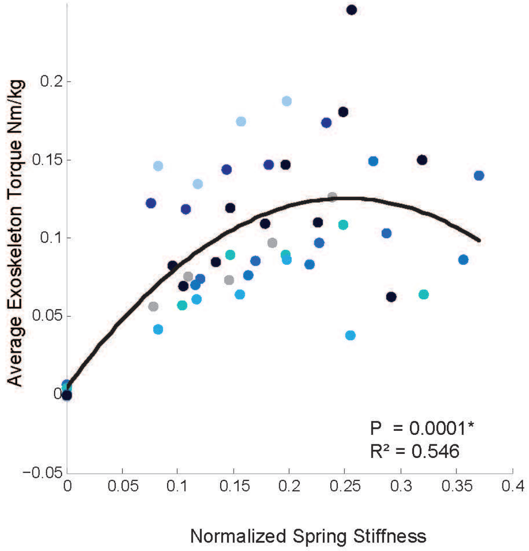

Average Exoskeleton Torque Nm/kg
Normalized Spring Stiffness
P = 0.0001*
R² = 0.546
0.2
0.15
0.1
0.05
0
−0.05
0
0.05
0.1
0.15
0.2
0.25
0.3
0.35
0.4

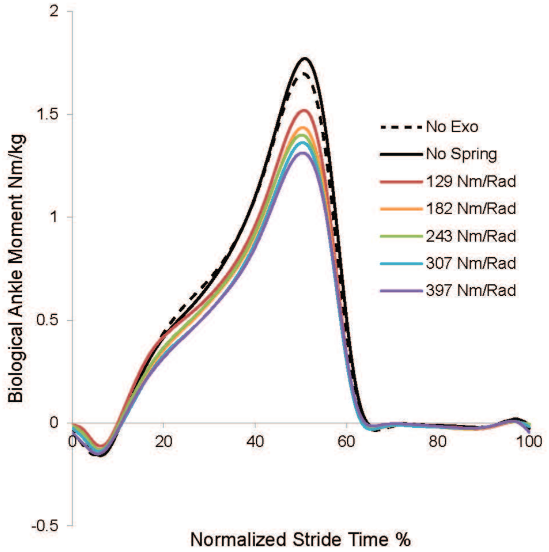

No Exo
No Spring
129 Nm/Rad
182 Nm/Rad
243 Nm/Rad
307 Nm/Rad
397 Nm/Rad
Biological Ankle Moment Nm/kg
Normalized Stride Time %
2
1.5
1
0.5
0
-0.5
0
20
40
60
80
100

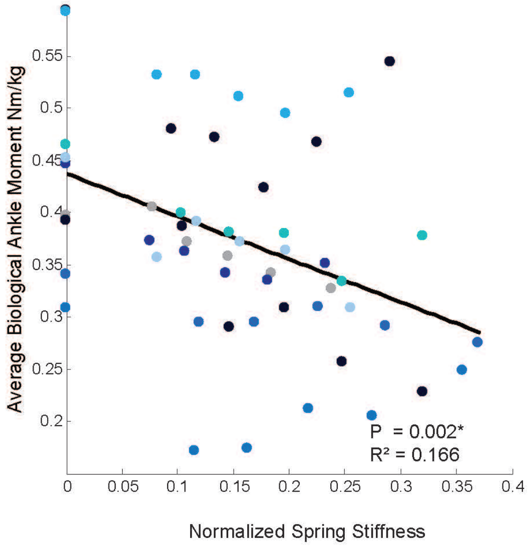

Average Biological Ankle Moment Nm/kg
Normalized Spring Stiffness
P = 0.002*
R² = 0.166
0.55
0.5
0.45
0.4
0.35
0.3
0.25
0.2
0
0.05
0.1
0.15
0.2
0.25
0.3
0.35
0.4

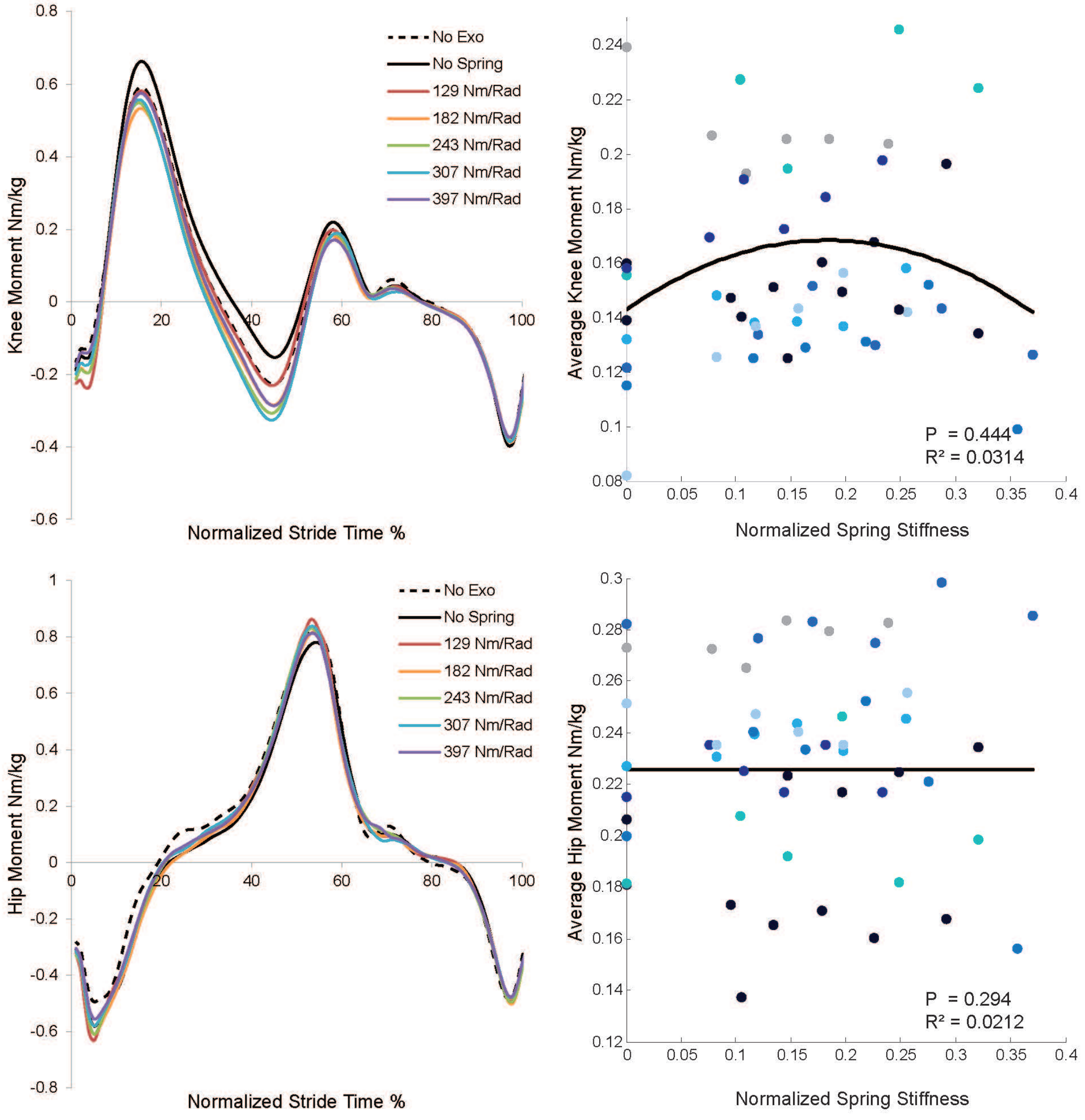
Knee Moment Nm/kg
0.8
0.6
0.4
0.2
0
-0.2
-0.4
-0.6
0
20
40
60
80
100
Normalized Stride Time %
No Exo
No Spring
129 Nm/Rad
182 Nm/Rad
243 Nm/Rad
307 Nm/Rad
397 Nm/Rad
Average Knee Moment Nm/kg
0.24
0.22
0.2
0.18
0.16
0.14
0.12
0.1
0.08
0
0.05
0.1
0.15
0.2
0.25
0.3
0.35
0.4
Normalized Spring Stiffness
P = 0.444
R² = 0.0314
Hip Moment Nm/kg
1
0.8
0.6
0.4
0.2
0
-0.2
-0.4
-0.6
-0.8
0
20
40
60
80
100
Normalized Stride Time %
No Exo
No Spring
129 Nm/Rad
182 Nm/Rad
243 Nm/Rad
307 Nm/Rad
397 Nm/Rad
Average Hip Moment Nm/kg
0.3
0.28
0.26
0.24
0.22
0.2
0.18
0.16
0.14
0.12
0
0.05
0.1
0.15
0.2
0.25
0.3
0.35
0.4
Normalized Spring Stiffness
P = 0.294
R² = 0.0212

Figure 19: Lower-limb Joint Mechanical Powers vs. Exoskeleton Spring Stiffness

Ankle, knee, hip and exoskeleton mechanical powers were averaged over the stride (heel strike to heel strike) and normalized by body mass, then plotted against percent stride time (left). Average mechanical power was calculated by integrating time-series data (work) and dividing by stride time. This was then plotted against normalized spring stiffness (right). We used least squares regression to find best fit polynomial curves to the scatter plot data with different color circles representing individual subjects. Biological ankle mechanical power is calculated from the difference in total ankle mechanical power and exoskeleton mechanical power. Regression equations are available in the Appendix C, Table 2. (n=9*)

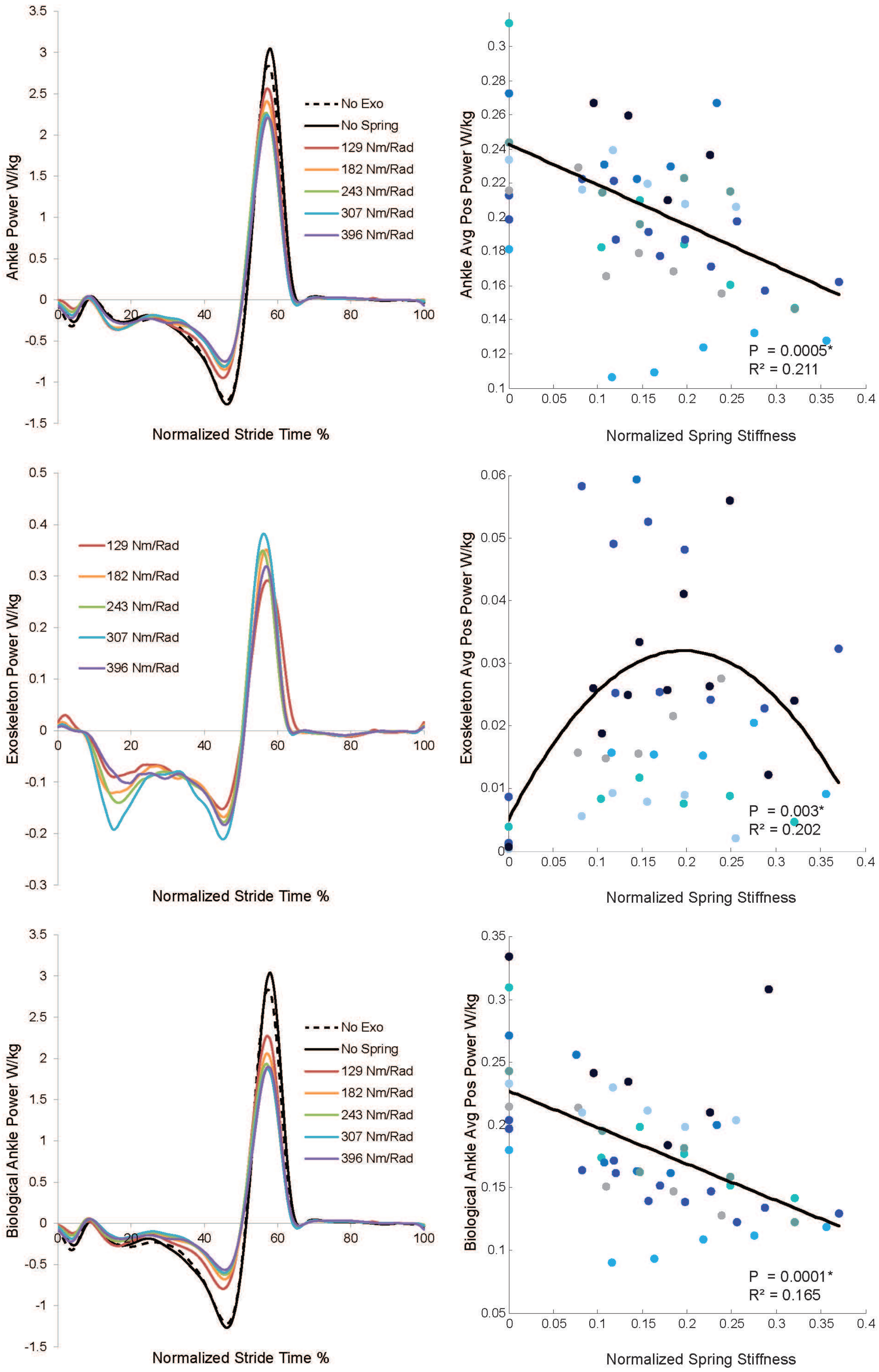

Ankle Power W/kg
Normalized Stride Time %
No Exo
No Spring
129 Nm/Rad
182 Nm/Rad
243 Nm/Rad
307 Nm/Rad
396 Nm/Rad
Ankle Avg Pos Power W/kg
Normalized Spring Stiffness
P = 0.0005*
R² = 0.211
Exoskeleton Power W/kg
Normalized Stride Time %
129 Nm/Rad
182 Nm/Rad
243 Nm/Rad
307 Nm/Rad
396 Nm/Rad
Exoskeleton Avg Pos Power W/kg
Normalized Spring Stiffness
P = 0.003*
R² = 0.202
Biological Ankle Power W/kg
Normalized Stride Time %
No Exo
No Spring
129 Nm/Rad
182 Nm/Rad
243 Nm/Rad
307 Nm/Rad
396 Nm/Rad
Biological Ankle Avg Pos Power W/kg
Normalized Spring Stiffness
P = 0.0001*
R² = 0.165

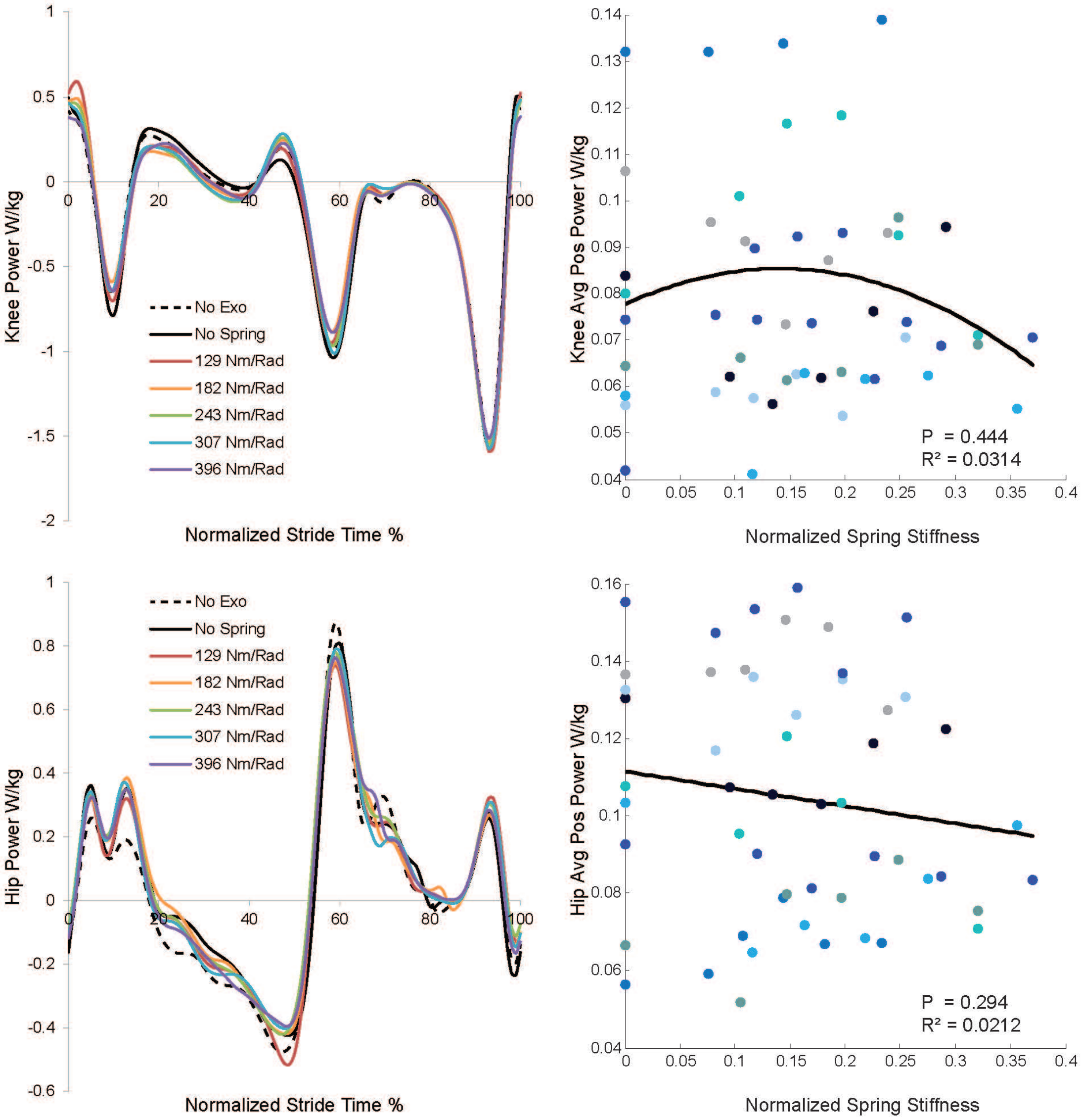

Knee Power W/kg
1
0.5
0
-0.5
-1
-1.5
-2
0
20
40
60
80
100
No Exo
No Spring
129 Nm/Rad
182 Nm/Rad
243 Nm/Rad
307 Nm/Rad
396 Nm/Rad
Normalized Stride Time %
Knee Avg Pos Power W/kg
0.14
0.13
0.12
0.11
0.1
0.09
0.08
0.07
0.06
0.05
0.04
0
0.05
0.1
0.15
0.2
0.25
0.3
0.35
0.4
P = 0.444
R² = 0.0314
Normalized Spring Stiffness
Hip Power W/kg
1
0.8
0.6
0.4
0.2
0
-0.2
-0.4
-0.6
0
20
40
60
80
100
No Exo
No Spring
129 Nm/Rad
182 Nm/Rad
243 Nm/Rad
307 Nm/Rad
396 Nm/Rad
Normalized Stride Time %
Hip Avg Pos Power W/kg
0.16
0.14
0.12
0.1
0.08
0.06
0.04
0
0.05
0.1
0.15
0.2
0.25
0.3
0.35
0.4
P = 0.294
R² = 0.0212
Normalized Spring Stiffness

Kinetic analysis indicates that the exoskeleton did not affect total joint average moment at the ankle, knee, or hip as the reported p-value of all curve fits was greater than 0.05 (Fig. 18). Additionally data from both average hip and knee power suggest the exoskeleton does not affect the knee or hip joint power (Fig. 19). Data for both average biological moment and average exoskeleton torque indicate the exoskeleton does reduce the biological moment as spring stiffness increases (Fig. 18). As spring stiffness increased total ankle power decreased (Fig. 19), suggesting that ankle angular velocity must decrease as spring stiffness increases. Maximum exoskeleton positive power occurs at a normalized spring stiffness of ~0.20. The largest change was seen in the negative biological ankle power, a reduction of up to 53% (Fig.19).

Kinematics data indicates that there was only a slight decrease in dorsiflexion angle during maximum torque production by the exoskeleton (40-60% stride cycle) (Fig. 20). Knee and hip joint angle curves suggest that the exoskeleton has little to no impact on normal gait kinematics (Fig. 20). The most notable change in gait kinematics, when users wore the exoskeletons, was a slight increase in step length. ANOVA analysis of step length and width and a post-hoc student's t-test indicate that during all exoskeleton trials, subjects had longer step lengths (p= 0.01) but not step widths (p=0.80) when compared to normal walking (Fig. 21).

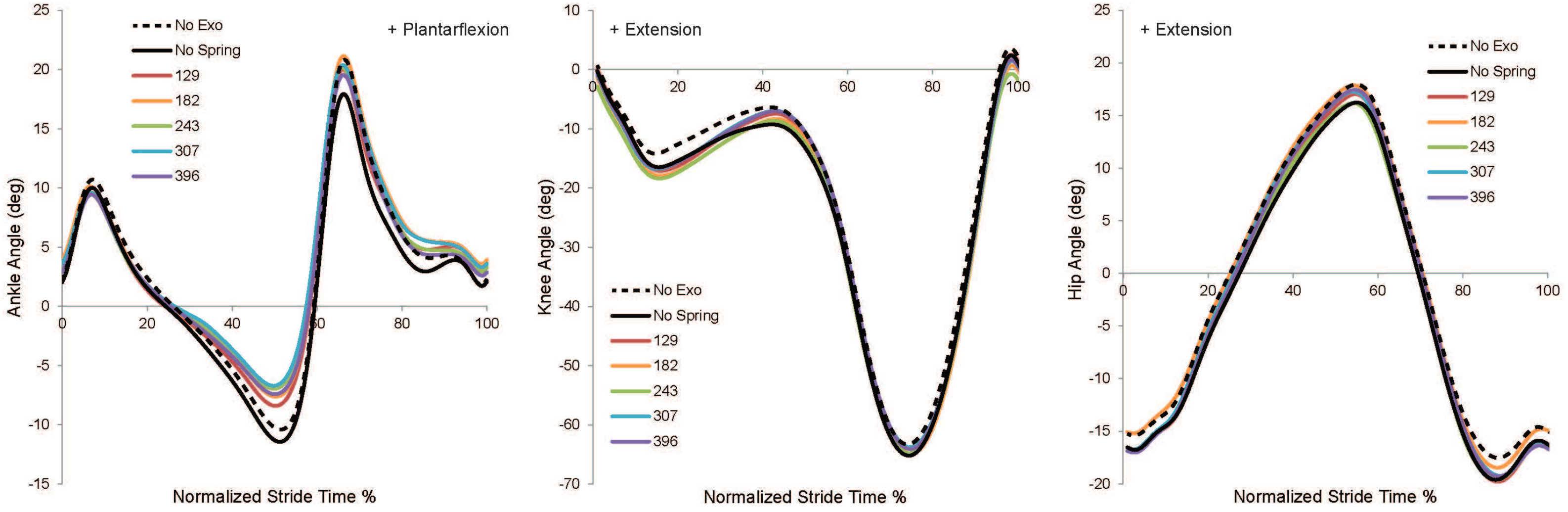

Figure 20: Lower Limb Joint Angles

Ankle, knee and hip joint angles were averaged over a stride (heel strike to heel strike), then plotted against percent stride time for each condition. Plantarflexion and extension are in the positive direction. (n=9*).

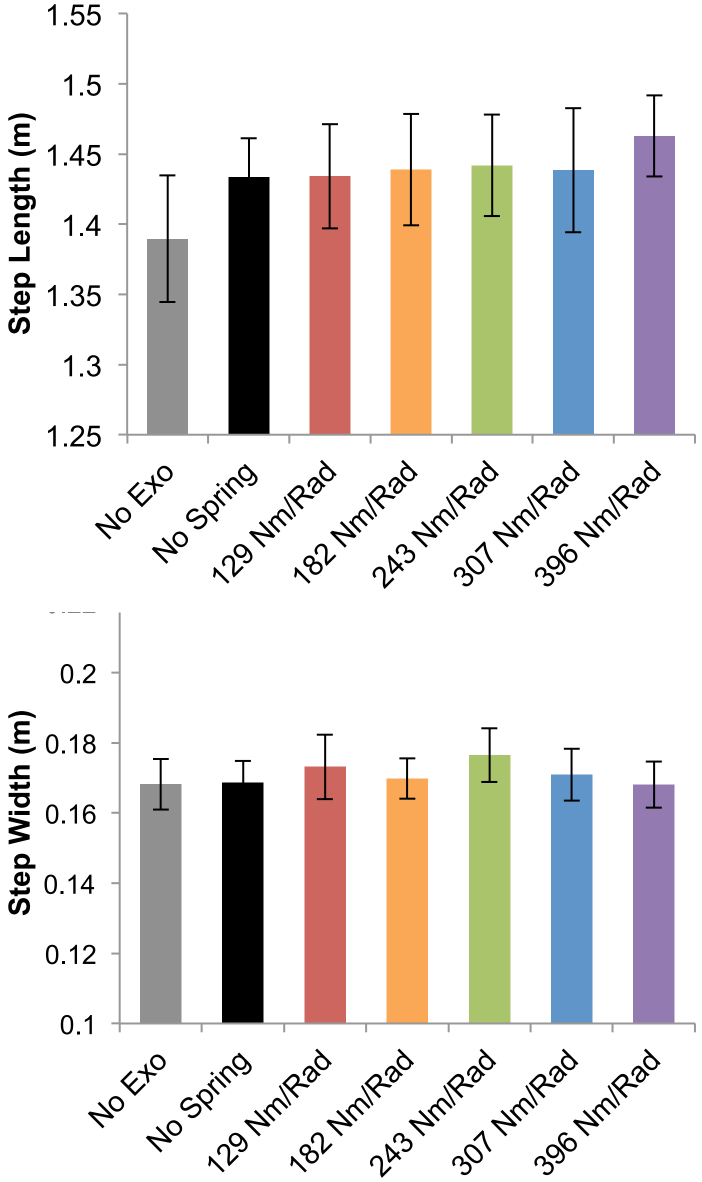

Figure 21: Step Length and Width vs. Exoskeleton Spring Stiffness

Foot kinematics data and ground reaction center of pressure measurements were used to calculate average step length and width of each individual across a minimum of 10 strides. The mean and standard error of individuals' average step length and width is plotted by spring condition. (n=9*)

Discussion

We hypothesized that there is an ideal parallel spring stiffness for reducing net metabolic energy consumption that is slightly stiffer than the parallel spring which provides the largest ankle torque. While there was a marked reduction in metabolic energy expenditure when walking in the exoskeleton the reason behind this is hard to pinpoint. EMG, kinetics, kinematics, and net metabolic power data all indicate that exoskeleton assistance reduces total metabolic energy use to a point (~7% below normal) with an ideal intermediate parallel spring. This ideal stiffness was actually less than the spring stiffness which provided the maximum torque, contrary to our original hypothesis based off a simulation study [15]. Springs stiffer than the ideal parallel spring drive back up net metabolic energy use, suggesting there might be compensation by other muscles in these higher stiffness conditions.

EMG activity of the soleus (SOL), a major plantarflexor, showed a significant linear decrease in activity as normalized spring stiffness increased however the tibialis anterior (TA) activity increased with spring stiffness up to 79% (normalized spring stiffness =.23) of the ankle quasi-stiffness during loading phase of stance during walking at 1.25 m/s. This co-activation might be key in understanding the shape of the metabolic cost curve. We speculate that subject used their TA to increase their dorsiflexion angle during stance, increasing exoskeleton torque. However after the spring stiffness reached approximately 79% ankle stiffness subjects decreased their TA activation and did not try to keep their heel on the ground, which would stretch the parallel spring more. This trend is also seen when examining the exoskeleton torque data which reached a maximum at approximately 86% ankle stiffness. While TA EMG increases more than SOL EMG, the SOL has 2.5 times the cross sectional area of the TA [29] indicating that changes in SOL EMG activity will have a larger impact on net metabolic energy expenditure.

To explain net reductions in metabolic power we examined a simulation study by Umberger et al. which suggest that the human plantarflexors are responsible for 27% of metabolic energy consumption during normal walking and that the majority of this energy in consumed during stance before push off, the period of negative ankle power [33]. Our data indicate that at the energetically ideal parallel spring, average biological negative power was reduced by 43%. This suggests that metabolic power could be reduced as much as 12%, if reducing negative biological power is key to decreasing metabolic energy expenditure. On the other hand, a hopping study performed with a similar ankle exoskeleton and fixed parallel spring stiffness suggests that reductions of muscle force, not work/power lead to reductions in metabolic energy use [49].

Recent attention has been drawn to confounding effects of assistive exoskeletons on the muscle-tendon dynamics of the ankle plantar flexors. Ultrasound studies performed in our lab [43] indicate that soleus muscle fascicles undergo higher length changes with parallel elastic assistance of plantarflexors during hopping movements. Reduced forces of the biological muscle were counteracted by increased length changes resulting in no difference in fassicle work. Increasing parallel spring stiffness did increase the reliance on contractile elements (i.e. muscles) for muscle-tendon unit power, shifting away from the large amount of power contributed by series elastic elements during hopping. In addition, parallel spring stiffness assistance increased tibialis anterior (TA) activation with increased spring stiffness, a potential compensation to maintain overall ankle joint moments during the task. These muscle-level phenomena may help explain why our metabolic reduction was lower than expected based on the model of Umberger describe above (i.e. 7% vs. 12%).

A recent study used a simple computational model of an elastic exoskeleton assisting the biological plantarflexors to further examine the underling muscle tendon interactions during exoskleleton assisted walking, recent study [50]. Simulation data indicate that as parallel spring stiffness increases, biological moment would decrease with increases in exoskeletal torque and that muscle activation and metabolic energy use would decrease nearly linearly, findings consistent with our observed decreases in biological moments, mechanical powers and SOL muscle activations. The study also investigated the muscle fascicle dynamics and determined that at an exoskeleton spring stiffness greater than 237 Nm/rad (~58% average ankle stiffness during loading) there was passive stretching of the muscle fascicles, shifting the operating point of the underlying muscles to longer lengths. This could be a factor that limits performance at high parallel spring stiffness values.

The simulation data also indicate that, due to compensatory mechanisms to maintain overall ankle joint moment, humans may lose the metabolic benefit of elastic exoskeletons with parallel springs over ~60% ankle stiffness. This is consistent with our data indicating maximum metabolic benefit with a parallel spring of ~50% ankle stiffness. As exoskeleton stiffness increases, there is less stretching of the biological series elastic element (tendon and aponeurosis) and more stretch in the length of the muscle fascicles. This could interrupt the clutch-like muscle-tendon dynamics seen in normal walking and limit the metabolic benefit at higher stiffnesses, due to higher added metabolic cost of muscle fascicle shortening.

These results indicate the need for future studies that aim to simultaneously maximize exoskeleton performance and study the underlying muscle-tendon dynamics during assisted walking. By establishing a testbed in which exoskeleton assistance could be adjusted by tethered interfaces, such as a cable driven exoskeleton, we could simulate the effects of applying both negative power and increased positive power at the ankle. In addition we could characterize assistance from nonlinear springs such as hardening or softening springs, and use those quantifications to design an exoskeleton that exceeds the new upper limits set here.

REFERENCES

[1] M. B. Wiggin, S. H. Collins, and G. S. Sawicki, "An Exoskeleton Using Controlled Energy Storage and Release to Aid Ankle Propulsion," *2011 Ieee International Conference on Rehabilitation Robotics (Icorr),* 2011.

[2] A. D. Kuo, J. M. Donelan, and A. Ruina, "Energetic consequences of walking like an inverted pendulum: step-to-step transitions," *Exerc Sport Sci Rev,* vol. 33, pp. 88-97, Apr 2005.

[3] D. J. Farris and G. S. Sawicki, "Human medial gastrocnemius force-velocity behavior shifts with locomotion speed and gait," *Proc Natl Acad Sci U S A,* vol. 109, pp. 977-82, Jan 17 2012.

[4] D. J. Farris and G. S. Sawicki, "The mechanics and energetics of human walking and running: a joint level perspective," *J R Soc Interface,* vol. 9, pp. 110-8, Jan 7 2012.

[5] C. P. McGowan, R. R. Neptune, and R. Kram, "Independent effects of weight and mass on plantar flexor activity during walking: implications for their contributions to body support and forward propulsion," *J Appl Physiol (1985),* vol. 105, pp. 486-94, Aug 2008.

[6] R. R. Neptune, S. A. Kautz, and F. E. Zajac, "Contributions of the individual ankle plantar flexors to support, forward progression and swing initiation during walking," *J Biomech,* vol. 34, pp. 1387-98, Nov 2001.

[7] A. M. Dollar and H. Herr, "Design of a Quasi-Passive Knee Exoskeleton to Assist Running," *2008 Ieee/Rsj International Conference on Robots and Intelligent Systems, Vols 1-3, Conference Proceedings,* pp. 747-754, 2008.

[8] A. M. Dollar and H. Herr, "Lower extremity exoskeletons and active orthoses: Challenges and state-of-the-art," *Ieee Transactions on Robotics,* vol. 24, pp. 144-158, Feb 2008.

[9] D. P. Ferris, "The exoskeletons are here," *J Neuroeng Rehabil,* vol. 6, p. 17, Jun 9 2009.

[10] J. Hitt, A. M. Oymagil, T. Sugar, K. Hollander, A. Boehler, and J. Fleeger, "Dynamically controlled ankle-foot orthosis (DCO) with regenerative kinetics: Incrementally attaining user portability," *Proceedings of the 2007 Ieee International Conference on Robotics and Automation, Vols 1-10,* pp. 1541-1546, 2007.

[11] A. Danielsson and K. S. Sunnerhagen, "Energy expenditure in stroke subjects walking with a carbon composite ankle foot orthosis," *J Rehabil Med,* vol. 36, pp. 165-8, Jul 2004.

[12] M. C. Faustini, R. R. Neptune, R. H. Crawford, and S. J. Stanhope, "Manufacture of Passive Dynamic ankle-foot orthoses using selective laser sintering," *IEEE Trans Biomed Eng,* vol. 55, pp. 784-90, Feb 2008.

[13] R. C. Browning, J. R. Modica, R. Kram, and A. Goswami, "The effects of adding mass to the legs on the energetics and biomechanics of walking," *Med Sci Sports Exerc,* vol. 39, pp. 515-25, Mar 2007.

[14] D. J. Bregman, J. Harlaar, C. G. Meskers, and V. de Groot, "Spring-like Ankle Foot Orthoses reduce the energy cost of walking by taking over ankle work," *Gait Posture,* vol. 35, pp. 148-53, Jan 2012.

[15] D. J. Bregman, M. M. van der Krogt, V. de Groot, J. Harlaar, M. Wisse, and S. H. Collins, "The effect of ankle foot orthosis stiffness on the energy cost of walking: a simulation study," *Clin Biomech (Bristol, Avon),* vol. 26, pp. 955-61, Nov 2011.

[16] K. N. Gregorczyk, L. Hasselquist, J. M. Schiffman, C. K. Bensel, J. P. Obusek, and D. J. Gutekunst, "Effects of a lower-body exoskeleton device on metabolic cost and gait biomechanics during load carriage," *Ergonomics,* vol. 53, pp. 1263-75, Oct 2010.

[17] S. Nadeau, D. Gravel, A. B. Arsenault, and D. Bourbonnais, "Plantarflexor weakness as a limiting factor of gait speed in stroke subjects and the compensating role of hip flexors," *Clin Biomech (Bristol, Avon),* vol. 14, pp. 125-35, Feb 1999.

[18] M. B. Wiggin, G. S. Sawicki, and S. H. Collins, "An exoskeleton using controlled energy storage and release to aid ankle propulsion," *IEEE Int Conf Rehabil Robot,* vol. 2011, p. 5975342, 2011.

[19] M. B. Wiggin, G. S. Sawicki, and S. H. Collins, "Apparatus and clutch for using controlled storage and release of mechanical energy to aid locomotion," US Patent, 2013.

[20] S. M. Cain, K. E. Gordon, and D. P. Ferris, "Locomotor adaptation to a powered ankle-foot orthosis depends on control method," *J Neuroeng Rehabil,* vol. 4, p. 48, 2007.

[21] G. S. Sawicki and D. P. Ferris, "Mechanics and energetics of level walking with powered ankle exoskeletons," *J Exp Biol,* vol. 211, pp. 1402-13, May 2008.

[22] P. Malcolm, W. Derave, S. Galle, and D. De Clercq, "A Simple Exoskeleton That Assists Plantarflexion Can Reduce the Metabolic Cost of Human Walking," *PLoS ONE,* vol. 8, p. e56137, 2013.

[23] M. K. Boes, M. Islam, Y. David Li, and E. T. Hsiao-Wecksler, "Fuel Efficiency of a Portable Powered Ankle-Foot Orthosis," in *Rehabilitation Robotics (ICORR), 2013 IEEE International Conference on*, 2013, pp. 1-6.

[24] K. E. Gordon and D. P. Ferris, "Learning to walk with a robotic ankle exoskeleton," *J Biomech,* vol. 40, pp. 2636-44, 2007.

[25] K. E. Gordon, G. S. Sawicki, and D. P. Ferris, "Mechanical performance of artificial pneumatic muscles to power an ankle-foot orthosis," *J Biomech,* vol. 39, pp. 1832-41, 2006.

[26] G. S. Sawicki and D. P. Ferris, "A pneumatically powered knee-ankle-foot orthosis (KAFO) with myoelectric activation and inhibition," *J Neuroeng Rehabil,* vol. 6, p. 23, 2009.

[27] G. S. Sawicki and D. P. Ferris, "Mechanics and energetics of incline walking with robotic ankle exoskeletons," *J Exp Biol,* vol. 212, pp. 32-41, Jan 2009.

[28] G. S. Sawicki and D. P. Ferris, "Powered ankle exoskeletons reveal the metabolic cost of plantar flexor mechanical work during walking with longer steps at constant step frequency," *J Exp Biol,* vol. 212, pp. 21-31, Jan 2009.

[29] J. M. Brockway, "Derivation of formulae used to calculate energy expenditure in man," *Hum Nutr Clin Nutr,* vol. 41, pp. 463-71, Nov 1987.

[30] J. M. Winters and L. Stark, "Estimated mechanical properties of synergistic muscles involved in movements of a variety of human joints," *Journal of biomechanics,* vol. 21, pp. 1027-1041, 1988.

[31] L. M. Mooney, E. J. Rouse, and H. M. Herr, "Autonomous exoskeleton reduces metabolic cost of human walking during load carriage," *Journal of NeuroEngineering and Rehabilitation,* vol. 11, p. 80, 2014.

[32] A. B. Zoss, H. Kazerooni, and A. Chu, "Biomechanical design of the Berkeley lower extremity exoskeleton (BLEEX)," *Mechatronics, IEEE/ASME Transactions on,* vol. 11, pp. 128-138, 2006.

[33] B. R. Umberger and J. Rubenson, "Understanding muscle energetics in locomotion: new modeling and experimental approaches," *Exerc Sport Sci Rev,* vol. 39, pp. 59-67, Apr 2011.

[34] B. R. Umberger, "Stance and swing phase costs in human walking," *J R Soc Interface,* vol. 7, pp. 1329-40, Sep 6 2010.

[35] G. Elliott, G. S. Sawicki, A. Marecki, and H. Herr, "The Biomechanics and Energetics of Human Running using an Elastic Knee Exoskeleton."

[36] A. M. Grabowski and H. M. Herr, "Leg exoskeleton reduces the metabolic cost of human hopping," *J Appl Physiol,* vol. 107, pp. 670-8, Sep 2009.

[37] S. Galle, P. Malcolm, W. Derave, and D. De Clercq, "Adaptation to walking with an exoskeleton that assists ankle extension," *Gait & posture,* vol. 38, pp. 495-499, 2013.

[38] S. Galle, P. Malcolm, W. Derave, and D. De Clercq, "Adaptation to walking with an exoskeleton that assists ankle extension," *Gait Posture,* vol. 38, pp. 495-9, Jul 2013.

[39] R. M. Alexander, *Principles of animal locomotion*: Princeton University Press, 2003.

[40] J. W. Beach, "Spring-heel," US Patent, 1891.

[41] A. M. Grabowski and H. M. Herr, "Leg exoskeleton reduces the metabolic cost of human hopping," *Journal of Applied Physiology,* vol. 107, pp. 670-678, 2009.

[42] W. van Dijk, H. van der Kooij, and E. Hekman, "A passive exoskeleton with artificial tendons: Design and experimental evaluation," in *Rehabilitation Robotics (ICORR), 2011 IEEE International Conference on*, 2011, pp. 1-6.

[43] D. J. Farris, B. D. Robertson, and G. S. Sawicki, "Elastic ankle exoskeletons reduce soleus muscle force but not work in human hopping," *Journal of Applied Physiology,* vol. 115, pp. 579-585, 2013.

[44] D. J. Farris and G. S. Sawicki, "Linking the mechanics and energetics of hopping with elastic ankle exoskeletons," *J Appl Physiol,* Oct 11 2012.

[45] L. E. Bratteby, B. Sandhagen, M. Lotborn, and G. Samuelson, "Daily energy expenditure and physical activity assessed by an activity diary in 374 randomly selected 15-year-old adolescents," *Eur J Clin Nutr,* vol. 51, pp. 592-600, Sep 1997.

[46] T. M. Manini, J. E. Everhart, K. V. Patel, D. A. Schoeller, L. H. Colbert, M. Visser*, et al.*, "Daily activity energy expenditure and mortality among older adults," *JAMA,* vol. 296, pp. 171-9, Jul 12 2006.

[47] R. L. Waters and S. Mulroy, "The energy expenditure of normal and pathologic gait," *Gait Posture,* vol. 9, pp. 207-31, Jul 1999.

[48] A. Grabowski, C. T. Farley, and R. Kram, "Independent metabolic costs of supporting body weight and accelerating body mass during walking," *Journal of Applied Physiology,* vol. 98, pp. 579-583, 2005.

[49] D. J. Farris and G. S. Sawicki, "Linking the mechanics and energetics of hopping with elastic ankle exoskeletons," *J Appl Physiol,* vol. 113, pp. 1862-72, Dec 15 2012.

[50] N. S. Khan, "A Data-driven Muscle-tendon Modeling Framework to Evaluate Muscle-level Performance of Ankle Exoskeletons during Human Walking.," Masters of Science, Biomedical Engineering, North Carolina State University, 2013.

APPENDICES

Appendix A

Mechanical Clutch Drawings

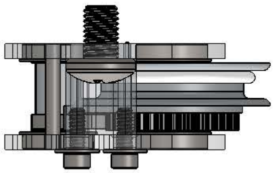

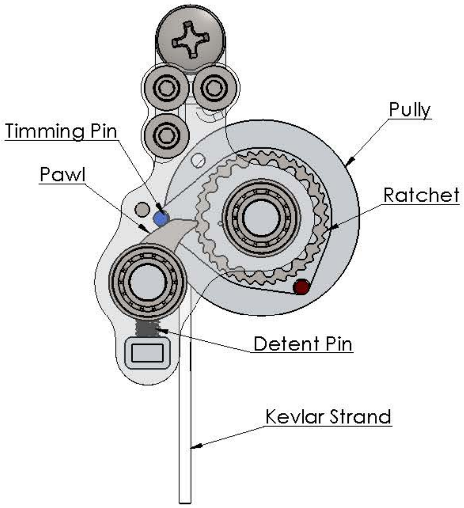
Pully
Timming Pin
Pawl
Ratchet
Detent Pin
Kevlar Strand

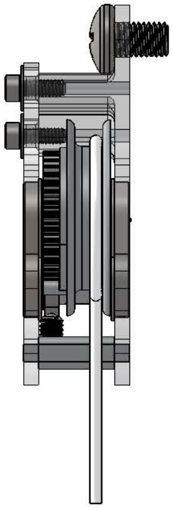

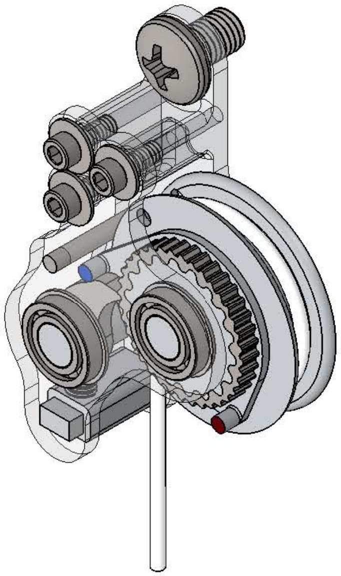

THIRD ANGLE PROJECTION

336-471-1934
mbwiggin@ncsu.edu

MATERIAL

FINISH

ALL DIMENSIONS ARE IN INCHES
TOLERANCES UNLESS OTHERWISE SPECIFIED
XX ± .01
XXX ± .005
ANGLES ± 0.1°
BEND RADII

NO BURRS OR SHARP EDGES.
ALL EDGES TO BE BROKEN .015 MIN.
UNLESS OTHERWISE SPECIFIED.

	BY	DATE
DESIGN		
DRAWN		
CHKD		
APPD		
CLASS CODE		

Bruce Wiggin
3111 Hemlock Forrest Circle Unit 103
Raleigh, NC 27612

TITLE
Mechanical Clutch

SIZE B
DRAWING NO.

SCALE Do Not Scale
SHEET 1 OF 1
REV.

LT102

ITEM NO.	PART NUMBER	QTY.
1	Support Plate	1
2	MMC# 91772A555	1
3	MMC# 57155K304	4
4	MMC# 90917A628	5
5	Pulley	1
6	Ratchet_Face	1
7	Pin Popper	1
8	Pawl	1
9	Pawl Shaft	1
10	Support Plate Flat	1
11	Pawl Backstop Pin	1
12	MMC# 96006A211	3
13	MMC# 96659A101	3
14	Kevlar Cable	1
15	Detent Holder	1
16	MMC# 3408A129	1
17	MMC# 9432K26	1

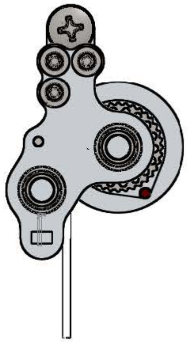

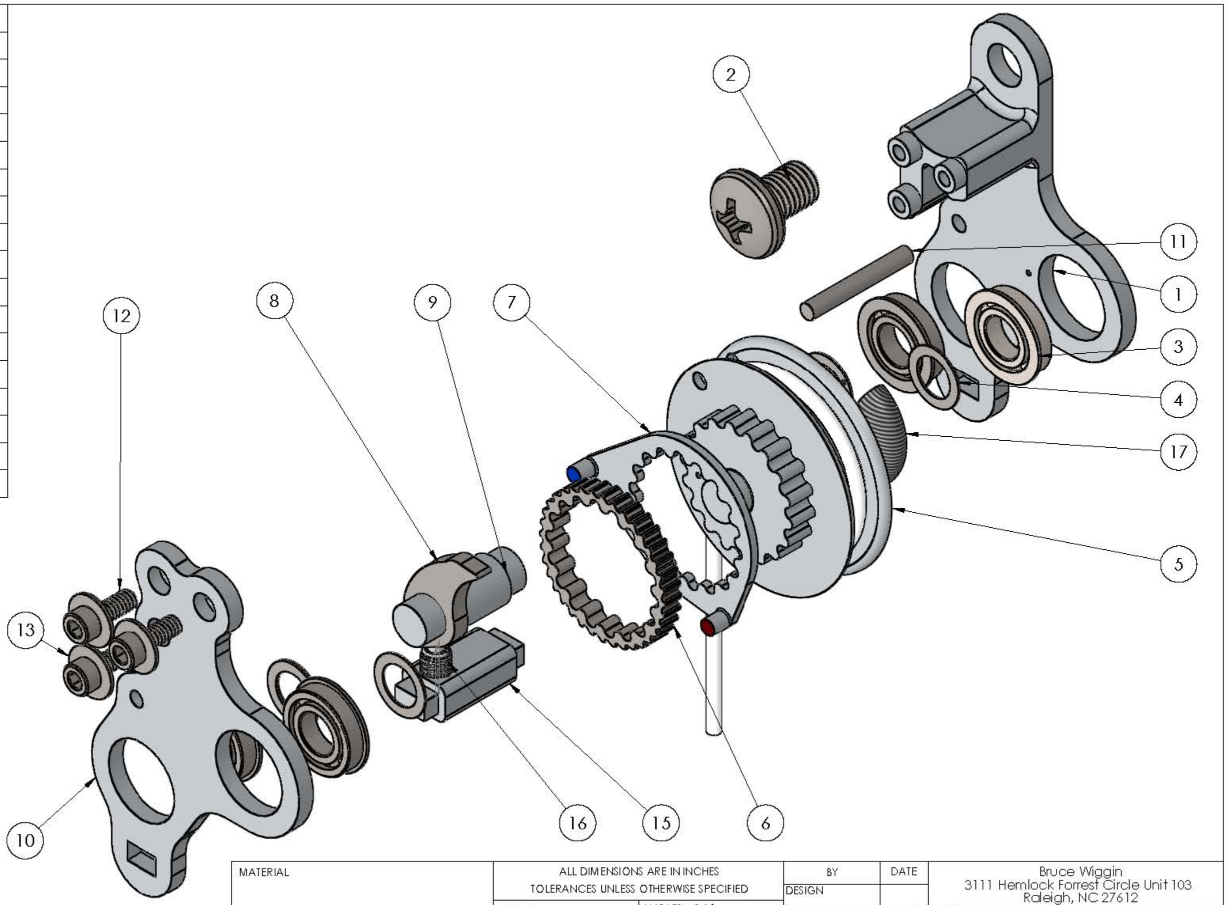

THIRD ANGLE PROJECTION

336-471-1934
mbwiggin@ncsu.edu

MATERIAL	ALL DIMENSIONS ARE IN INCHES TOLERANCES UNLESS OTHERWISE SPECIFIED XX ± .01 XXX ± .005 ANGLES ± 0.1° BEND RADII	BY	DATE	Bruce Wiggin 3111 Hemlock Forrest Circle Unit 103 Raleigh, NC 27612
		DESIGN		
		DRAWN		TITLE Mechanical Clutch Bill of Materials
FINISH	NO BURRS OR SHARP EDGES. ALL EDGES TO BE BROKEN .015 MIN. UNLESS OTHERWISE SPECIFIED.	CHKD		SIZE B
		APPD		DRAWING NO.
		CLASS CODE		SCALE Do Not Scale | SHEET 1 OF 1 | REV.

LT102

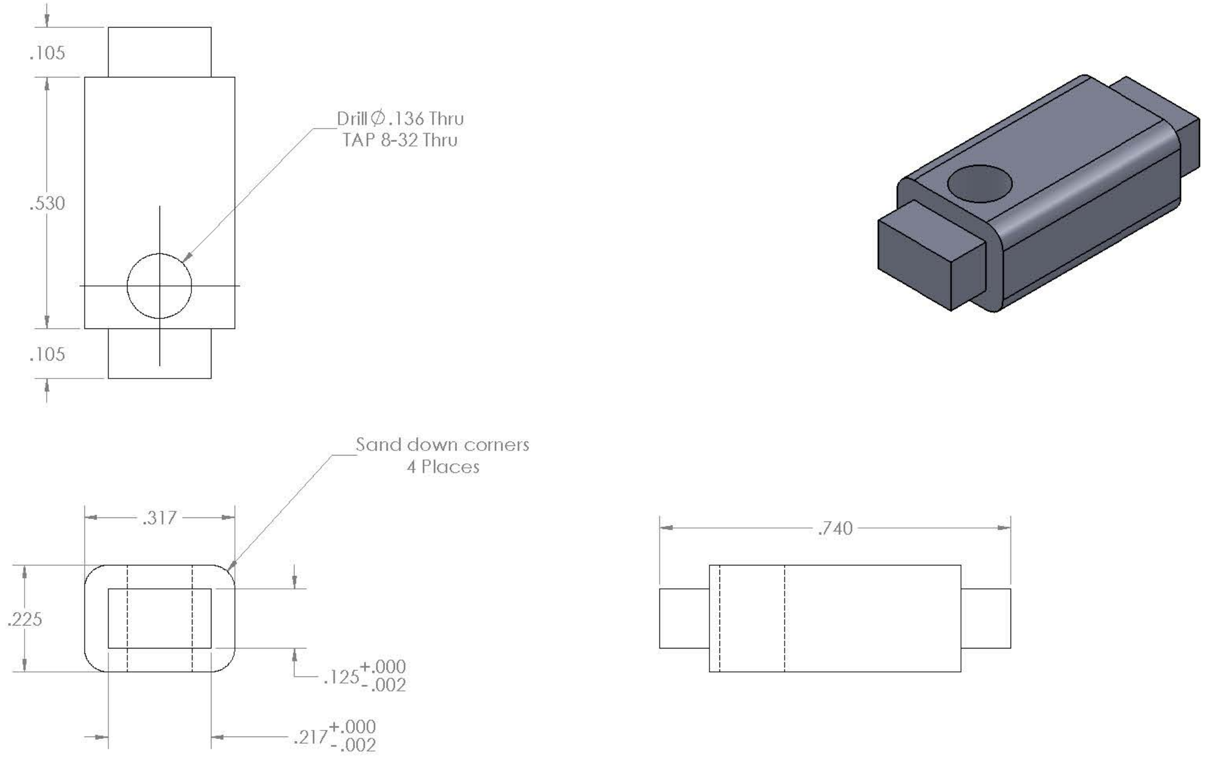
.105
.530
.105
Drill ∅ .136 Thru
TAP 8-32 Thru
Sand down corners
4 Places
.317
.225
.125 +.000 -.002
.217 +.000 -.002
.740

MATERIAL 7075-T6 Al	ALL DIMENSIONS ARE IN INCHES TOLERANCES UNLESS OTHERWISE SPECIFIED XX ± .01 XXX ± .005 ANGLES ± 0.1° BEND RADII	BY	DATE	Bruce Wiggin 3111 Hemlock Forrest Circle Unit 103 Raleigh, NC 27612
		DESIGN		TITLE Detent Holder
FINISH	NO BURRS OR SHARP EDGES. ALL EDGES TO BE BROKEN .015 MIN. UNLESS OTHERWISE SPECIFIED.	DRAWN CHKD APPD		SIZE B DRAWING NO.
		CLASS CODE		SCALE Do Not Scale SHEET 1 OF 1 REV.

THIRD ANGLE PROJECTION

336-471-1934
mbwiggin@ncsu.edu

LT102

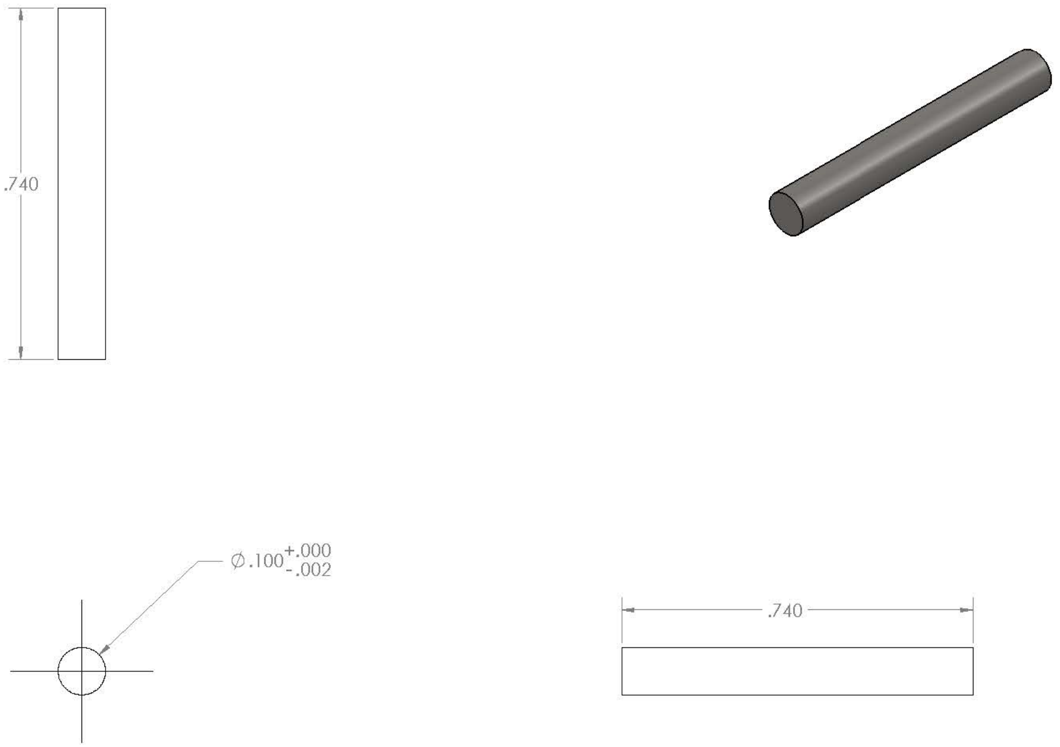

MATERIAL

302 or 304 SST

FINISH

ALL DIMENSIONS ARE IN INCHES
TOLERANCES UNLESS OTHERWISE SPECIFIED

XX ± .01
XXX ± .005

ANGLES ± 0.1°
BEND RADII

NO BURRS OR SHARP EDGES.
ALL EDGES TO BE BROKEN .015 MIN.
UNLESS OTHERWISE SPECIFIED.

	BY	DATE
DESIGN		
DRAWN		
CHKD		
APPD		
CLASS CODE		

Bruce Wiggin
3111 Hemlock Forrest Circle Unit 103
Raleigh, NC 27612

TITLE
Pawl Backstop Pin

SIZE B

DRAWING NO.

SCALE Do Not Scale

SHEET 1 OF 1

REV.

THIRD ANGLE PROJECTION

336-471-1934
mbwiggin@ncsu.edu

LT102

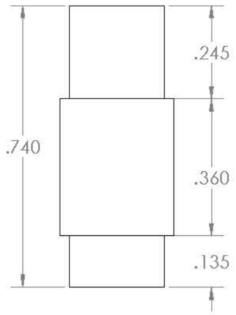

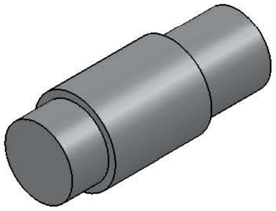

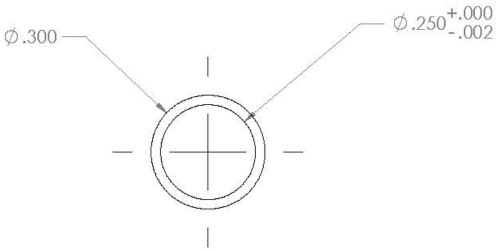

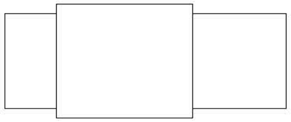

MATERIAL
7075-T6 Aluminum

FINISH

ALL DIMENSIONS ARE IN INCHES
TOLERANCES UNLESS OTHERWISE SPECIFIED
XX ± .01
XXX ± .005
ANGLES ± 0.1°
BEND RADII

NO BURRS OR SHARP EDGES.
ALL EDGES TO BE BROKEN .015 MIN.
UNLESS OTHERWISE SPECIFIED.

	BY	DATE
DESIGN		
DRAWN		
CHKD		
APPD		
CLASS CODE		

Bruce Wiggin
3111 Hemlock Forrest Circle Unit 103
Raleigh, NC 27612

TITLE
Pawl Shaft

SIZE
B
DRAWING NO.

SCALE
Do Not Scale
SHEET 1 OF 1
REV.

THIRD ANGLE PROJECTION

336-471-1934
mbwiggin@ncsu.edu

LT102

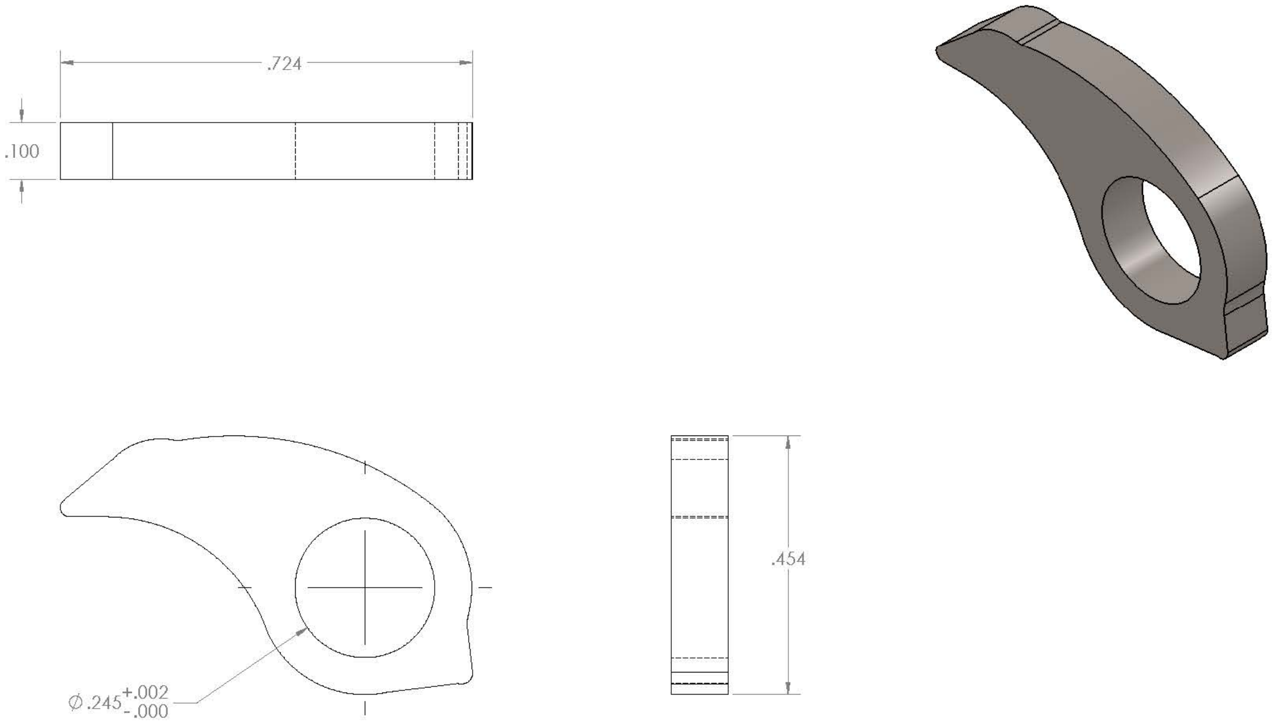

THIRD ANGLE PROJECTION

336-471-1934
mbwiggin@ncsu.edu

MATERIAL
17-4 PH stainless steel

FINISH

ALL DIMENSIONS ARE IN INCHES
TOLERANCES UNLESS OTHERWISE SPECIFIED
XX ± .01
XXX ± .005
ANGLES ± 0.1°
BEND RADII

NO BURRS OR SHARP EDGES.
ALL EDGES TO BE BROKEN .015 MIN.
UNLESS OTHERWISE SPECIFIED.

BY	DATE
DESIGN	
DRAWN	
CHKD	
APPD	
CLASS CODE	

Bruce Wiggin
3111 Hemlock Forrest Circle Unit 103
Raleigh, NC 27612

TITLE
Pawl

SIZE B
DRAWING NO.

SCALE Do Not Scale
SHEET 1 OF 1
REV.

LT102

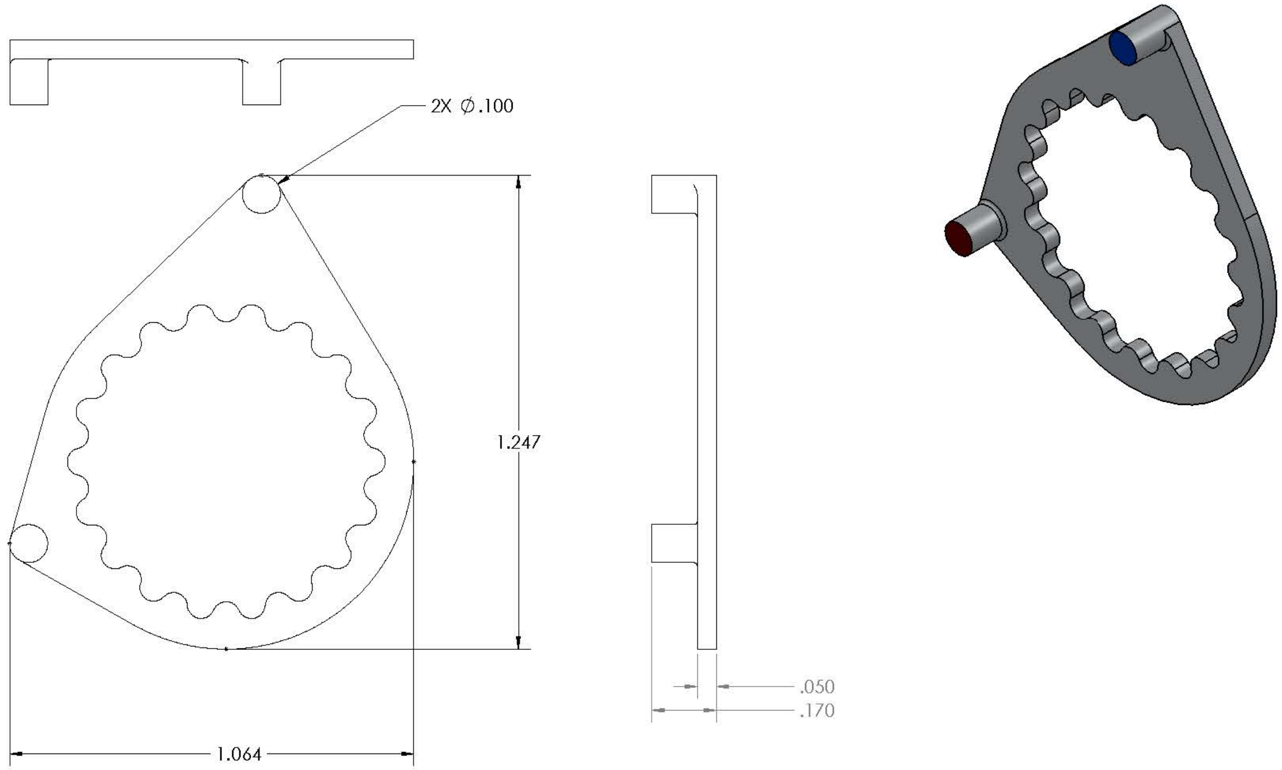

MATERIAL

7075-T6 Aluminum

FINISH

ALL DIMENSIONS ARE IN INCHES
TOLERANCES UNLESS OTHERWISE SPECIFIED
XX ± .01
XXX ± .005
ANGLES ± 0.1°
BEND RADII

NO BURRS OR SHARP EDGES.
ALL EDGES TO BE BROKEN .015 MIN.
UNLESS OTHERWISE SPECIFIED.

	BY	DATE
DESIGN		
DRAWN		
CHKD		
APPD		
CLASS CODE		

Bruce Wiggin
3111 Hemlock Forrest Circle Unit 103
Raleigh, NC 27612

TITLE
Pin Popper

SIZE B
DRAWING NO.

SCALE Do Not Scale
SHEET 1 OF 1
REV.

THIRD ANGLE PROJECTION

336-471-1934
mbwiggin@ncsu.edu

LT102

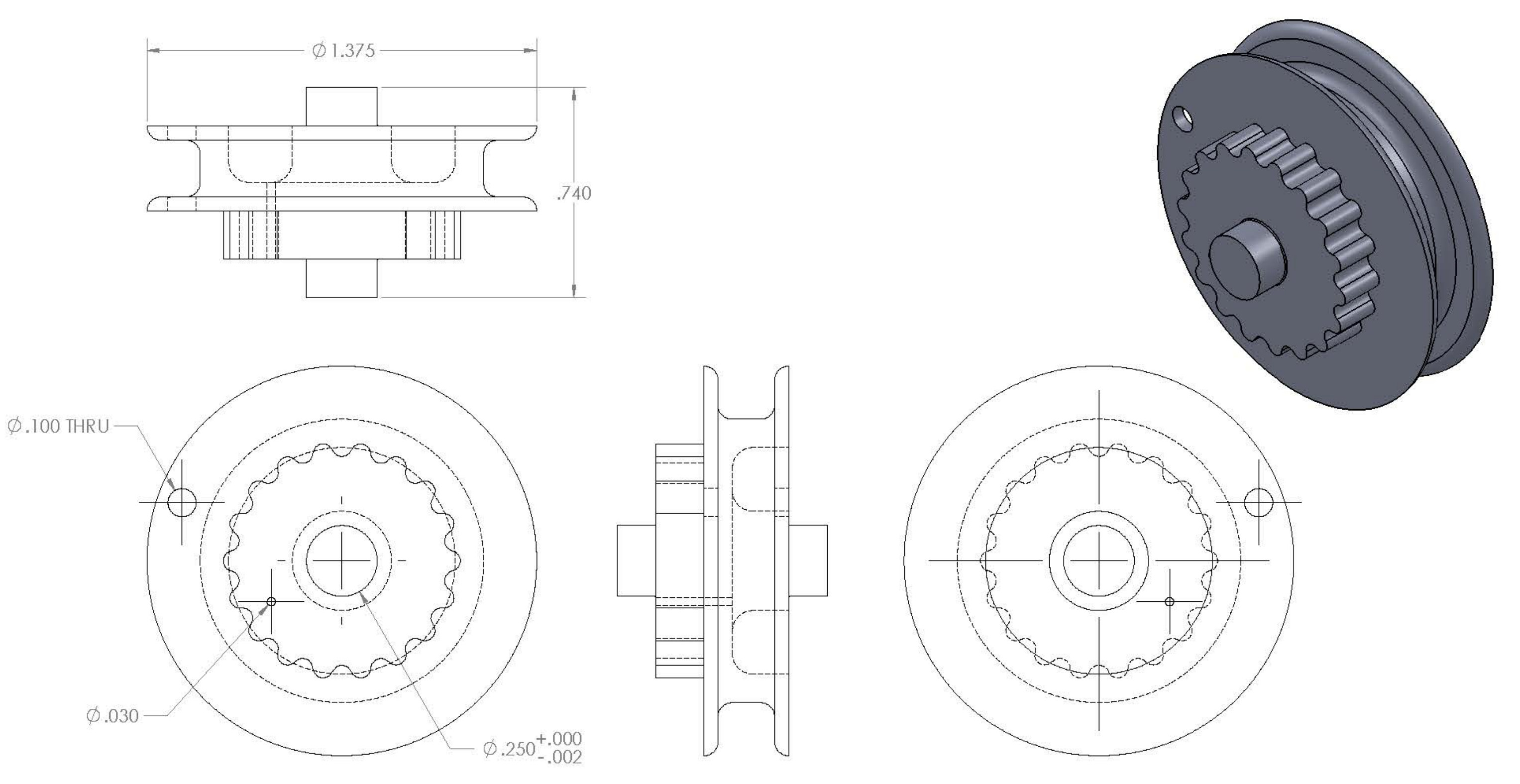

THIRD ANGLE PROJECTION

336-471-1934
mbwiggin@ncsu.edu

MATERIAL
7075-T6 Aluminum

FINISH

ALL DIMENSIONS ARE IN INCHES
TOLERANCES UNLESS OTHERWISE SPECIFIED
XX ± .01
XXX ± .005
ANGLES ± 0.1°
BEND RADII

NO BURRS OR SHARP EDGES.
ALL EDGES TO BE BROKEN .015 MIN.
UNLESS OTHERWISE SPECIFIED.

BY	DATE
DESIGN	
DRAWN	
CHKD	
APPD	
CLASS CODE	

Bruce Wiggin
3111 Hemlock Forrest Circle Unit 103
Raleigh, NC 27612

TITLE Pulley

SIZE B
DRAWING NO.

SCALE Do Not Scale
SHEET 1 OF 1
REV.

LT102

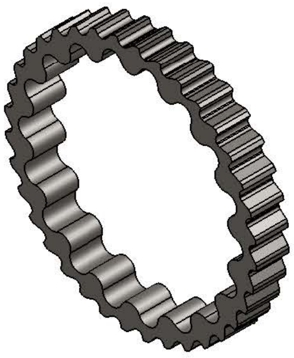

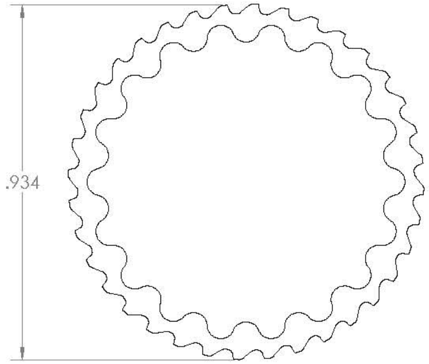

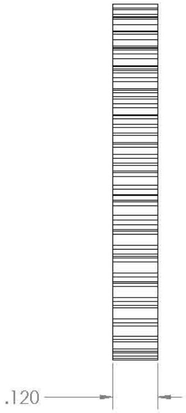

Suggested fabrication method: water-jet or laser cutting

THIRD ANGLE PROJECTION

336-471-1934
mbwiggin@ncsu.edu

MATERIAL
17-4 PH stainless steel

FINISH

ALL DIMENSIONS ARE IN INCHES
TOLERANCES UNLESS OTHERWISE SPECIFIED
XX ± .01
XXX ± .005
ANGLES ± 0.1°
BEND RADII

NO BURRS OR SHARP EDGES.
ALL EDGES TO BE BROKEN .015 MIN.
UNLESS OTHERWISE SPECIFIED.

BY
DATE
DESIGN
DRAWN
CHKD
APPD
CLASS CODE

Bruce Wiggin
3111 Hemlock Forrest Circle Unit 103
Raleigh, NC 27612

TITLE
Ratchet Face

SIZE
B
DRAWING NO.

SCALE
Do Not Scale
SHEET 1 OF 1
REV.

LT102

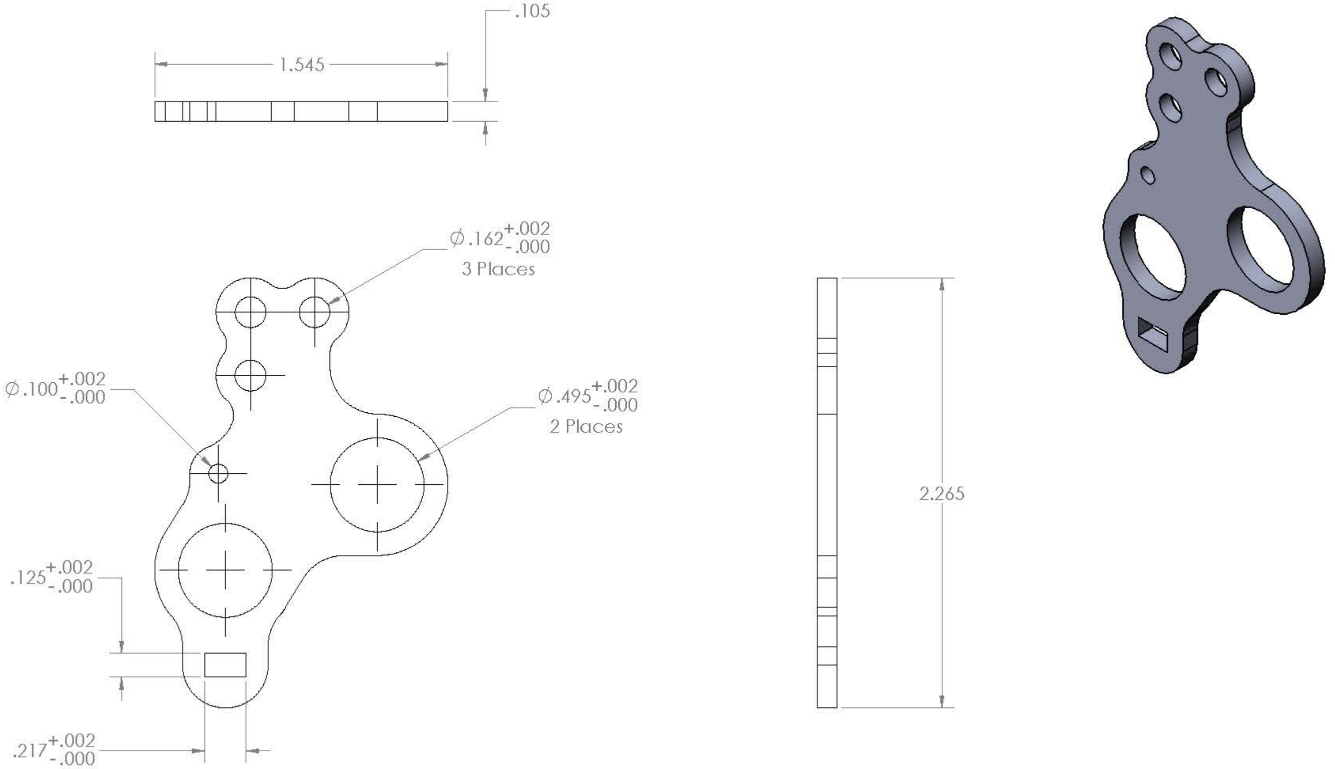

.105
1.545
$\varnothing .162^{+.002}_{-.000}$
3 Places
$\varnothing .100^{+.002}_{-.000}$
$\varnothing .495^{+.002}_{-.000}$
2 Places
2.265
$.125^{+.002}_{-.000}$
$.217^{+.002}_{-.000}$

MATERIAL

7075-T6 Aluminum

FINISH

ALL DIMENSIONS ARE IN INCHES
TOLERANCES UNLESS OTHERWISE SPECIFIED
XX ± .01
XXX ± .005
ANGLES ± 0.1°
BEND RADII

NO BURRS OR SHARP EDGES.
ALL EDGES TO BE BROKEN .015 MIN.
UNLESS OTHERWISE SPECIFIED.

	BY	DATE
DESIGN		
DRAWN		
CHKD		
APPD		
CLASS CODE		

Bruce Wiggin
3111 Hemlock Forrest Circle Unit 103
Raleigh, NC 27612

TITLE
Support Plate Flat

SIZE B
DRAWING NO.

SCALE Do Not Scale
SHEET 1 OF 1
REV.

THIRD ANGLE PROJECTION

336-471-1934
mbwiggin@ncsu.edu

LT102

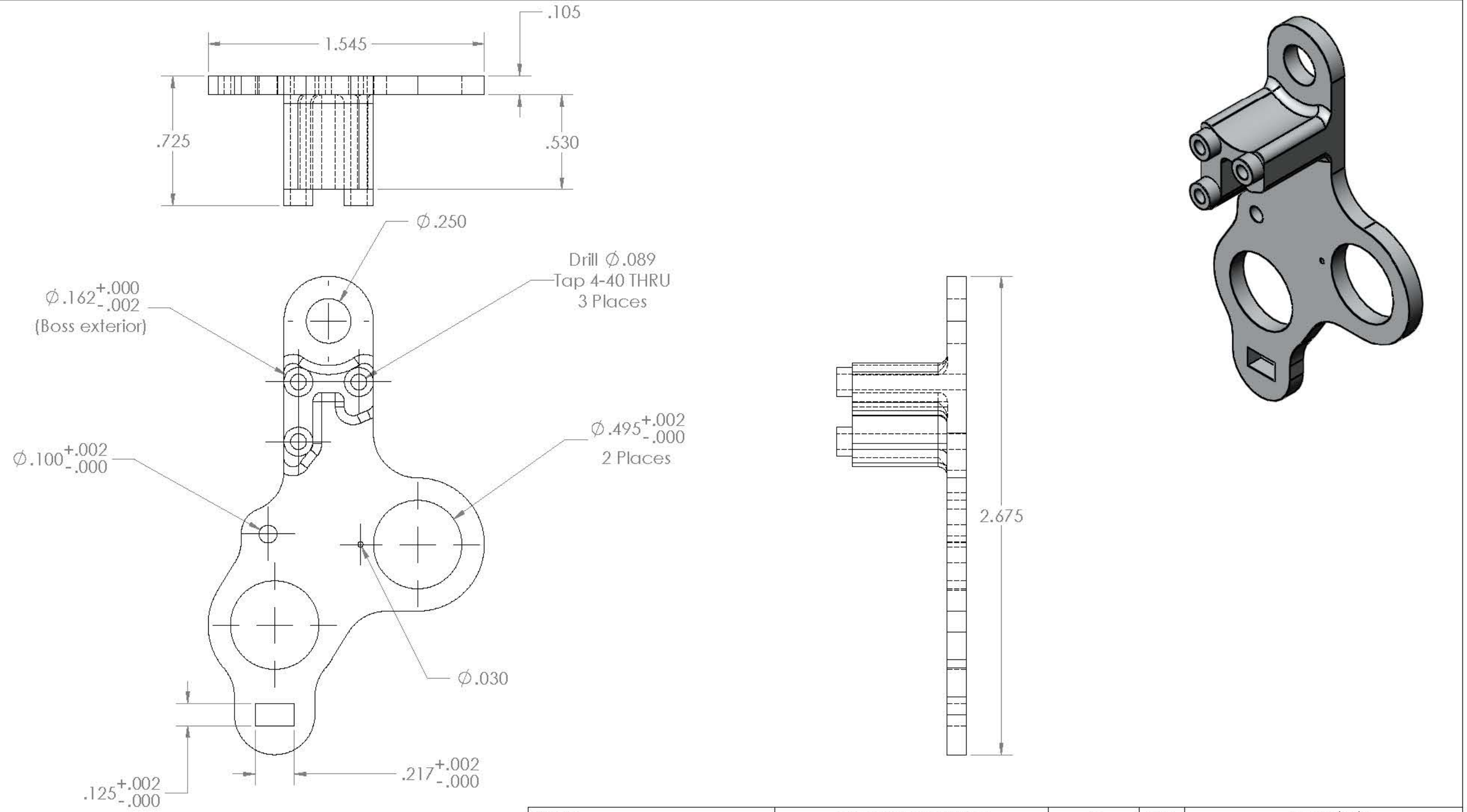
.105
1.545
.725
.530
Ø.250
Drill Ø.089
Tap 4-40 THRU
3 Places
Ø.162 +.000 -.002
(Boss exterior)
Ø.495 +.002 -.000
2 Places
Ø.100 +.002 -.000
2.675
Ø.030
.217 +.002 -.000
.125 +.002 -.000

MATERIAL **7075-T6 Aluminum**	ALL DIMENSIONS ARE IN INCHES TOLERANCES UNLESS OTHERWISE SPECIFIED XX ± .01 XXX ± .005 ANGLES ± 0.1° BEND RADII	BY	DATE	Bruce Wiggin 3111 Hemlock Forrest Circle Unit 103 Raleigh, NC 27612
		DESIGN		TITLE Support Plate
		DRAWN		
FINISH	NO BURRS OR SHARP EDGES. ALL EDGES TO BE BROKEN .015 MIN. UNLESS OTHERWISE SPECIFIED.	CHKD		SIZE B DRAWING NO.
		APPD		
		CLASS CODE		SCALE Do Not Scale SHEET 1 OF 1 REV.

THIRD ANGLE PROJECTION

336-471-1934
mbwiggin@ncsu.edu

LT102

Appendix B

Electromechanical Clutch Drawings

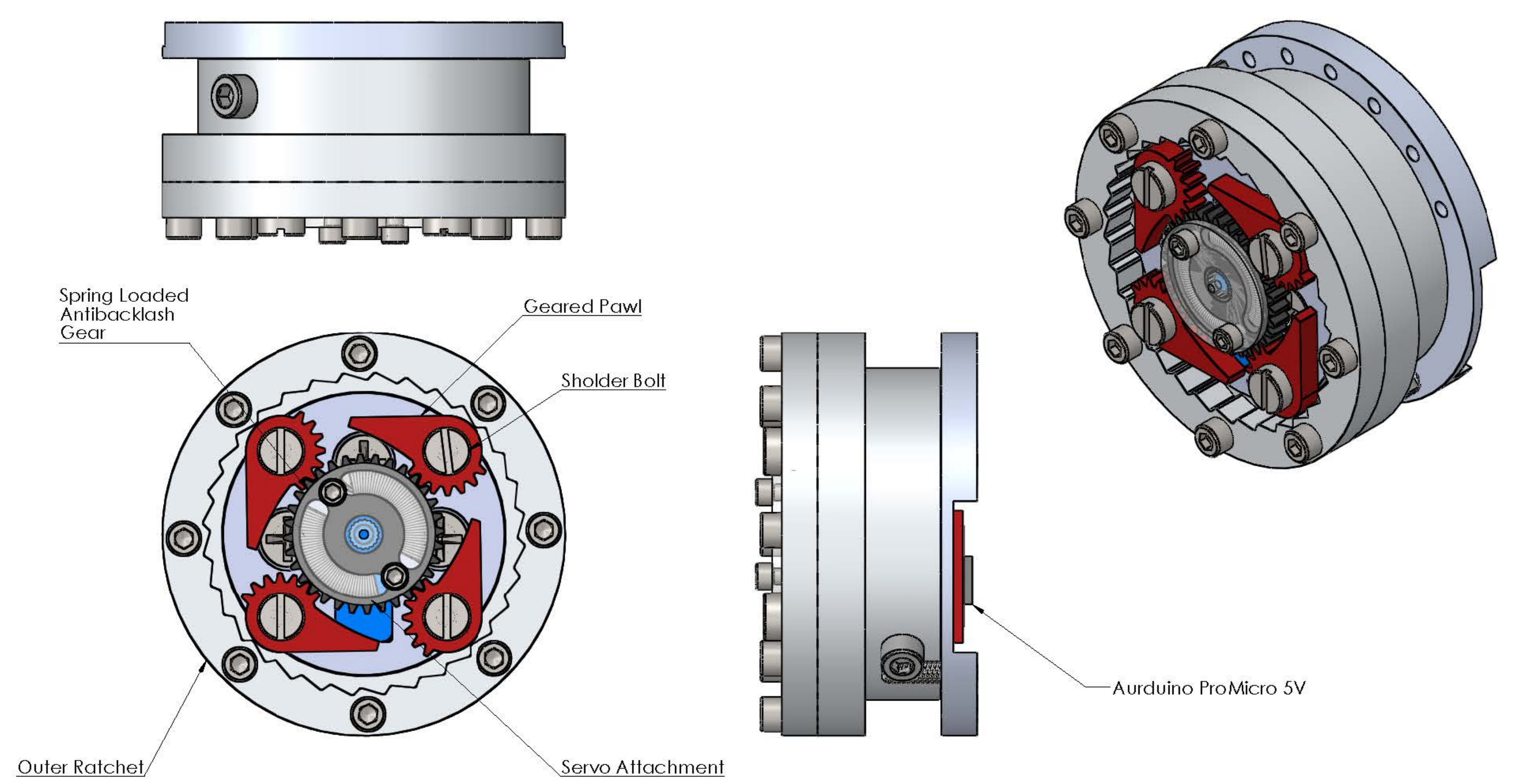
Spring Loaded Antibacklash Gear
Geared Pawl
Sholder Bolt
Outer Ratchet
Servo Attachment
Aurduino ProMicro 5V

MATERIAL

FINISH

ALL DIMENSIONS ARE IN INCHES
TOLERANCES UNLESS OTHERWISE SPECIFIED
XX ± .01
XXX ± .005
ANGLES ± 0.1°
BEND RADII

NO BURRS OR SHARP EDGES.
ALL EDGES TO BE BROKEN .015 MIN.
UNLESS OTHERWISE SPECIFIED.

	BY	DATE
DESIGN		
DRAWN		
CHKD		
APPD		
CLASS CODE		

Bruce Wiggin
3111 Hemlock Forrest Circle Unit 103
Raleigh, NC 27612

TITLE
Electromechanical Clutch

SIZE
B
DRAWING NO.

SCALE
Do Not Scale
SHEET 1 OF 1
REV.

THIRD ANGLE PROJECTION

336-471-1934
mbwiggin@ncsu.edu

LT102

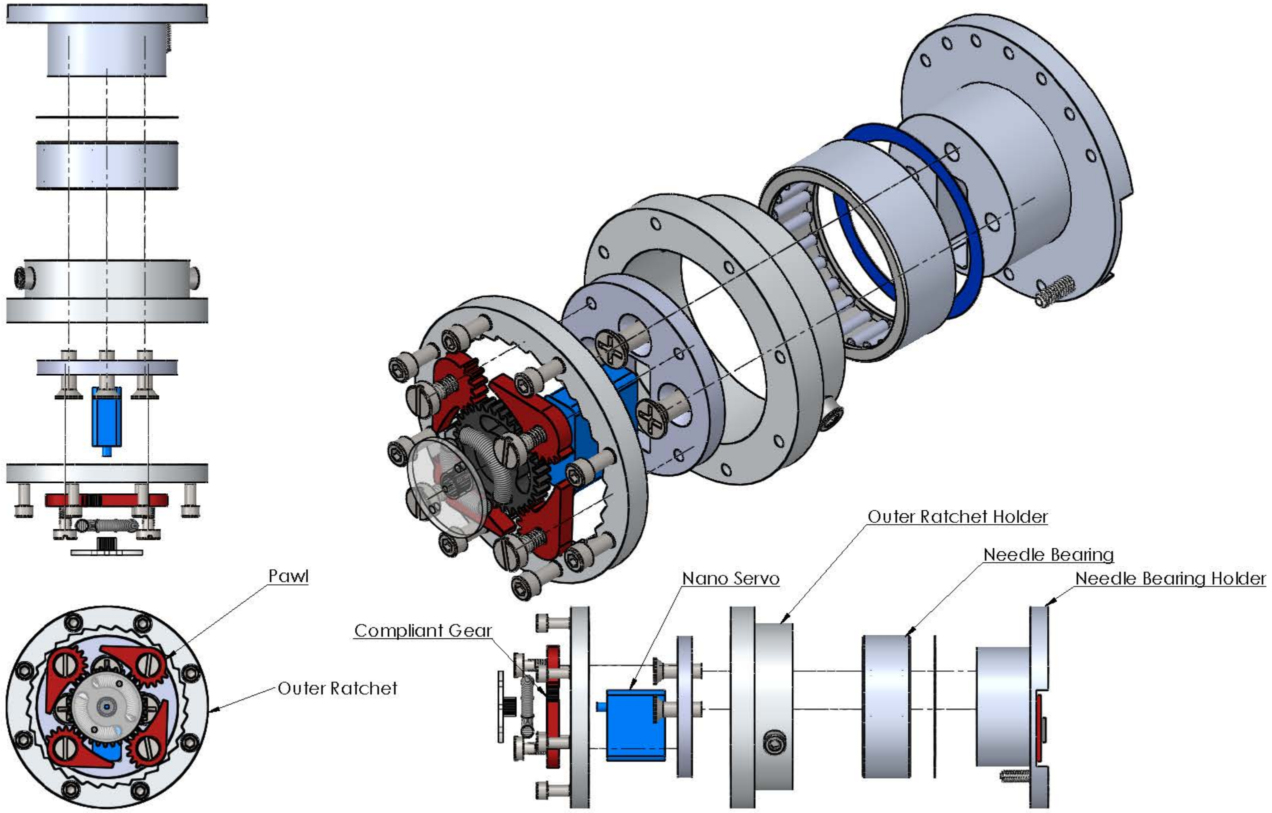
Pawl
Outer Ratchet
Compliant Gear
Nano Servo
Outer Ratchet Holder
Needle Bearing
Needle Bearing Holder

MATERIAL

FINISH

ALL DIMENSIONS ARE IN INCHES
TOLERANCES UNLESS OTHERWISE SPECIFIED
XX ± .01
XXX ± .005
ANGLES ± 0.1°
BEND RADII

NO BURRS OR SHARP EDGES.
ALL EDGES TO BE BROKEN .015 MIN.
UNLESS OTHERWISE SPECIFIED.

	BY	DATE
DESIGN		
DRAWN		
CHKD		
APPD		
CLASS CODE		

Bruce Wiggin
3111 Hemlock Forrest Circle Unit 103
Raleigh, NC 27612

TITLE
Electromechanical Clutch

SIZE B
DRAWING NO.
SCALE Do Not Scale
SHEET 1 OF 2
REV.

THIRD ANGLE PROJECTION

336-471-1934
mbwiggin@ncsu.edu

LT102

ITEM NO.	PART NUMBER	DESCRIPTION	QTY.
1	Servo Motor	HITEC HS-5035HD	1
2	Servo Attachment	WHEN TURNED APPLIES FORCE TO (17) OR (3) BASED ON DIRECTION	1
3	AntiBacklashGear	ALLOWS COMPLIANT OR DIRECT TORQ BASED OFF DIR OF ROT	1
4	Pawl	ALLOWS UNI-DIR ROT WHEN ENGAGED	4
5	Pawl Holder	COUPLES TORQ FROM (4) TO (8)	1
6	MMC 99154A330	McMaster 99154A330	4
7	MMC 5905K29	STANDARD BEARING PRESS FIT TO (9) MCMASTER 5905K29	1
8	Needle Bearing Holder	BACK MOUNTING PLATE AND KEY ATTACHMENT POINT	1
9	Outer Ratchet Holder	PRESS FIT TO (7)	1
10	Outer Ratchet	COUPLES EXTERNAL FORCES TO (4) WHEN ENGAGED AND TURNED IN LOCKING DIR	1
11	CR-FHMS 0.164-32x0.5x0.5-N		3
12	Arduino Promicro5v	5v MICRO CONTROLLER TO DRIVE (1)	1
13	HX-SHCS 0.112-40x0.25x0.25-N		8
14	MMC 98090A635		1
15	MMC 92313A109		1
16	GearSpring	McMaster 9657K282	2

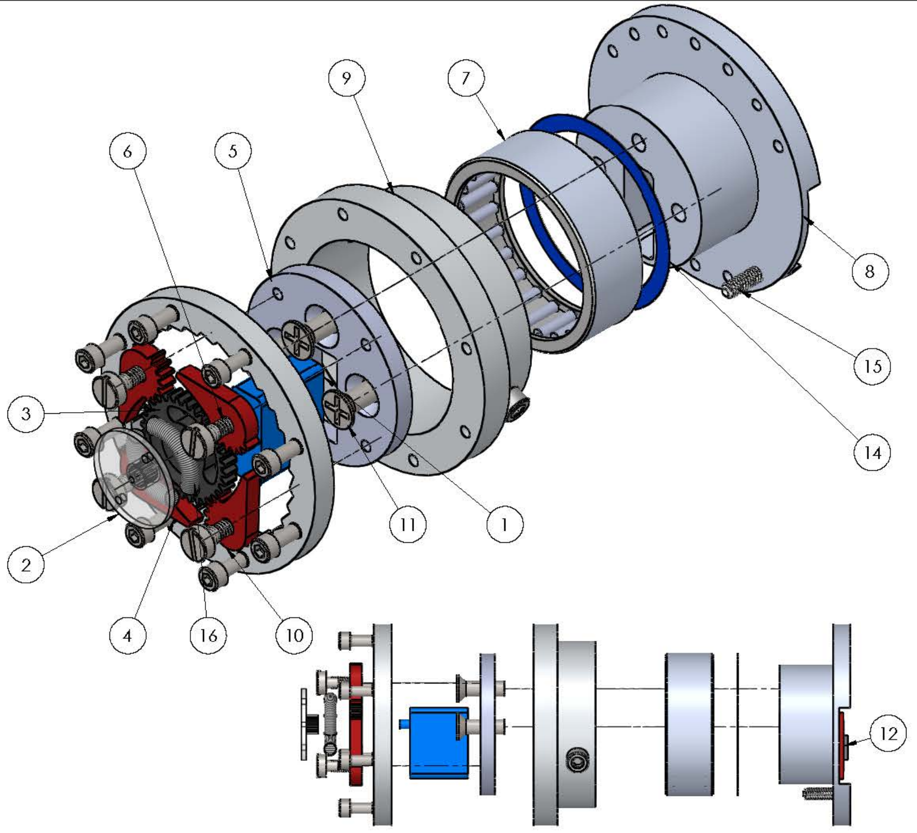

MATERIAL	ALL DIMENSIONS ARE IN INCHES TOLERANCES UNLESS OTHERWISE SPECIFIED	BY	DATE	Bruce Wiggin 3111 Hemlock Forrest Circle Unit 103 Raleigh, NC 27612
	XX ± .01 XXX ± .005 | ANGLES ± 0.1° BEND RADII	DESIGN		
		DRAWN		TITLE Electromechanical Clutch
FINISH	NO BURRS OR SHARP EDGES. ALL EDGES TO BE BROKEN .015 MIN. UNLESS OTHERWISE SPECIFIED.	CHKD		SIZE B | DRAWING NO.
		APPD		
		CLASS CODE		SCALE Do Not Scale | SHEET 2 OF 2 | REV.

THIRD ANGLE PROJECTION

336-471-1934
mbwiggin@ncsu.edu

LT102

DRAWING NO.

REV/ECN LEVEL	CHANGE DESCRIPTION	BY:	DATE

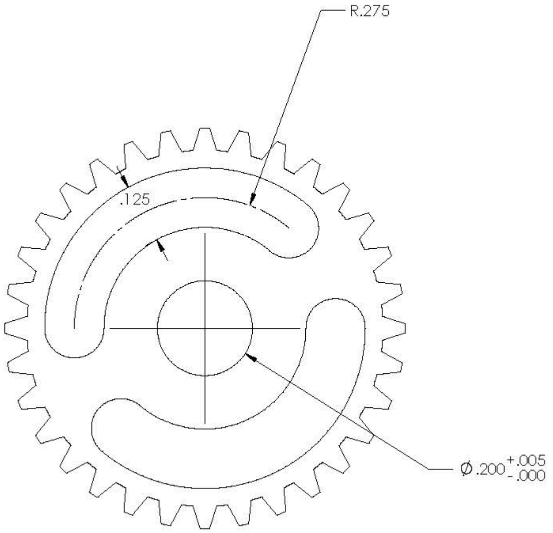

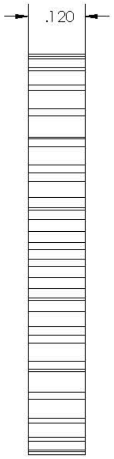

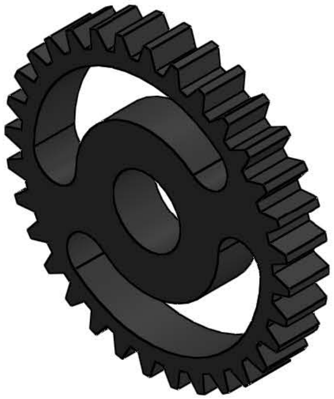

THIRD ANGLE PROJECTION

336-471-1934
mbwiggin@ncsu.edu

MATERIAL 6061 Al	ALL DIMENSIONS ARE IN INCHES TOLERANCES UNLESS OTHERWISE SPECIFIED XX ± .01 / XXX ± .005 ANGLES ± 1° / BEND RADII	BY	DATE	Bruce Wiggin 3111 Hemlock Forrest Circle Unit 103 Raleigh, NC 27612
		DESIGN		
		DRAWN		TITLE Anti Backlash Gear
FINISH	NO BURRS OR SHARP EDGES. ALL EDGES TO BE BROKEN .015 MIN. UNLESS OTHERWISE SPECIFIED.	CHKD		SIZE B | DRAWING NO.
		APPD		
		CLASS CODE		SCALE 1/1 | SHEET 1 OF 1 | REV.

LT102

DRAWING NO.

REV/ECN LEVEL	CHANGE DESCRIPTION	BY:	DATE

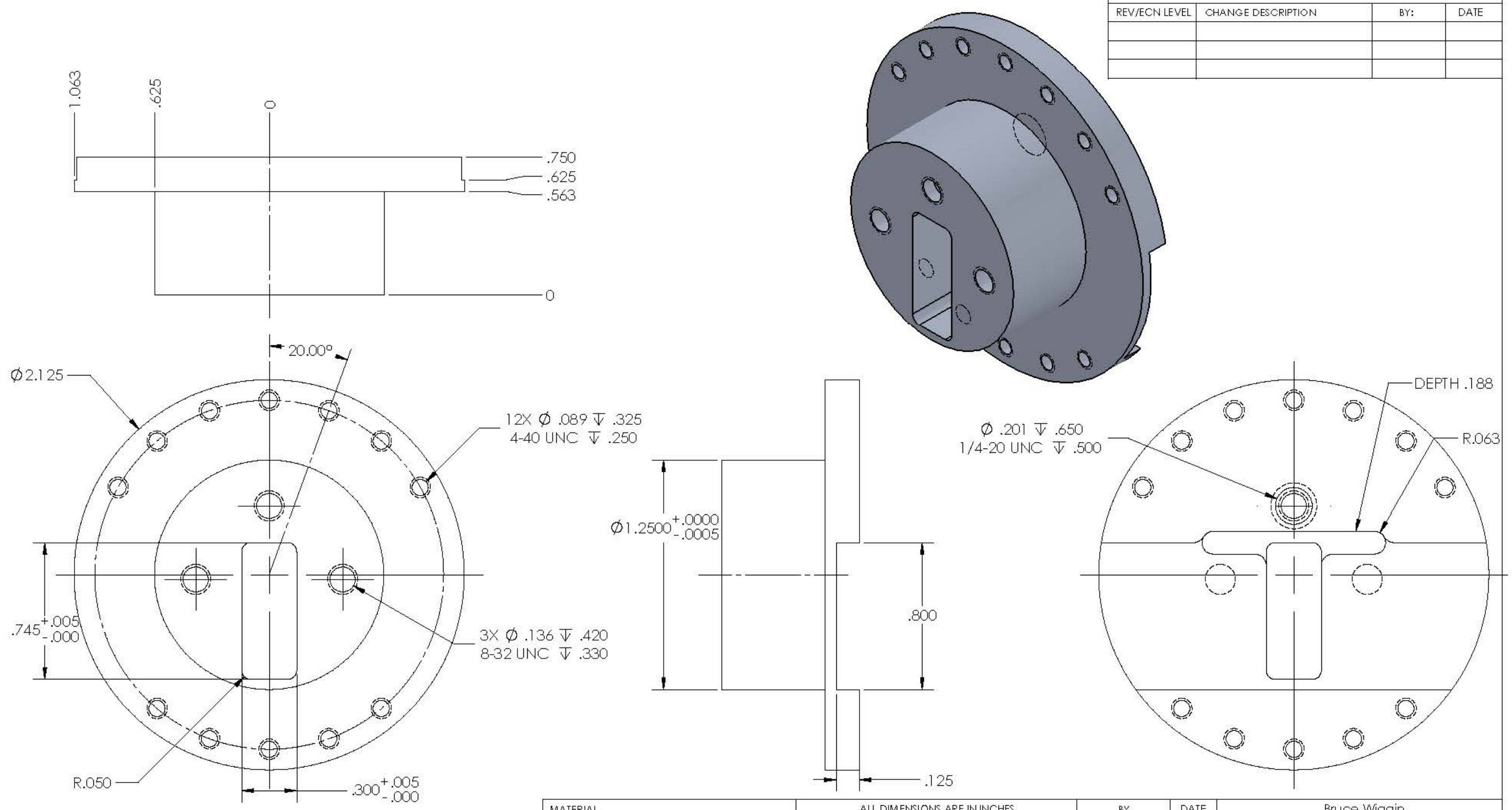

1.063
.625
0
.750
.625
.563
0
20.00°
Ø2.125
12X Ø .089 ⊽ .325
4-40 UNC ⊽ .250
.745 +.005 -.000
3X Ø .136 ⊽ .420
8-32 UNC ⊽ .330
R.050
.300 +.005 -.000
Ø1.2500 +.0000 -.0005
.800
.125
Ø .201 ⊽ .650
1/4-20 UNC ⊽ .500
DEPTH .188
R.063

THIRD ANGLE PROJECTION

336-471-1934
mbwiggin@ncsu.edu

MATERIAL

6061 Al

FINISH

ALL DIMENSIONS ARE IN INCHES
TOLERANCES UNLESS OTHERWISE SPECIFIED
XX ± .01
XXX ± .005
ANGLES ± 1°
BEND RADII

NO BURRS OR SHARP EDGES.
ALL EDGES TO BE BROKEN .015 MIN.
UNLESS OTHERWISE SPECIFIED.

	BY	DATE
DESIGN		
DRAWN		
CHKD		
APPD		
CLASS CODE		

Bruce Wiggin
3111 Hemlock Forrest Circle Unit 103
Raleigh, NC 27612

TITLE
Needle Bearing Holder

SIZE B
DRAWING NO.

SCALE 1/1 SHEET 1 OF 1 REV.

LT102

DRAWING NO.			
REV/ECN LEVEL	CHANGE DESCRIPTION	BY:	DATE

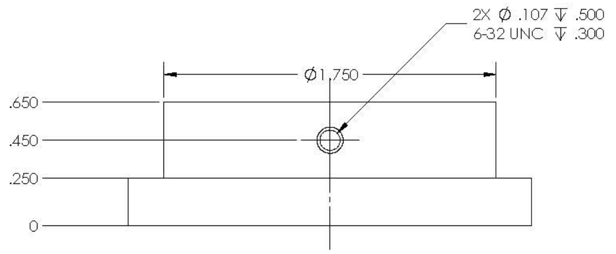
2X Ø .107 ↧ .500
6-32 UNC ↧ .300
Ø1.750
.650
.450
.250
0

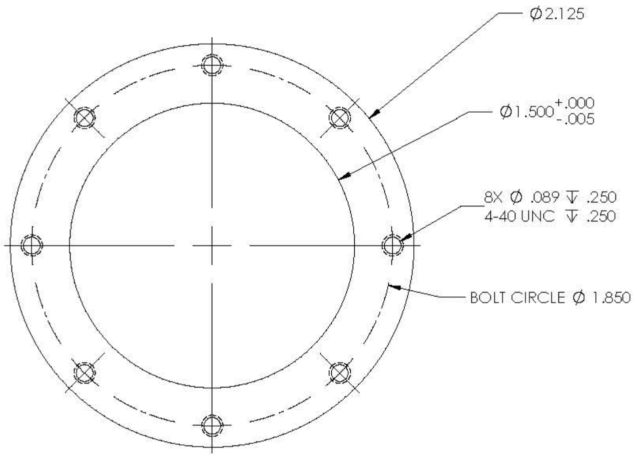
Ø2.125
Ø1.500 +.000 -.005
8X Ø .089 ↧ .250
4-40 UNC ↧ .250
BOLT CIRCLE Ø 1.850

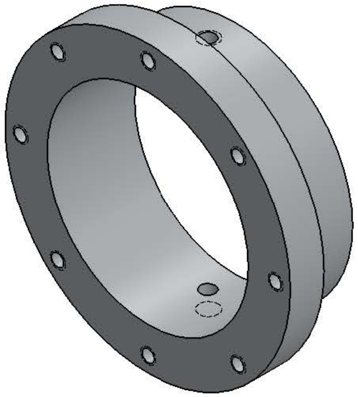

THIRD ANGLE PROJECTION

336-471-1934
mbwiggin@ncsu.edu

MATERIAL 6061 Al	ALL DIMENSIONS ARE IN INCHES TOLERANCES UNLESS OTHERWISE SPECIFIED XX ± .01 / XXX ± .005 ANGLES ± 1° / BEND RADII	BY	DATE	Bruce Wiggin 3111 Hemlock Forrest Circle Unit 103 Raleigh, NC 27612
		DESIGN		
		DRAWN		TITLE Outer Ratchet Holder
FINISH	NO BURRS OR SHARP EDGES. ALL EDGES TO BE BROKEN .015 MIN. UNLESS OTHERWISE SPECIFIED.	CHKD		SIZE B / DRAWING NO.
		APPD		
		CLASS CODE		SCALE 1/1 / SHEET 1 OF 1 / REV.

LT102

DRAWING NO.

REV/ECN LEVEL	CHANGE DESCRIPTION	BY:	DATE

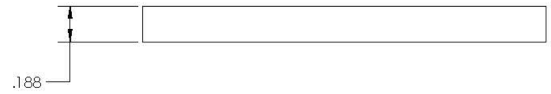

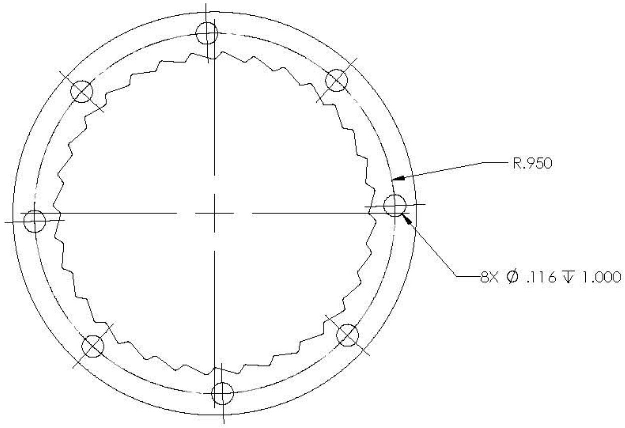

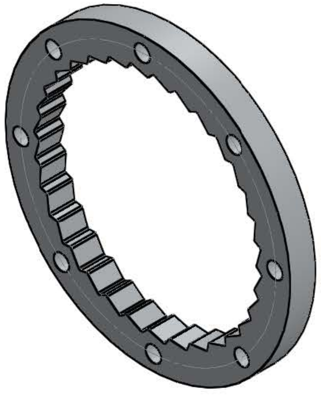

THIRD ANGLE PROJECTION

336-471-1934
mbwiggin@ncsu.edu

MATERIAL
6061 Al

FINISH

ALL DIMENSIONS ARE IN INCHES
TOLERANCES UNLESS OTHERWISE SPECIFIED
XX ± .01
XXX ± .005
ANGLES ± 1°
BEND RADII

NO BURRS OR SHARP EDGES.
ALL EDGES TO BE BROKEN .015 MIN.
UNLESS OTHERWISE SPECIFIED.

	BY	DATE
DESIGN		
DRAWN		
CHKD		
APPD		
CLASS CODE		

Bruce Wiggin
3111 Hemlock Forrest Circle Unit 103
Raleigh, NC 27612

TITLE
Outer Ratchet

SIZE B
DRAWING NO.

SCALE 1/1
SHEET 1 OF 1
REV.

LT102

DRAWING NO.

REV/ECN LEVEL	CHANGE DESCRIPTION	BY:	DATE

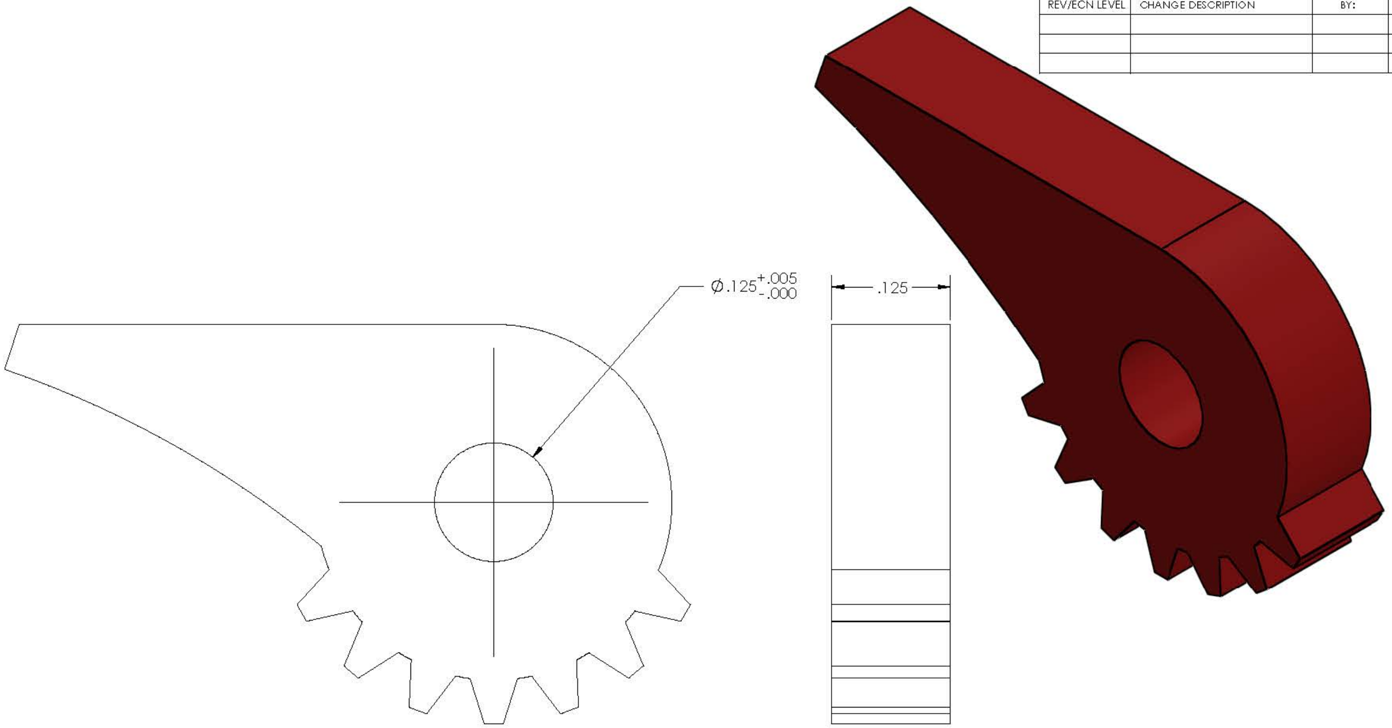

MATERIAL 6061 Al	ALL DIMENSIONS ARE IN INCHES TOLERANCES UNLESS OTHERWISE SPECIFIED XX ± .01 XXX ± .005 ANGLES ± 1° BEND RADII	BY	DATE	Bruce Wiggin 3111 Hemlock Forrest Circle Unit 103 Raleigh, NC 27612
		DESIGN		TITLE Pawl
FINISH	NO BURRS OR SHARP EDGES. ALL EDGES TO BE BROKEN .015 MIN. UNLESS OTHERWISE SPECIFIED.	DRAWN		SIZE B
		CHKD		DRAWING NO.
		APPD		SCALE 1/1
		CLASS CODE		SHEET 1 OF 1 REV.

THIRD ANGLE PROJECTION

336-471-1934
mbwiggin@ncsu.edu

LT102

DRAWING NO.

REV/ECN LEVEL	CHANGE DESCRIPTION	BY:	DATE

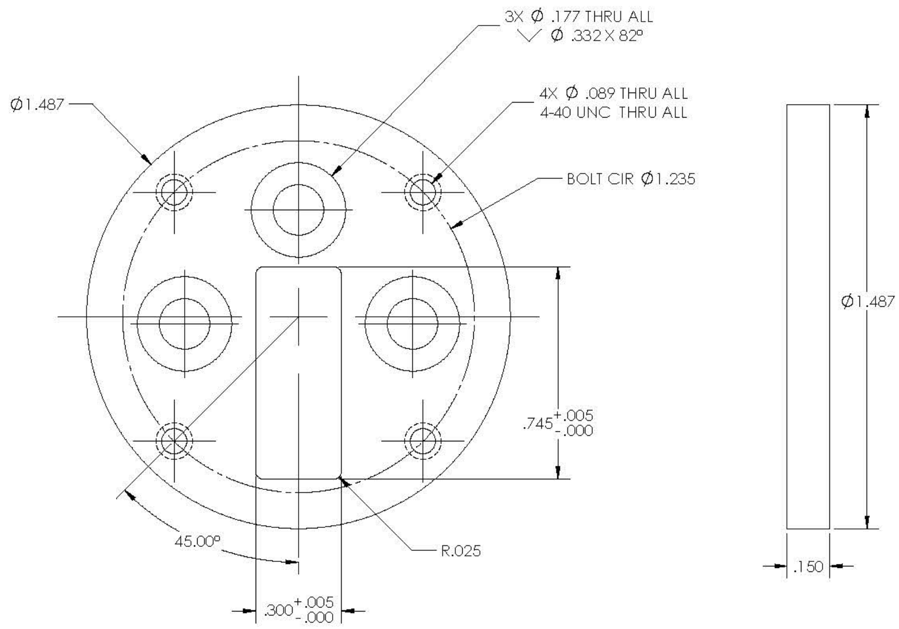

3X Ø .177 THRU ALL
⌵ Ø .332 X 82°
Ø1.487
4X Ø .089 THRU ALL
4-40 UNC THRU ALL
BOLT CIR Ø1.235
.745 +.005 -.000
45.00°
R.025
.300 +.005 -.000
Ø1.487
.150

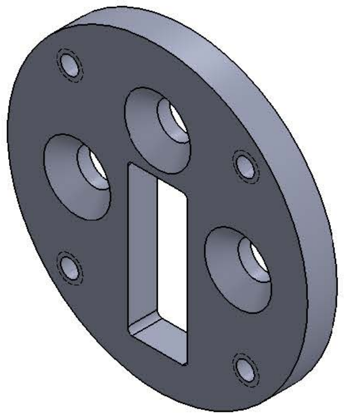

MATERIAL	6061 Al
FINISH	

ALL DIMENSIONS ARE IN INCHES
TOLERANCES UNLESS OTHERWISE SPECIFIED

XX ± .01 XXX ± .005	ANGLES ± 1° BEND RADII

NO BURRS OR SHARP EDGES.
ALL EDGES TO BE BROKEN .015 MIN.
UNLESS OTHERWISE SPECIFIED.

	BY	DATE
DESIGN		
DRAWN		
CHKD		
APPD		
CLASS CODE		

Bruce Wiggin
3111 Hemlock Forrest Circle Unit 103
Raleigh, NC 27612

TITLE Pawl Holder

SIZE	DRAWING NO.		
B			
SCALE 1/1	SHEET 1	OF 1	REV.

THIRD ANGLE PROJECTION

336-471-1934
mbwiggin@ncsu.edu

LT102

DRAWING NO.

REV/ECN LEVEL	CHANGE DESCRIPTION	BY:	DATE

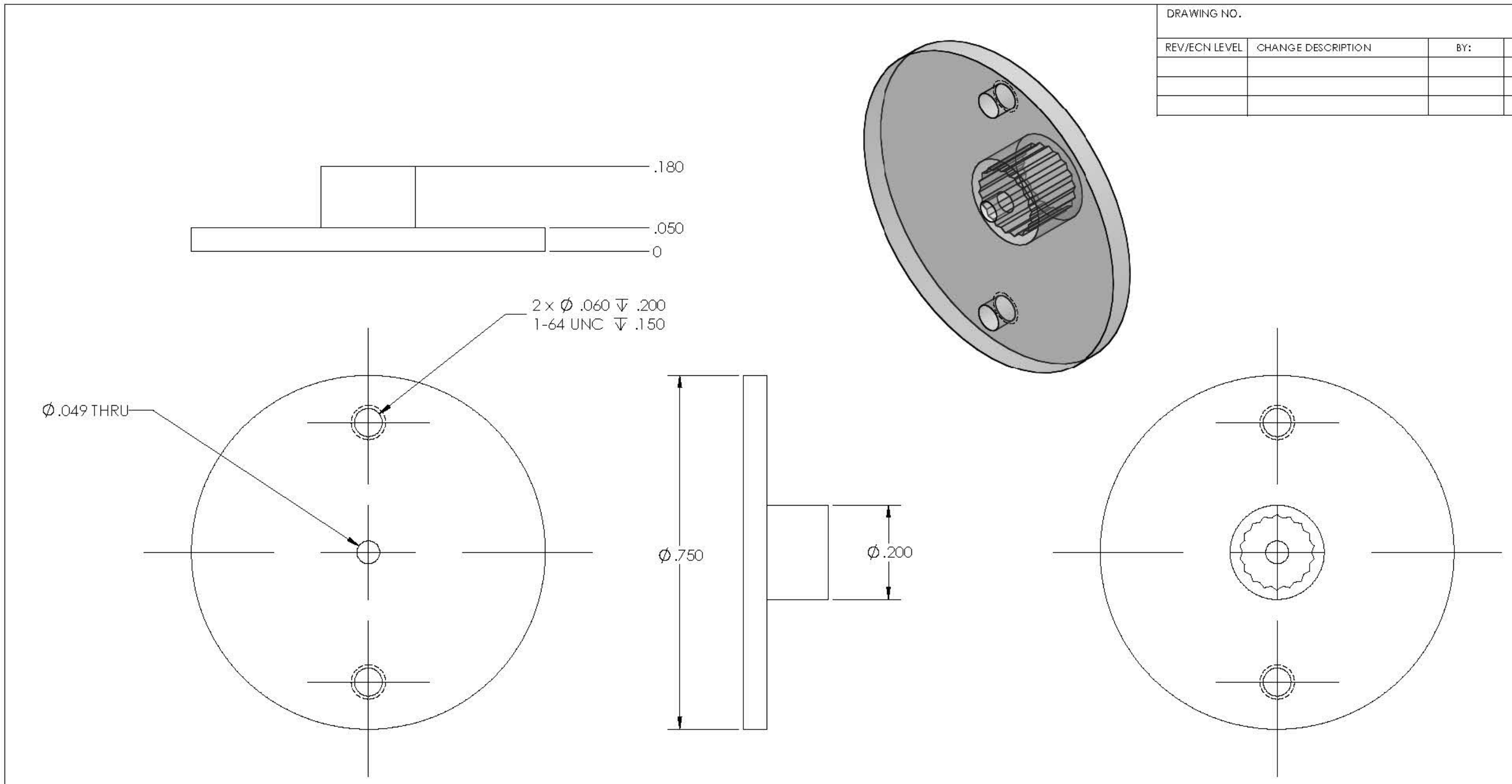

MATERIAL 6061 Al	ALL DIMENSIONS ARE IN INCHES TOLERANCES UNLESS OTHERWISE SPECIFIED XX ± .01 XXX ± .005 ANGLES ± 1° BEND RADII
FINISH	NO BURRS OR SHARP EDGES. ALL EDGES TO BE BROKEN .015 MIN. UNLESS OTHERWISE SPECIFIED.

BY	DATE
DESIGN	
DRAWN	
CHKD	
APPD	
CLASS CODE	

Bruce Wiggin
3111 Hemlock Forrest Circle Unit 103
Raleigh, NC 27612

TITLE Servo Attachment

SIZE B
DRAWING NO.
SCALE 1/1
SHEET 1 OF 1
REV.

THIRD ANGLE PROJECTION

336-471-1934
mbwiggin@ncsu.edu

LT102

Appendix C

Table C1: Regression equations for key outcome metrics vs. normalized spring stiffness during walking at 1.25 m/s.

Metric	Fit Order	Fit Equation	R2	p-value
Δ NetMetCost	1	Δ NetMetPow(W/kg) = -0.009075 - 2.3377815(Kns) + 8.3286823(Kns)^2	0.134	0.026
Exo Torque	2	ExoTorque(N-m/kg) = 0.0041179 + 0.9647767(Kns) - 1.9181047(Kns)^2	0.546	0.0001
Ank Bio Mom	1	AnkBioMom(N-m/kg) = 0.4374749 - 0.4100184(Kns)	0.167	0.002
Total Bio Mom	1	TotalBioMom(N-m/kg) = 0.818822 - 0.3595645(Kns)	0.114	0.015
Tot Ank +Pow	1	TotAnk+Pow(W/kg) = 0.2428553 - 0.2378337(Kns)	0.213	0.0005
Exo +Pow	2	Exo+Pow(W/kg) = 0.0049768 + 0.2750216(Kns) - 0.6998508(Kns)^2	0.202	0.003
Ank Bio +Pow	1	AnkBio+Pow(W/kg) = 0.2271446 - 0.2911921(Kns)	0.337	0.0001
Total Bio +Pow	1	TotBio+Pow(W/kg) = 0.4226346 - 0.3519215(Kns)	0.244	0.0002
Grand Total +Pow	1	GrandTot+Pow(W/kg) = 0.4383128 - 0.2982346(Kns)	0.171	0.0022
Tot Ank -Pow	1	TotAnk-Pow(W/kg) = -0.217201 + 0.2332674(Kns)	0.358	0.0001
Exo -Pow	2	Exo-Pow(W/kg) = -0.003351 - 0.4058288(Kns) + 0.8548961(Kns)^2	0.436	0.0001
Ank Bio -Pow	2	AnkBio-Pow(W/kg) = -0.225295 + 0.874113(Kns) - 1.5961034(Kns)^2	0.705	0.0001
Total Bio -Pow	2	TotBio-Pow(W/kg) = -0.460028 + 1.361092(Kns) - 3.3451545(Kns)^2	0.221	0.017
Grand Total -Pow	2	GrandTot-Pow(W/kg) = -0.463399 + 0.957605(Kns) - 2.4987741(Kns)^2	0.115	0.045
Norm Sol EMG	1	IntSolEMG(norm) = 0.9500082 - 0.2627736(Kns)	0.1	0.03

Norm TA EMG	2	IntTAEMG(norm) = 0.994444 + 2.3664023(Kns) - 5.2660847(Kns)^2	0.191	0.01

* Kns = Normalized Spring Stiffness

Table C2: Regression equations for net metabolic power vs. time training with elastic ankle exoskeletons of varying spring stiffness during walking at 1.25 m/s.

Metric	Fit Order	Fit Equation	R2	p-value
No Spring	2	No Spring = 0.4828546 - 0.013859*Time (Min) - 0.0001168*Time (Min)^2	0.28	P=.009
129	2	129 Nm/Rad = 0.5245192 - 0.0267731*Time (Min) + 0.0001284*Time (Min)^2	0.18	P=.064
182	2	182 Nm/Rad = 0.4634496 - 0.0255925*Time (Min) + 8.8951e-5*Time (Min)^2	0.28	P=.009
243	2	243 Nm/Rad = 1.142391 - 0.0829873*Time (Min) + 0.00123*Time (Min)^2	0.36	P=0.002
307	2	307 Nm/Rad = 0.5335541 - 0.0243367*Time (Min) + 0.0006954*(Time (Min)-17.8182)^2	0.23	P=0.021
396	2	396 Nm/Rad = 0.3232031 + 0.0019089*Time (Min) - 0.0004309*Time (Min)^2	0.1	P=0.35